**TRIBHUVAN UNIVERSITY**

**INSTITUTE OF ENGINEERING**

**PULCHOWK CAMPUS**

**THESIS NO: PUL079MSPSE010**

# "Experimental Investigation of the Dielectric Strength of the Insulating stand-offs of Electrically Insulated Lightning Protection Systems under Standard Lightning Impulse Voltages"


**By**

**Gyanendra Kumar Kurmi**

**PUL079MSPSE010**


**A THESIS**

**SUBMITTED TO THE DEPARTMENT OF ELECTRICAL ENGINEERING IN PARTIAL FULFILMENT OF THE REQUIREMENTS FOR THE DEGREE OF MASTER OF SCIENCE IN ELECTRICAL ENGINEERING IN POWER SYSTEM ENGINEERING**


**DEPARTMENT OF ELECTRICAL ENGINEERING**

**LALITPUR, NEPAL**



**April 2025**

**Experimental Investigation of the Dielectric Strength of the Insulating Stand-offs of Electrically Insulated Lightning Protection Systems under Standard Lightning Impulse Voltages**

By

Gyanendra Kumar Kurmi

Roll No: PUL079MSPSE010

Thesis Supervisor:

Associate Professor Dr. Basanta Kumar Gautam

Department of Electrical Engineering

Pulchowk, Nepal

A Thesis

submitted to the Department of Electrical Engineering in partial fulfillment of the

requirements for the Degree of

Master of Science in Electrical Engineering in Power System Engineering

Department of Electrical Engineering

Institute of Engineering, Pulchowk Campus

Tribhuvan University

Lalitpur, Nepal

April 2025

त्रिभुवन विश्वविद्यालय
TRIBHUVAN UNIVERSITY
इन्जिनियरिङ्ग अध्ययन संस्थान
INSTITUTE OF ENGINEERING
पुल्चोक क्याम्पस
PULCHOWK CAMPUS
DEPARTMENT OF ELECTRICAL ENGINEERING
Pulchowk, Lalitpur





## CERTIFICATE OF APPROVAL

The undersigned certify that they have read and recommended to the Institute of Engineering for acceptance, a dissertation entitled "**Experimental Investigation of the Dielectric Strength of the Insulating Stand-offs of Electrically Insulated Lightning Protection Systems under Standard Lightning Impulse Voltages**", submitted by **Gyanendra Kumar Kurmi** in partial fulfillment of the requirement for the award of the degree of **Master of Science in Power System Engineering.**

Assoc. Prof. Lalit Bikram Rana
Faculty of Science and Technology
Pokhara University
(External Examiner)

Asst. Prof. Dr. Bishal Silwal
Program Coordinator
M. Sc. in Power System Engineering
Department of Electrical Engineering
Pulchowk Campus, Lalitpur

Assoc. Prof. Dr. Basanta Kumar Gautam
Head of Department
Department of Electrical Engineering
Pulchowk Campus, Lalitpur
(Supervisor)

April 2025

## DECLARATION AND AUTHORIZATION

This statement formally certifies that the enclosed thesis represents the candidate's authentic and independent research, undertaken solely by them and not previously presented for any other academic qualification or used to obtain a prior degree. It further grants the Institute of Engineering, Pulchowk Campus, explicit permission to disseminate this work for scholarly purposes, including lending copies to other institutions or individuals, and reproducing it through photocopying or other means, in its entirety or in part, ensuring its availability for academic research.

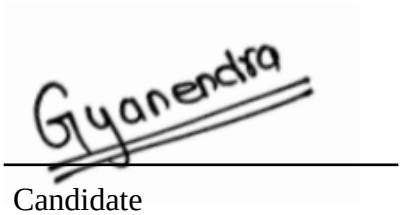

Candidate

Gyanendra Kumar Kurmi

PUL079MSPSE010

Department of Electrical Engineering

Pulchowk Campus

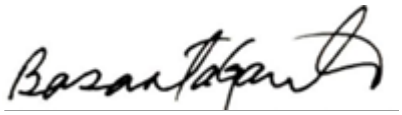

Supervisor

Assoc. Prof. Dr. Basanta Kumar Gautam

Head of Department

Department of Electrical Engineering

Pulchowk Campus

## COPYRIGHT©

## ACKNOWLEDGEMENT

I would like to express my deepest gratitude to my supervisor Associate Prof. Dr. Basanta Kumar Gautam, for his invaluable guidance, insightful comments, and continuous support and encouragement throughout the progress of this research work. Furthermore, I am immensely thankful to Prof. Dr. Navaraj Karki, Asst. Prof. Yuba Raj Adhikari, Asst. Prof. Anil Panjiyar, Asst. Prof. Dr. Bishal Silwal and the whole team of Department of Electrical Engineering, IOE, Pulchowk Campus for providing the necessary resources and environment conducive to academic growth and learning.

I am also grateful for the opportunity to participate in student mobility funded by Erasmus International Student Program of the European Union. This experience not only enriched my academic journey but also broadened my perspectives, allowing me to engage with diverse cultures and academic traditions. The financial sup- port provided under this project made it possible for me to pursue this invaluable learning experience abroad.

I express my sincere thanks go to School of Electrical and Computer Engineering, Electrical Sector, High Voltage Laboratory at Aristotle University of Thessaloniki, Greece and to Prof. Pantelis N. Mikropoulos and Petros P. Tsouris for their precious suggestion and kind support throughout this research work.

Lastly, I would like to extend my appreciation to my friends and parents for their unwavering encouragement and understanding during this challenging yet rewarding endeavor. Their moral support has been a constant source of strength throughout my academic pursuits. This thesis would not have been possible without the contributions and support of all those mentioned above. Thank you all for believing in me and for being part of this journey.

Gyanendra Kumar Kurmi

PUL079MSPSE010

## ABSTRACT

Lightning protection systems (LPS) are crucial for safeguarding structures, electrical equipment, and personnel from the destructive impacts of lightning strikes. Insulating stand-offs, vital components of these systems, support and electrically isolate down conductors from the protected structure. These stand-offs must withstand the high-voltage surges generated during lightning events, which often exceed hundreds of kilovolts. Evaluating their performance under standardized lightning impulse voltages (typically aligned with IEC standards) helps determine their ability to maintain insulation integrity during real-world lightning strikes. However, the dielectric strength of insulating stand-offs, critical to LPS effectiveness is influenced by factors such as material composition, geometric design, environmental exposure, and voltage waveform characteristics. Standard lightning impulse voltages are defined by extremely short durations and high peak voltages, such as the 1.2/50 µs waveform. Under these transient conditions, insulating materials may behave differently compared to steady-state or gradually applied voltages. Testing under lightning impulse conditions is therefore essential to verify that materials can endure the rapid voltage rise and brief, high-energy nature of actual lightning strikes. Insulating stand-offs that fail under such impulses risk compromising the entire lightning protection system. Assessing their dielectric strength minimizes failure risks and ensures system functionality during lightning events. This research involves laboratory experiments to evaluate the dielectric strength of insulating stand-offs of varying lengths under standardized lightning impulse (LI) voltage conditions. The resulting data will be analyzed to identify key factors influencing performance. The findings aim to optimize LPS design, enhancing reliability and effectiveness in protecting critical infrastructure.

Positive polarity exhibits higher flashover voltage and better withstand capability, while negative polarity shows increased discharge current and variability, especially with longer standoffs. Flashover voltage and discharge current increase with standoff length. Negative polarity yields higher maximum currents at longer lengths. Spark conductance increases linearly with voltage, with negative polarity showing higher conductance



**Keywords:** Electrically Insulated Lightning Protection System, Insulating Standoffs, Standard Lightning Impulse Voltages, Dielectric Strength

## TABLE OF CONTENTS

## LIST OF FIGURES

## LIST OF TABLES

## LIST OF ABBREVIATIONS

| | |
|---|---|
| ATP-EMTP | Alternative Transient Program-Electromagnetic Transient program |
| DCB | Dielectric Breakdown |
| $\eta$ | Efficiency |
| EILPS | Electrically Insulated Lightning Protection System |
| FOV | Flashover Voltage |
| HV | High voltage |
| IEC | International Electrotechnical Commission |
| kV | Kilo Volt |
| LI | Lightning Impulse |
| LPS | Lightning Protection System |
| µs | Microsecond |
| NFPA | National Fire Protection Association |
| SIL | Standard Lightning Impulse |
| $T_1$ | Front Time |
| $T_2$ | Tail Time |
| $U_{ap}$ | Applied Voltage |
| $U_p$ | Flashover Voltage |
| LPL | Lightning Protection Level |

# CHAPTER ONE: INTRODUCTION

## 1.1 Introduction

Lightning protection systems are critical in safeguarding structures, electrical equipment, and personnel from the damaging effects of lightning strikes. Insulating stand-offs are essential components in electrically insulated lightning protection systems (EILPS) as they support and electrically isolate conductors or rods from the structure being protected. Insulating stand-offs used in EILPS, must endure the overvoltage's arising during a lightning strike (often in the range of hundreds of kilovolts). Investigating how these materials behave under standard lightning impulse voltages helps assess their capability to maintain insulation properties during real-world lightning events. The surface dielectric strength of insulating stand-offs, a critical component of EILPS, is influenced by various factors such as material properties, geometry, environmental conditions, and surge overvoltage waveform.

The surface dielectric behaviour of insulating materials under fast-front transients differs significantly from their behaviour under steady or slowly increasing voltages. Therefore, testing the dielectric behaviour of insulating materials under lightning impulse voltages is of crucial importance. Failure of insulating stand-offs can lead to undesired flashovers to the metal installation within a structure is maintained resulting in catastrophic consequences. By testing the surface dielectric strength of these stand-offs, it's possible to minimize the risk of failure and ensure the structure remains protected in the event of a lightning strike.

A lightning strike can cause immense arising overvoltages, with peak values ranging from several hundred kilovolts to megavolts. The rising surge is very steep and it is typically characterized as a lightning overvoltage, a transient electrical phenomenon that can damage or compromise the integrity of electrical equipment and structural components.

## 1.2 Overvoltage

Overvoltage in power system is defined as the increase in voltage for the very short time in the power system. It is also known as the voltage transients or voltage surge. It is also defined as voltages that exceed in value the maximum allowable operating voltage value of the equipment. They are categorized according to their origin into temporary, long

duration front, short duration front and very short duration front. Earth faults, or lightning strikes on line conductors for long-distance transit from the system are the main causes of long-duration surges or internal surges in a system. Direct or indirect lightning strikes, as well as system manipulations and failures, can cause short-duration front surges or external surges.

**Types of overvoltage**

Overvoltage phenomena in the power system can be classified into two types and they are given below.

### 1.2.1 Internal overvoltage

Switching impulse voltages, which replicate internal overvoltage in the lab, are defined as impulse voltages with a front duration longer than 20 μs and typically a larger overall duration. The main causes of internal overvoltages in a system are lightning strikes on transmission line conductors located far from the system, handling, and ground faults. the subject of this work and therefore a simple reference is deemed sufficient. The waveform of laboratory-generated standard switching impulse voltage, SI, of 250/2500 μs front duration and half-width respectively, as defined by IEC[1] is presented in Figure 1.1.

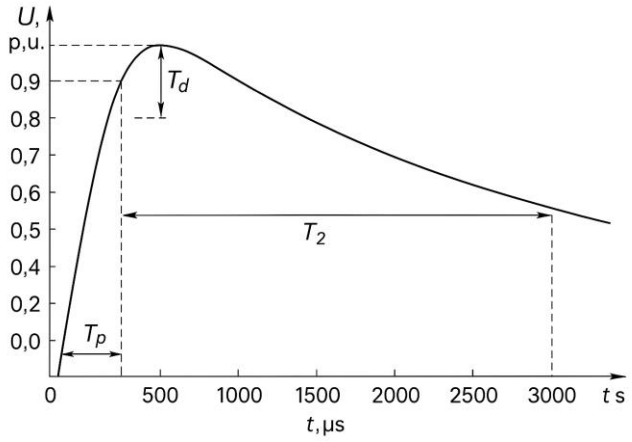


Figure 1.1: Waveform of Switching Impulse Voltage

### 1.2.2 External overvoltage

Lightning impulse voltages mimic external overvoltages in the lab and are characterized as impulse voltages with a front duration of less than 20 μs [1]. Short-duration front surges or external surges can be caused by direct or indirect lightning strikes, system manipulations, or malfunctions. Lightning impulse high voltages are characterized by the

amplitude or peak voltage Up, the front duration $T_1$ and the half-width duration $T_2$. Direct or indirect lightning strikes can cause external surges, which are replicated in the lab by using lightning impulse high voltages.

### 1.3 Lightning Phenomena

Lightning is a natural event caused by electrostatic discharges between charged areas in the atmosphere, releasing energy almost instantly. This discharge generates electromagnetic radiation, such as heat and visible light. Thunderstorms form when moist, warm air rises to higher altitudes, which can happen through different types: heat thunderstorms driven by strong sunlight, frontal thunderstorms caused by cold air pushing under warm air, and orographic thunderstorms triggered by terrain elevation. Orographic thunderstorms develop when ground-level warm air is forced to rise. This upward motion is intensified by physical factors, leading to strong updraft channels that can reach speeds of up to 100 km/h. As a result, large cumulonimbus clouds form, typically standing between 5 and 12 kilometres tall and spanning 5 to 10 kilometres wide[2]. Electrostatic charge separation processes charge water droplets and ice particles, with positive and negative charges. Thunderstorms generate corona discharge from ground objects, transported by wind. If space charge densities in a thundercloud produce strong local field, leader discharges initiate lightning discharges. Cloud-to-cloud flashes neutralize charge between cloud and ground centres, but their electromagnetic impulses pose a threat to electrical and electronic systems. Flashes to earth neutralize charge between cloud and ground charges, with two types distinguishable.

Downward flashes involve lightning discharges from the cloud to the ground, typically occurring in areas with flat landscapes and shorter structures, cloud-to-ground lightning strikes are typically observed. These flashes are recognizable by their branches extending toward the ground. The most frequent form is a negative downward strike, in which a leader carrying a negative charge from the cloud descends toward the earth. as in Figure 1.2. This leader propagates at a speed of around 300 km/h in steps of a few 10 m. When the leader draws close to the earth, the electric field strength of objects near the leader increases, exceeding the air's dielectric strength.

Positive downward lightning can originate from the lower, positively charged regions of a thundercloud, though such strikes are less common—making up roughly 10% compared to 90% for negative flashes, depending on the region. Upward lightning typically occurs from tall, isolated structures or mountaintops, initiated by strong distortions in the surrounding electric field. These upward discharges can carry either a negative or positive charge. Because the lightning leaders travel from the ground-based object up to the cloud, a single lightning event can strike tall structures multiple times during a thunderstorm.

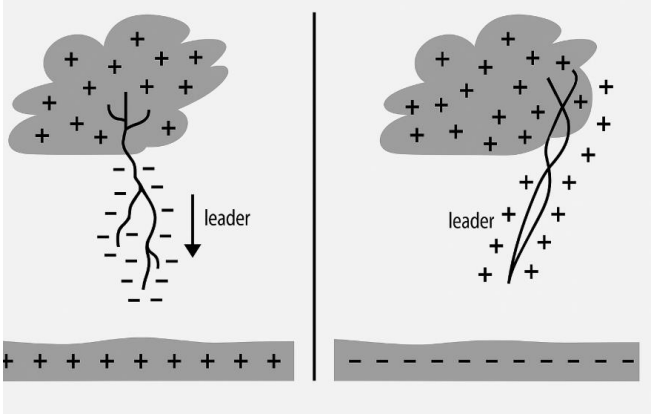


Figure 1.2: Discharge mechanism of negative and positive downward flash

### 1.4 Lightning Impulse Voltage

A lightning impulse is the sharp, transient electrical pulse generated during a lightning strike, characterized by high voltage and current. This impulse can cause electrical surges, damage to infrastructure, and interference with electronics. In lab, impulse high voltages replicate surges that might occur in an electrical power system as a result of lightning strikes or manipulations.

IEC 60060-1:2010[1] defines an impulse as any purposefully induced aperiodic pulse of voltage or current that typically increases quickly to its maximum and then gradually decays to zero. Impulse high voltages are classified as switching (SI) or lightning (LI) based on the length of time their front lasts. Lightning impulse high voltages have a front duration of less than 20 μs, whereas switching impulse high voltages have a front duration of more than 20 μs.

In our project lightning impulses voltages are produced in lab, which are characterized by the range or peak voltage Up, the front duration $T_1$, and the half width duration $T_2$ as in

Figure 1.3 while for their description it is customary to refer to them as: "Up(kV), T1/T2 (μs)'.

IS-2071-1 [1] and IEC 60060-1 [1] specify that the Standard Lightning Impulse (SLI) shall be a (1.2/50 μs) wave, meaning that it must have a 1.2 μs rise time and a 50 μs tail period. With a rise time of 1.2 μs, a conventional value, the impulse waveform has to reach its maximum value from zero approximately in 2.2 μs, and a tail time of 50 μs indicates that it will take 50 μs for the impulse waveform to reach its half amplitude from the origin. Less than ±3% for the peak value, ±30% for the front time, and ±20% for the tail time is the allowable tolerance [1]. Additionally, the SLI voltage waveform needs to be unipolar and free of significant oscillations.

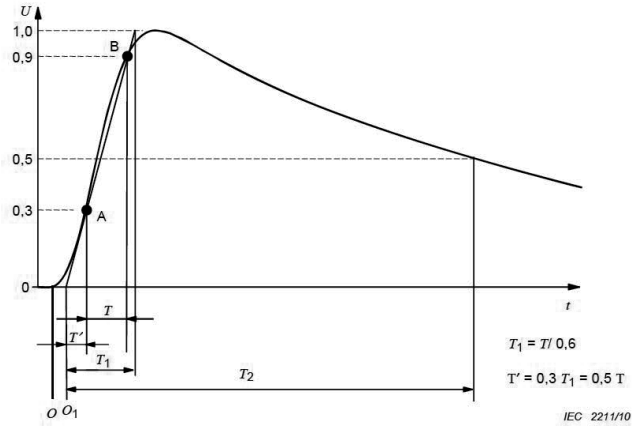


Figure 1.3: Waveform of Lightning impulse voltage

### 1.5 Dielectric strength and flashover mechanism

Dielectric strength refers to the ability of a material to withstand high-voltage stress without breaking down and allowing electrical conduction. Breakdown occurs when the material's dielectric strength is exceeded, leading to a loss of insulation. Breakdown can occur in several forms.

**Surface Flashover:** When the electric field along the surface of the insulator exceeds its threshold, causing the voltage to arc over the surface.

**Partial Discharge:** Localized discharges within the material that do not lead to full breakdown but cause long-term degradation.

**Bulk Breakdown:** When the material's internal electric field exceeds its dielectric limit, causing a complete breakdown.

Insulating stand-offs are vital in EILPS to prevent flashovers. Dielectric strength testing is crucial to ensure these stand-offs can withstand high lightning voltages without failing, guaranteeing safety and system reliability, and meeting standards. Different stand-off materials require this testing to verify their insulating capabilities and long-term performance.

The Lightning Protection Level (LPL I-IV) dictates the severity of the expected lightning strike. Based on the chosen LPL, IEC standards provide formulas to calculate the minimum separation distance (s) needed to prevent flashovers. The length of the insulating stand-off must be at least this calculated distance. Higher LPLs typically require larger separation distances and thus potentially longer stand-offs. Crucially, the stand-off material's dielectric strength ensures this physical separation effectively prevents flashovers under the voltage stresses associated with the specific LPL. Therefore, both the calculated separation distance based on the LPL and the inherent dielectric strength of the stand-off material are critical factors in selecting appropriate components for effective EILPS.

For LPS, the dielectric strength of insulating materials is of critical importance. The materials must resist these breakdown mechanisms, especially under lightning impulse voltages, which have very different characteristics compared to steady-state AC or DC voltages[3].

### 1.6 Lightning Impulse Voltages and Their Effect on Dielectric Strength

Lightning impulse voltages are characterized by their very fast rise time (1.2 μs) and relatively long tail (50 μs), mimicking the conditions experienced by electrical systems during a lightning strike. These voltages induce high electric fields in insulating materials, which may lead to different breakdown mechanisms compared to AC or DC voltages. The high peak voltage and rapid rise time stress the insulating material, making it more susceptible to failure, particularly under adverse environmental conditions (e.g., moisture, surface contamination)[4].

The study of dielectric strength under lightning impulse conditions is critical because it provides more accurate insights into the performance of LPS under actual lightning strike

conditions. It is necessary to test materials under such conditions to ensure that they remain functional and prevent breakdown during real-world lightning events[5].

## 1.7 Lightning Protection System

As Lighting is a magnificent manifestation of nature's might, it can all be damaging. Its massive electrical discharge has the potential to seriously harm equipment, buildings, and even people. Lightning protection systems (LPS) have been created to safely intercept and redirect lightning strikes to the ground in order to reduce these hazards[6]. A lightning protection system's purpose is to shield buildings from mechanical or fire damage and to prevent injuries or even fatalities to occupants. An external and an internal lightning protection system make up a lightning protection system.

The functions of external lightning protection system are

- To intercept direct lightning strikes via an air termination system[8].
- To safely conduct the lightning current to the ground via a down-conductor system[8].
- To distribute the lightning current in the ground via an earth termination system[8].

### 1.7.1 Component of External LPS

#### 1.7.1.1 Air-termination system

This system consists of conductive components (air terminals) which are positioned strategically on building's highest points to form this system. These objects serve as a preferred for lighting strikes[9]. The LPS's air-termination system prevents direct lightning strikes from damaging the area that needs to be protected. It must be made to prevent uncontrollably occurring lightning strikes on the structure or building that needs to be protected.

#### 1.7.1.2 Down-conductors

They are a critical component of a lightning protection system (LPS). They provide a low-resistance path for the lightning current to travel safely from the air termination system to the grounding system[10]. This helps to minimize the risk of side-flashing, structural damage, and fire hazards caused by lightning strikes. Similarly, multiple conductors ensure lightning current division and that if one path is damaged or overloaded, the current is still

safely directed to the ground. Down conductors are installed externally away from the structure to maintain isolation. They are routed vertically and in a direct path to the ground to minimize inductance and potential arcing[9].

#### 1.7.1.3 Earthing system

The earthing system is a crucial component of any lightning protection system. The purpose of an earth termination network (earthing system) is to provide a low impedance pathway for lightning discharge currents to dissipate into the ground safely. An earthing network should be designed to provide a low resistance path to the earth, typically as per IEC/BS EN 62305 standards which recommend being below 10 ohms.

#### 1.7.1.4 Insulating stand-off

These are essential parts of the system, ensuring that conductors are held in place and electrically insulated from the structure being protected. The insulating stand-offs play a significant role in maintaining the integrity of the lightning protection system by preventing direct electrical contact between the lightning conductors and the protected structure, thus avoiding potential damage to the structure and any electrical systems. Insulating stand-off, also referred to as insulators, are used to support and electrically isolate the components of the lightning protection system, particularly the conductors or cables, from the structures. It also ensures that the lightning conductors do not become grounded through contact with the structures, which could cause arcing thus fail to properly dissipate the lighting energy into the earth[11]. By keeping conductors electrically insulated, insulating stand-offs prevent the lightning current from affecting the building's electrical and communication systems, which could lead to fires or system failures, due to induced overvoltages.

**Why Insulating Standoffs are Used**

1. **Prevent Side Flashes (Arcing)**

   Lightning currents can exceed 200 kA, creating massive voltages. If the down conductor contacts the structure, a portion of the current may arc ("side flash") to conductive parts of the building, causing fires, equipment damage, or electrocution. Insulating standoffs maintain a physical and electrical gap to block this arcing.

2. **Avoid Galvanic Corrosion**
   Direct contact between dissimilar metals (e.g., copper down conductor and steel structure) in humid environments causes electrochemical corrosion. Standoffs eliminate this contact, preserving structural integrity.
3. **Isolate Ground Loops**
   In systems with sensitive electronics, conductive paths between the LPS and equipment can create ground loops, leading to electromagnetic interference (EMI). Insulating standoffs break these paths.
4. **Enhance System Reliability**
   By isolating the LPS from the structure, standoffs ensure lightning current follows the intended low-resistance path to ground, improving system performance.

**Types of insulating stand-off**

Insulating stand-offs are generally Categorized by length (Voltage Withstand) and material (environmental/mechanical durability).

**1. By Length**

The required length depends on the lightning impulse voltage and clearance needed to prevent arcing. Standards like IEC 62305 define minimum distances based on lightning protection levels (LPL I–IV).

- **Short Standoffs (10–30 cm)**
  For low-risk applications (e.g., residential buildings) or structures with limited lightning exposure.
- **Medium Standoffs (30–100 cm)**
  Used in industrial facilities or taller structures requiring higher voltage isolation (e.g., 100–500 kV withstand).
- **Long Standoffs (>1 m)**
  For critical infrastructure (e.g., power substations, telecom towers) where lightning currents exceed 100 kA, requiring extreme voltage isolation (e.g., >1 MV).

## 2. By Material

On the basis of material insulating standoffs can be classified as follows.

### a. Polymers

This material boasts several desirable properties, including high dielectric strength for excellent electrical insulation, a lightweight composition for ease of handling and reduced structural burden, inherent resistance to degradation from ultraviolet (UV) radiation, and a flexible nature that allows for versatile application across various surfaces. These characteristics make it a compelling choice for numerous electrical and structural contexts where durability and adaptability are key considerations.

However, a significant limitation of this material is its susceptibility to surface tracking, particularly in environments characterized by high levels of pollution or humidity. The accumulation of contaminants on its surface under moist conditions can lead to the formation of conductive pathways, potentially compromising its insulating capabilities and increasing the risk of electrical faults. Despite this drawback, its beneficial attributes have led to its adoption in specific applications such as telecom towers, rooftops, and coastal installations, where the advantages often outweigh the risks associated with surface tracking, provided appropriate mitigation measures are in place.

### b. Composites

This material presents a compelling set of properties that make it suitable for demanding applications. Its high strength-to-weight ratio signifies that it can bear significant loads relative to its mass, offering structural integrity without excessive bulk. Furthermore, its inherent corrosion resistance ensures longevity and reliability even in harsh or chemically active environments, minimizing the need for frequent maintenance or replacement. The non-conductive nature of the material provides crucial electrical insulation, expanding its utility in applications where electrical isolation is paramount for safety and performance.

Despite these considerable advantages, a notable limitation of this material is its higher cost when compared to more basic polymer alternatives. This economic factor can influence material selection decisions, particularly in high-volume or cost-sensitive

projects. However, the superior performance and extended lifespan often associated with its unique properties can, in many cases, justify the initial investment by reducing long-term operational costs and enhancing overall system reliability.

### 1.8 Statement of Problems

The dielectric strength of insulating stand-offs in lightning protection systems under simulated lightning impulse conditions has not been sufficiently studied, and existing data on their performance is limited. The lack of comprehensive experimental investigations into the breakdown characteristics of insulating stand-offs under these conditions could lead to inadequate lightning protection and the failure of critical electrical systems in Lightning Protection Systems (LPS), insulating stand-offs play a critical role in ensuring the proper functioning of the system by electrically isolating lightning conductors from the protected structure. These insulating stand-offs must withstand the extreme conditions created by lightning strikes, which can involve high-voltage impulse currents with very short durations.

However, the dielectric strength of insulating stand-offs under standard lightning impulse voltages (typically characterized by a 1.2/50 μs waveform, as defined by standards like IEC 62305) has not been sufficiently characterized in some materials used for these stand-offs. The behavior of these materials under such conditions particularly their ability to maintain insulation and mechanical support when subjected to high-voltage lightning surges is not fully understood. The performance of insulating materials under lightning impulse conditions is uncertain, and testing their dielectric strength is crucial to prevent damage to structures or electrical systems. New materials like ceramics, polymers, and composites need to be evaluated for durability, weight, and cost. Understanding the dielectric strength is crucial for designing lightning protection systems, as inadequate or poorly selected stand-offs can compromise overall structure protection.

## 1.9 Objectives

### 1.9.1 Primary Objective

- To experimentally investigate the dielectric strength of insulating stand-offs used in electrically insulated lightning protection systems (EILPS) under standard lightning impulse voltages

### 1.9.2 Secondary Objective

- To identify the factors influencing the dielectric strength of insulating stand-offs, such as length of insulating standoffs and polarity of applied voltage waveforms.
- To identify the effect of material and length of insulating stand-offs on Electric field distribution by using COMSOL Multiphysics.
- To assess the electrical properties of insulating materials, focusing on their strength to lightning impulse voltages and their ability to maintain integrity during repeated surge events.

## 1.10 Scopes

- The experimental setup focused on simulating positive and negative lightning surge voltages using a standard impulse waveform of 1.2/50 μs, as defined by the IEEE and IEC standards.
- The study considered resin as the insulating material used for standoffs and examined three different lengths of standoffs: 25 cm, 50 cm, and 75 cm.
- The investigation also examined the dielectric strength of the standoffs by overstressing the insulating components.
- This investigation further examined the effect of materials and the length of standoffs on the electric field distribution using COMSOL Multiphysics
- This investigation examined the effect of materials and length of stand-offs on the electric filed distribution in COMSOL Multiphysics.

## 1.11 Limitations

- The investigation of insulating standoff flashover using lightning impulse voltages with differing waveforms was not considered.
- The spark path during electrical discharge were not observed with a camera and its correlation with the electrical characteristics of the discharge, were not considered.
- Testing was conducted in a laboratory environment, and real-world environmental factors such as pollution, humidity, and temperature variations, as well as mechanical wear, were not considered.

## 1.12 Report Organization

Chapter 2 presents a concise literature review on physical aspect and factors influencing the flashover mechanism in insulating materials.

Chapter 3 describes the High Voltage Laboratory of Aristotle University of Thessaloniki (AUTH), including the experimental setup, equipment, and specifications of the lightning impulse voltages applied. Details of the insulating stand-offs tested and the experimental configuration are also outlined.

Chapter 4 analyzes the surface electric field distribution around the stand-offs. This chapter explains the methodology used to calculate the field distribution, presents the results, and investigates how variations in material properties affect electric field patterns.

Chapter 5 defines key experimental parameters and measurement techniques, ensuring clarity for readers, and elaborates on the experimental procedure.

Chapter 6 presents and discusses the experimental results for stand-offs of varying lengths. Processed measurement data are visualized in diagrams, with analysis of the effects of voltage polarity, amplitude, and stand-off length on dielectric performance.

Chapter 7 summarizes key conclusions derived from the experimental measurements.

Chapter 8 proposes directions for future research on improving the dielectric strength of insulating stand-offs in EILPS.

# CHAPTER TWO: LITERATURS REVIEW

The development of insulating standoffs for lightning protection systems (LPS) has paralleled advancements in electrical and materials engineering, primarily driven by the need to prevent damaging side flashes. Early LPS, like those pioneered by Benjamin Franklin, focused on diverting lightning strikes using conductive rods. However, these systems often lacked proper insulation between conductors and structures, leading to arcing risks as buildings grew taller and incorporated metal frameworks. Initial attempts at insulation, using glass, porcelain, or wood, were limited in durability and performance.

The mid-20th century, with its rise in steel-framed structures, demanded more reliable insulation. Post-World War II innovations in synthetic polymers and advanced ceramics revolutionized standoff design, offering superior dielectric strength and weather resistance. Standards like IEC 62305[8] formalized insulation requirements, highlighting the critical role of standoffs in LPS.

Recent decades have seen significant refinements in standoff design, aided by computational modelling and lessons from real-world failures. Tools like COMSOL Multiphysics have allowed engineers to optimize standoff geometry and materials, addressing issues like sharp edges and air gaps that can lead to ionization. Modern standoffs are engineered for extreme environments, using composite materials and hybrid designs, and are rigorously tested to meet standards like IEC 62305-3[12].

Today, insulating standoffs are essential in protecting critical infrastructure, ensuring lightning energy is safely dissipated. Their evolution reflects a century of innovation, integrating physics, materials science, and computational engineering.

## 2.1 Physical aspect of standoffs

Insulating standoffs are essential components in lightning protection systems. Their primary function is to electrically isolate the lightning protection conductor (usually a metal rod or cable) from the building structure it's attached to. The Figure 2.1 shows the different aspect of insulating standoffs.

1. Insulating Material: The central, dark-coloured section appears to be the insulating material. It's likely made of a high-dielectric strength polymer such as:

2. End Fittings (Metal Caps): The metallic components on either end of the insulator are the end fittings. These are typically made of corrosion-resistant metals like

   Stainless Steel: Provides excellent corrosion resistance and strength.

   Aluminium: Lightweight and corrosion-resistant, often used in less demanding applications.

3. Length and Diameter: The length and diameter of the standoff are critical parameters. They determine the creepage distance (the shortest path along the surface of the insulator between the energized conductor and the grounded structure) and the strike distance (the minimum air gap between the conductor and the structure). These distances must be sufficient to prevent flashover.

4. Surface Condition: The surface of the insulator should be smooth and clean to minimize the risk of surface tracking (the formation of conductive paths on the insulator surface due to contaminants).

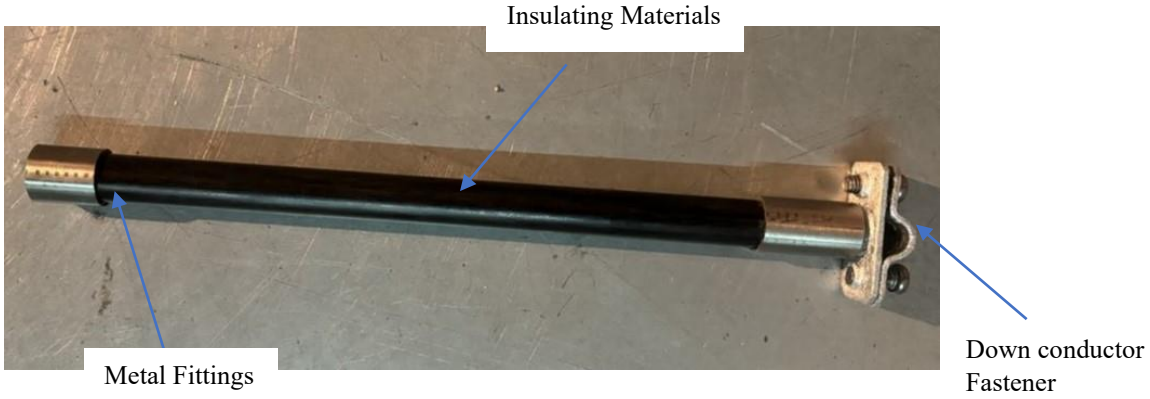


Figure 2.1: Physical Aspect of insulating standoff

## 2.2 Insulating Materials

Insulating materials in electrical applications require more than just strong dielectric properties. They must also endure various environmental stressors, including radiation, contamination, and lightning surges. Additionally, these materials need sufficient tensile, compressive, and mechanical strength to handle the physical loads they will encounter. Essentially, they must be robust against both electrical and physical challenges to ensure reliable performance.

### 2.2.1 Polymer

Polymer insulating standoffs are widely used in modern lightning protection systems (LPS) to electrically isolate down conductors from protected structures, preventing side flashes and ensuring safe dissipation of lightning currents. These standoffs leverage advanced polymer materials, such as polypropylene, polyethylene, and fiberglass-reinforced composites, which offer a balance of dielectric performance, mechanical durability, and environmental resistance. Unlike traditional ceramic or glass insulators, polymers are lightweight, corrosion-resistant, and easier to mold into complex geometries, making them ideal for diverse architectural and industrial applications. Their adoption has grown due to advancements in polymer science, enabling tailored designs that meet stringent international standards (e.g., IEC 62305, NFPA 780). However, while polymer standoffs provide significant advantages, they also exhibit limitations that engineers must address during system design and installation.

The Positive Features of Polymer Insulating Standoffs are

1. High Dielectric Strength: Polymers like polyethylene can withstand electric fields up to 20–50 kV/mm, effectively isolating down conductors even during high-current lightning strikes.
2. Corrosion Resistance: Unlike metallic components, polymers are immune to rust and electrochemical degradation, ensuring longevity in humid or coastal environments.
3. Lightweight and Easy to Install: Reduced weight simplifies mounting on structures and lowers logistical costs compared to ceramics or glass.
4. Design Flexibility: Polymers can be molded into custom shapes (e.g., flanged, curved) to accommodate complex structural geometries or aesthetic requirements.
5. Cost-Effective: Lower manufacturing and material costs compared to ceramics make polymers economically viable for large-scale projects.

The limitations of Polymer Insulating Standoffs are

1. Temperature Sensitivity: Prolonged exposure to high temperatures (>100°C) can degrade thermoplastic polymers, reducing dielectric and mechanical performance.

2. Lower Mechanical Strength: Compared to ceramics, polymers have lower compressive strength, limiting their use in applications requiring heavy load-bearing capacity.
3. Aging and Degradation: UV exposure, ozone, and chemical pollutants can cause gradual embrittlement or surface cracking over time.
4. Limited Thermal Conductivity: Polymers trap heat, potentially leading to thermal stress in high-current scenarios if not properly ventilated.
5. Surface Contamination Risks: Dust, salt, or industrial pollutants on polymer surfaces can create conductive paths, increasing leakage current risks.

### 2.2.2 Epoxy resin

Epoxy resin insulating standoffs are widely utilized in lightning protection systems (LPS) due to their unique combination of electrical, mechanical, and chemical properties. These standoffs serve as critical components to isolate down conductors from protected structures, preventing side flashes and ensuring lightning currents follow a controlled path to ground. Epoxy resins are favored for their ability to be molded into complex shapes, high adhesion to metals, and resistance to environmental stressors. However, like all materials, they present trade-offs between performance benefits and limitations, which must be carefully evaluated during LPS design and installation.

The positive features of epoxy resin insulating standoffs are

1. High Dielectric Strength: Epoxy resins exhibit excellent dielectric properties (typically 15–25 kV/mm), effectively insulating against lightning-induced voltages and preventing arcing between the down conductor and structure.
2. Mechanical Durability: They offer high compressive strength and rigidity, maintaining structural integrity under mechanical loads such as wind, vibration, or thermal expansion.
3. Environmental Resistance: Epoxy is inherently resistant to moisture, chemicals (e.g., acids, alkalis), and corrosion, making it suitable for harsh environments like coastal or industrial areas.

4. Adhesion and Sealing Properties: Epoxy bonds strongly to metals and other substrates, creating a seamless interface that prevents moisture ingress and reduces partial discharge risks.
5. Thermal Stability: Retains insulating properties across a broad temperature range (-40°C to +150°C), ensuring reliability in extreme climates[13].

The limitations of epoxy resin insulating standoffs are

1. Brittleness at Low Temperatures: Epoxy becomes brittle in sub-zero conditions, increasing susceptibility to cracking under mechanical stress (e.g., ice loads or impact).
2. UV Degradation: Prolonged exposure to ultraviolet radiation can cause surface chalking or microcracking unless UV-stabilized additives or protective coatings are applied.
3. Cost and Complexity: High-performance epoxy formulations and precision molding processes are costlier compared to basic polymers like polyethylene.
4. Weight: Epoxy standoffs are heavier than polymer alternatives, potentially complicating installation on lightweight structures.
5. Limited Flexibility: Rigid epoxy designs may not accommodate structural movement as effectively as elastomeric materials, risking fatigue failure over time.

In the Literature Review the various existing techniques of measuring the dielectric strength, flashover of insulator stand-off and development of various scholars have been briefly reviewed. During the past few decades there has been a continually increasing interest and investigation in the flashover and dielectric strength of the insulators.

*Zhang et al. 2018* investigates the flashover performance of two types of insulators, composite and glass, in lightning impulse flashover tests at the National Engineering Laboratory. The tests recorded discharge path and 50% impulse flashover voltage, and electric fields in the vicinity of the insulators were calculated using the finite element

method. The study found a relationship between flashover performance and electric field distribution[14].

In paper *Mikropoulos et al. 2022* an investigation of lightning impulse flashover characteristics of a 24 kV pin-type porcelain insulator reveals flashover probability distributions under standard impulses of both polarities, with higher applied voltages causing flashover sooner and lower voltages under negative impulses[15].

Lightning protection systems (LPS) use insulating stand-offs and down conductors to maintain separation distance from grounded objects. However, these components are stressed by non-standard fast-front overvoltage's due to lightning currents. *Samaras et al. 2023* assesses the electric stress experienced by these components through ATP-EMTP simulations, determining critical values for separation distance and dielectric strength[16].

*Aristotelous George Petros et al. 2020* examined the dielectric behavior of insulators influenced by waveform and voltage polarity. It found that shorter lead durations led to higher breakdown voltage and shorter breakdown time. Polarity affects maximum current value by insulator and waveform. As insulator dimensions increase, so does the breakdown time. As dimensions decrease, discharge current increases, and spark conductivity increases for smaller insulators. Overall, insulator characteristics influence breakdown voltage and discharge current[17].

*Brocke et al. 2014* evaluates the dielectric strength of insulated LPS components under pollution and humidity effects, highlighting the significant impact on insulation properties. It also reveals that impulse duration significantly influences insulation efficiency, with longer impulse durations potentially decreasing insulation[18].

*ICEPE 2018: 2nd International 2018* examines the impact of lightning on insulator flashover characteristics in railway traction masts. It explores the influence of footing resistance and soil ionization on flashover behavior, using the CIGRE model[19] and double exponential model using EMTP software. Results show that increased footing resistance increases the likelihood of flashover, and the CIGRE model predicts early flashover[20].

According to paper *Kovalev et al. 2022*, the use of micro and nano-sized inert particles in insulation increases dielectric strength, and the prototype's serviceability has been confirmed, making it recommended for use in solid-insulated busbar design in various sectors, including agro-industrial, to improve power supply reliability[21].

*pereirabraz2011 n.d* evaluates the dielectric behavior of medium voltage insulators exposed to non-standard impulse voltages and two methods for predicting their dielectric strength against such impulses. It presents test results and volt-time characteristics for positive and negative polarities of different voltage waveforms, discussing the critical lighting impulse flashover voltage[22].

*Alexandrov et al. n.d.* investigates that insulating suspension sets' switching surge flashover voltages depend on the distance between the conductor and tower components and do not depend on the type of insulator used. Under positive polarity lightning impulses, the flashover voltage increases linearly with the length of the insulator string, with an average flashover field of 0.5 MV/m. Under negative polarity impulses long strings of cap-and-pin insulators have lower flashover voltages, with a rate of decrease with larger string lengths. Enhancing impulse strength can increase negative polarity flashover voltage by 25-40%[23].

# CHAPTER THREE: EXPERIMENTAL SETUP AND EQUIPMENT

## 3.1 High Voltage Laboratory area

The experimental measurements were carried out at the High Voltage Laboratory of the School of Electrical and Computer Engineering of the Aristotle University of Thessaloniki. The laboratory consists of two high-voltage test areas accompanied by corresponding control and measurement areas, an auxiliary laboratory, as well as office and warehouse areas (Figure 3.1). The experimental measurements were carried out in the main testing area of the laboratory, which is completely enclosed in a grounded metal mesh in all dimensions (Faraday cage), in order to avoid the inadvertent entry of personnel and also to reduce the electromagnetic noise in the quantities under measurement. The dimensions of the metal mesh are 6.5m high, 12m long and 7m wide. Along the roof is a 10-ton overhead crane.


Figure 3 1: Floor Plan of the High voltage laboratory of AUTH

The height of the metal cage (6m), which is also the smallest dimension of the test area, corresponds to a minimum safety distance of 3.25m. This minimum safety distance limits the generation of AC high voltages HVAC to 650kV (rms), DC high voltages HVDC to

900kV, Lightning impulse high voltages LI at 1 MV and Switching impulse high voltages SI at 1.4 MV.

The grounding system of the high-voltage laboratory includes the foundation grounding of the building, the independent protective grounding in the main testing area, which is a grounding rod to which the high-voltage generation and measurement devices are directly connected with a copper grounding tape, as well as other grounding systems such as the automatic ground, the manual ground and the floor layer sheets.

In particular, the floor of the laboratory is covered with metal layer sheets intended to limit the development of potential difference between different points of grounding of equipment or high voltage circuits and especially to limit the development of step voltages. All metal parts of the test area that do not carry high voltage are properly earthed and connected to the laboratory earthing installation through specially designed earthing conductors of suitable cross-section. The cables used in the high voltage measurements are coaxial with a reliably grounded shield.

### 3.2 Generation and measurement of Impulse High Voltages

The complete circuit required for the testing of the equipment with high voltage consist of high voltage generation system, connection to the test and voltage measurement system.

The general arrangement of the high voltage test circuit is shown below as in Figure 3.2 [24].

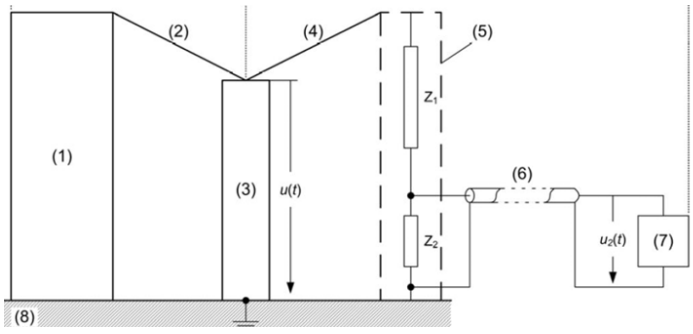


Figure 3.2: High Voltage test Circuit

(1) High voltage generation device, (2) Connection of high voltage generation device (3) Test, (4) Test - Voltage Divider Connection, (5) Voltage Divider, (6) Test Lead, (7) Voltage Recorder, (8) Grounded Lab Floor.

The high voltage measurement system includes the test connection to the voltage divider, the voltage divider, the measuring cable inserted between the output of the voltage divider and the input of the recording instrument and the recording instrument itself. When testing high voltage surge equipment, the voltage divider is usually a component of the surge generator so as not to load the generator by altering the output waveform[24].

Next, some basic theoretical elements are described regarding impulse high voltage generators and later the impulse high voltage production and measurement systems used during the preparation of this thesis are analyzed.

### 3.3 Theoretical elements

The mathematical representation of impulse high voltages can be carried out by using biexponential function which is given by equation 3.1

$$U(t) = Up[\exp(-a_1 t) - \exp(-a_2 t)] \quad (3.1)$$

where $a_2$ is greater than $a_1$

These waveforms can easily be represented in the laboratory using capacitor discharge circuits through resistors of suitable value, thus making it possible to generate impulse high voltage. Such circuits are the single stage or multi-stage generators of impulse high voltages. The two basic circuits of the single stage impulse high voltage generator are shown in Figure 3.3.

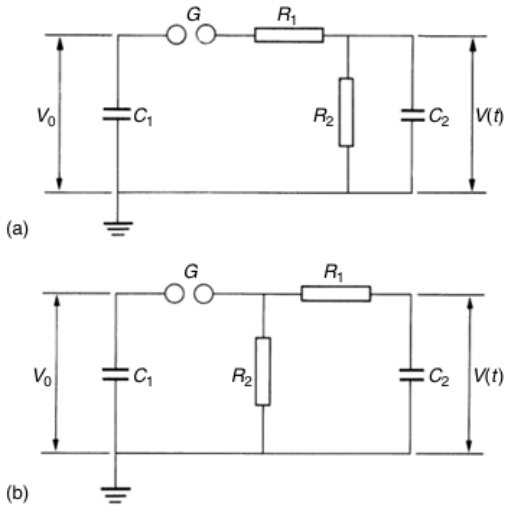


Figure 3.3: Circuits of a single stage high voltage shock generator

The capacitor $C_1$ is slowly charged from d.c. source until the spark gap G breaks down. This spark gap act as a voltage-limiting and voltage- sensitive switch, whose ignition time is very short. The components $R_1$, $R_2$, and $C_2$ together make up the wave-shaping circuit. Resistor $R_1$ mainly serves to dampen the circuit and regulate the rise time, $T_1$. Resistor $R_2$ is responsible for discharging the capacitors, thereby influencing the duration of the waveform's tail. The capacitor $C_2$ represents the total load, which includes the test object along with any other parallel capacitances, such as measurement equipment or added load capacitors used to maintain consistent $T_1/T_2$ values when switching test objects.

The output voltage of the generator, v(t), is the voltage across the load capacitor, $C_2$. For the generation of impulse high voltages requires a rapid increase of the voltage to its maximum value and a slow decrease to zero value. Circuit-wise this means that the impulse capacitor $C_2$ must be charged quickly, while the parallel combination of $C_1$ and $C_2$ needs to be discharged slowly. These requirements are met as long as

$$R_2 >> R_1$$

$$C_1 >> C_2$$

Neglecting any stray inductances and capacitances, the charging duration of $C_2$ with time constant $C_1R_2$ approximately coincides with the front duration of the high voltage surge, while the discharging duration with time constant $R_2(C_1+C_2)$ coincides with the tail duration.

The maximum value of the generator output voltage V(t), peak voltage, can never exceed the value of the generator charging voltage, $V_0$ and this is because the initial available charge of the capacitor $C_1$ is distributed proportionally to the capacitors, $C_1$ and $C_2$, during its breakdown auxiliary gap. The utilization factor, η, of the generator, defined as the ratio of the peak voltage to the input voltage for the type a and type b circuit arrangement, is shown in equations 3.2 and 3.3 respectively.

$$\eta = \frac{V_p}{V_0} \leq \frac{R_2}{R_2+R_1} \cdot \frac{C_1}{C_1+C_2} \tag{3.2}$$

$$\eta = \frac{V_p}{V_0} \leq \frac{C_1}{C_1+C_2} \tag{3.3}$$

From the above equation, it can be seen that the utilization factor of the circuit arrangement of type b is greater than the corresponding one of the circuit arrangements of type a. Therefore, the b-type circuit is able to produce impulse high voltages with a higher peak voltage compared to the a-type circuit. This is the main reason why the type b circuit arrangement was preferred for the experimental tests of the present study.

The generation of the desired impulse voltage waveform is obtained for given values of generator capacitances by using a suitable pair of front and tail resistor values, while the peak value can be varied by controlling the generator charging voltage. If it is desired to produce large peak value impulse high voltages then multistage generators or Marx generators are used[25].

The generator output voltage after mathematical analysis is given by equation 3.4

$$V(t) = \frac{V_0}{R_2 \cdot C_2} \cdot \frac{T_1 \cdot T_2}{T_1 - T_2}\left(e^{-\frac{t}{T_1}} - e^{-\frac{t}{T_2}}\right) \tag{3.4}$$

Under the assumption $R_2C_1 >> R_1C_2$. The time constant $T_1$ and $T_2$, for the circuit b are given by the following equation 3.5, 3.6.

$$T_1 = R_2 \cdot (C_2 + C_1) \tag{3.5}$$

$$T_2 = R_1 \cdot \left(\frac{C_1 \cdot C_2}{C_1 + C_2}\right) \tag{3.6}$$

The front duration of the generated shock stress can be calculated from the time at which the equation 3.7 exhibits a maximum.

$$T_{cr} = \frac{T_1 \cdot T_2}{T_1 - T_2} \cdot ln\left(\frac{T_1}{T_2}\right) \tag{3.7}$$

If the half width duration, Tt, is assumed to be much longer than the front duration, it is given by equation 3.8.

$$T_t = T \cdot ln\left(\frac{2}{\eta}\right) \tag{3.8}$$

### 3.4 Multistage High Voltage Impulse Generator- Marx Generator

As shown in figure 3.4, in Marx generators a number of charging capacitors, Cc, as many stages of the generator, connected in parallel through load resistors, RL, are charged under

continuous high voltage and then discharged, through the breakdown of spherical gaps, connected in series to a load capacitor, Cf. In this way the output voltage of the generator is a multiple of the charging voltage, in proportion to the number of stages [24]. Marx generators combine, in addition to impulse capacitors, front and tail resistors as well as auxiliary spherical gaps in a manner similar to that of single-stage generators. These elements are usually distributed among the stages of the generator and equal. Therefore, the equivalent circuit of an n-stage generator is the same with that of the single-stage generator with equivalent values of elements and charging voltage as shown below:

$$\mathrm{Cc} = C_{cn}/\mathrm{n},$$

$$R_f = \mathrm{n} \cdot R_{fn},$$

$$R_t = \mathrm{n} \cdot R_{tn},$$

$$U_0 = \mathrm{n} \cdot U_{0n},$$

where the index n denotes the values of the individual elements of the Marx generator.

Depending on its circuit type, the Marx generator may additionally combine a lumped front resistance, Rfe (Figure 3.4), and/or a lumped tail resistor, Rte. The ignition of the impulse high voltage generator is done by the breakdown of the auxiliary gap of the first stage which triggers the successive breakdown of the gaps and the remaining stages. The ignition is either automatic or controlled. During generator auto-start, either a specific value of charging voltage is applied and the distance between the spheres of the auxiliary gap is reduced until breakdown, or the distance between the spheres of the auxiliary sphere gap is set to a specified value and the charging voltage of the generator is increased until the auxiliary gap splits.

## 3.5 Generation of External shock high voltages

### 3.5.1 Marx 10-stage Generator

The production of the lightning impulse high voltages during the experimental measurements was carried out using the 10-stage Marx generator, from Ferranti, which is installed in the main testing area of the high voltage laboratory of the AUTH. This particular generator produces standard lightning impulse high voltages of the 1.2/50μs type waveform used to simulate direct lightning strikes and by changing the polarity of the diode

we can obtained high voltages negative polarity. The generator ratings are nominal voltage 1MV and rated power (energy) 7kJ[24]. However, the actual values of impulse voltages that can be produced, due to losses, are 850 kV switching impulse voltages and 885kV lightning impulse voltages. The circuit arrangement of the generator used in the laboratory tests is shown in Figure 3.5.

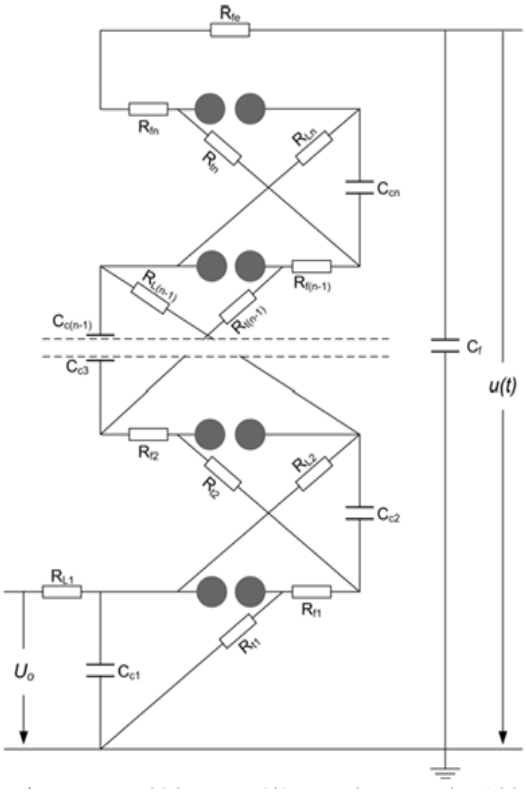


Figure 3.4: Schematic Diagram of n-stage Marx generator

The process of generating the lightning impulse high voltages using the Marx generator is first carried out by supplying the generator with continuous high voltage through a test transformer and the rectifier voltage doubler, Greinacher. The test transformer, 220V/50kV, 5kVA, supplies the rectifier. The output voltage of the test transformer, which is measured using a CM type 100pF measurement capacitor through a digital voltmeter, is rectified with the help of the rectifier device which consists of two capacitors and two rectifier diodes. The polarity of the charging voltage depends on the direction of the rectifier diodes and polarity reversal is accomplished by essentially reversing the diodes of the rectifier device by means of the manual handle.

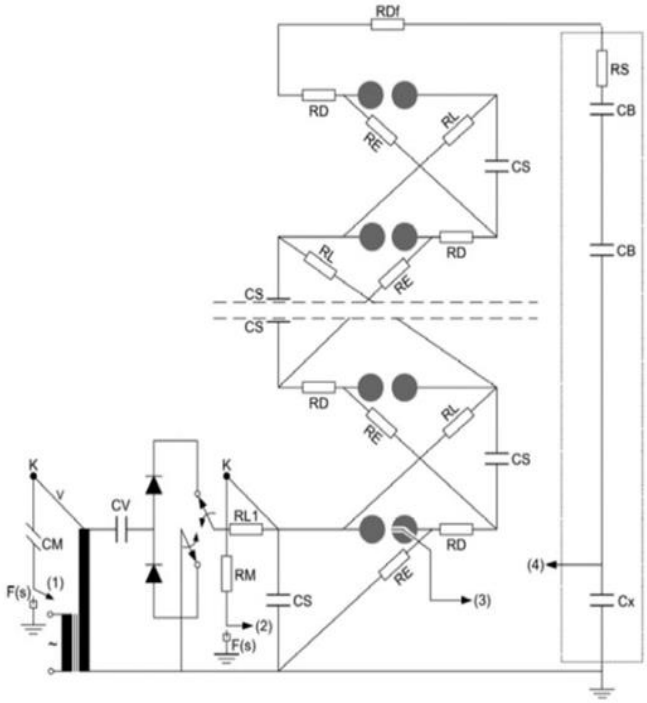


Figure 3.5: Schematic diagram of Marx Generator experimental setup

The smoothing, Greinacher arrangement capacitors CS is used as the charging capacitor for the first stage of the Marx generators. The experimental arrangement of the rectifier Greinacher, together with the test M/S, is shown in Figure 3.6.

Figure 3.6: Experimental setups of Greinacher

The DC voltage, $V_0$, charges, through the charging resistor, $RL_1$, the charging capacitor of the first stage, $CS_1$. The charging capacitor of the next stage, $CS_2$, is charged through the next charging resistor, $RL_2$, to the same potential, $V_0$. All ten impulse capacitors of the

generator are charged in exactly the same way. The other ends of the capacitors are grounded through the tail resistors, RE [19]. The actual layout of the generator Marx, of the High Voltage Laboratory of AUTH is presented in Figure 3.7. The splitting of the auxiliary spacers, during the experiment, is carried out in a controlled manner by means of the Trigatron device. Once the high voltage pulse is applied to the auxiliary gap of the Trigatron device, the first gap, $G_1$, breaks down. The capacitor $CS_1$ is under voltage $V_0$ and after the breakdown of $G_1$ is added to the voltage of the charging capacitor of the second stage, $CS_2$, which is also under voltage $V_0$, resulting in a voltage equal to $2V_0$. Capacitors $CS_1$ and $CS_2$ are now in series. The auxiliary gap is under a voltage of $2V_0$ and breaks down almost instantaneously with the result that the $2V_0$ voltage is added to the voltage $V_0$ of the capacitor of the third stage, $CS_3$, the end of which will be under a voltage $G_2$, of $3V_0$, as well as the auxiliary gap of the third stage which will break down almost instantly.

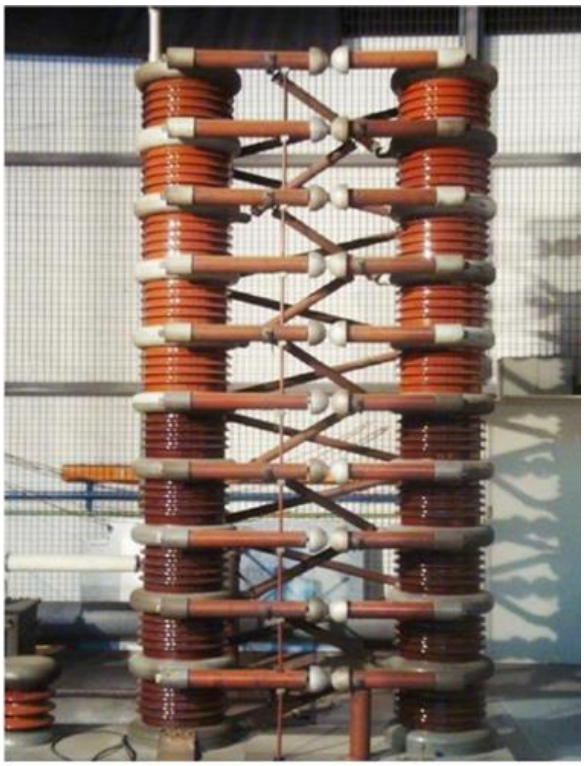

Figure 3.7: Marx generator of AUTH Laboratory

The same process is repeated in all stages of the Marx generator, sequentially and almost instantaneously [25]. Once all ten generator gaps are broken, the total voltage to ground will theoretically be $10V_0$, as given by the equation 3.9.

$$U_p = n \cdot V_0 = 10 \cdot V_0 \quad (3.9)$$

In practice, however, the output voltage of the generator also depends on its utilization factor and results which is shown in equation 3.10.

$$U_p = n \cdot \eta \cdot V_0 = 10 \cdot V_0 \quad (3.10)$$

where n is the number of stages of the generator and $\eta$ is the utilization factor. It is noted that, for a standard lightning impulse voltage of 1.2/50μs, the utilization factor of the generator has been determined experimentally equal to $\eta$ =0.95 for positive shock high voltages and $\eta$ =0.944 for negative shock high voltages[17].

The series charged capacitors discharge into the load capacitor, CB, through the front resistors, RD, and the external front resistor, RDf. The voltage across the load capacitor becomes equal to the output voltage of the generator. The discharge of the load capacitor is done through the front resistors, RD, and tail resistors, RE, as a type b circuit arrangement is used [19]. The load capacitor of the high voltage laboratory of the AUTH is shown in Figure 3.8.

Figure 3.8: Load capacitor and external front resistor of the AUTH laboratory

### 3.5.2 Trigatron device

As we know that, the start of the impulse high voltage generator can be done either automatically or controlled. Controlled starting of the generator can be carried out by

means of the Trigatron device. The device combines two basic electrodes that form between them a homogeneous field gap and a third auxiliary electrode that together with one of the basic electrodes, usually the grounded one, forms an auxiliary gap. During operation of the device, a voltage of less than the gap breakdown voltage (DC output voltage of the rectifier) is applied to the base electrodes Greinacher). At the desired time, a high voltage pulse is imposed on the auxiliary gap.

The application of the voltage pulse leads to the breakdown of the auxiliary gap and subsequently, as a result of the electric discharge, the almost homogeneous field in the main gap space becomes locally strongly inhomogeneous and its breakdown occurs. To more precisely control the operation of the Trigatron device, the design of the auxiliary gap is changed so that when the voltage pulse is applied, the gap between the high voltage electrode and the auxiliary electrode is broken first, and then the auxiliary gap[24].

A Trigatron device, of the MWB house, of the High Voltage Laboratory of AUTH, is shown in figure 2.9. It combines a spherical gap of the KE type with an auxiliary electrode, an auxiliary high voltage generation device, in the form of a damping oscillation and a coupling capacitor. In the grounded sphere of the spherical gap is the insulated auxiliary electrode, which does not protrude from the surface of the sphere and forms with it an annular gap of 1mm. The coupling capacitor, Ctr, withstands the maximum charging voltage of the shock capacitor and is used to protect the operator and the device. The layout of the Trigatron device is shown in the Figure 3.9.

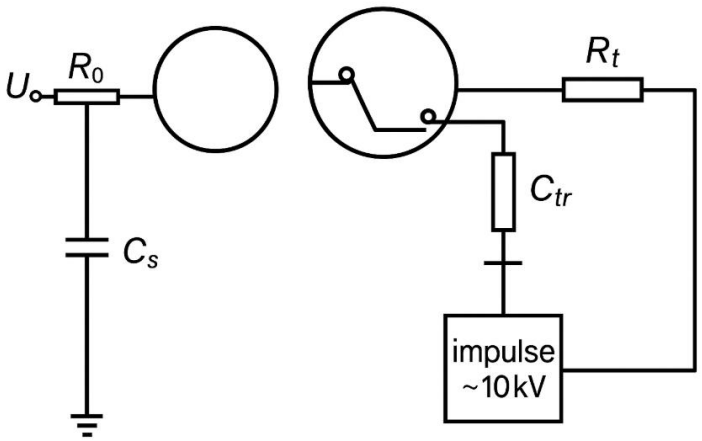


Figure 3.9: Trigatron Device

### 3.6 Control desk

The control desk illustrated in Figure 3.10 was utilized to regulate the high voltage generation circuit during the experimental measurements. The SRP 0.5/5E control desk has a rated supply voltage of 220V, 50Hz, and a rated power of 5kVA. In order to make the breakdown phenomenon evident during the measuring procedure, it is positioned adjacent to one of the two entrance doors of the laboratory's main area.

In particular, the control desk is used to regulate a Digital AC voltmeter which used to measure the output voltage of the autotransformer, which controls the output voltage of the test transformer (output 1. Figure 3.15). A DC digital voltmeter was used to measure the Marx generator charging circuit's output voltage (output 2, Figure 3.15). Through a switch (output 3, Figure 3.15), the Trigatron device is utilized to start the generator. Using switches and a digital indicator to measure the separations between the Marx generator's auxiliary spherical gaps [26].

It also features switches for managing the immediate power cutoff safety switch, opening and closing the console, and connecting and disconnecting the test transformer's main. Additionally, it incorporates devices to measure the supply voltage and the constructed protective relays, control switches, fuses, high voltages, and operating switches.

Figure 3.10: Bank control and Handling

### 3.7 Digital oscilloscope-voltage transformer-signal attenuator

The LeCroy WR64Xi oscilloscope was used to visualize and measure the impulse high voltage waveforms during the experimental process, as well as to determine the breakdown time, breakdown voltage, current and other measurements. The bandwidth of this

oscilloscope is 600 MHz and the sampling frequency is 5 Gs/s. The oscilloscope was connected to the low voltage side of the capacitive voltage divider (Output 4, Figure 3.15), high voltage capacitance of the load capacitor, of the Marx generator, 200 pF and low voltage capacitance of 0.296 μF [15]. The digital oscilloscope used is shown in Figure 3.11.

Figure 3.11: LeCroy WR64Xi Digital Oscilloscope

To record and measure the current signal, a current transformer of the PEARSON company type 301X, 0.01 Volts per Amp and a signal attenuator of the PEARSON company type A10, 10:1 Voltage Ratio is used. The device's ground wire runs from the current transformer while the output of the transformer is connected to the oscilloscope through the signal attenuator (attenuator). Using the two devices helps to downscale the signal by a factor of 1 to 1000 so that the current waveform can be displayed on the oscilloscope. The Current transformer and the attenuator are shown in Figures 3.12 and 3.13 respectively.

The connection of the digital oscilloscope to the capacitive voltage divider was carried out using a coaxial cable with a grounded jacket, shielded against electromagnetic noise by means of a metal jacket. In the same way, the connection of the transformer was carried out, through the signal attenuator[24]. The digital oscilloscope operates within a shielding cage which is connected to the earthing facility of the main test room of the high voltage laboratory through the earthed sheath surrounding the coaxial cable. In this way, closed earth loops between the coaxial cable and the earthing system are avoided.


Figure 3.12: PEARSON 302X current Transformer


Figure 3.13: Signal Attenuator PERSON Attenuator A10

### 3.8 Insulating stand-offs

In the context of this thesis work, the samples under study are three insulating stand-offs differing in length i.e 75 cm, 50 cm and 25 cm respectively, which are shown in Figure 3.14. For each insulating standoff, its surface dielectric behaviour was studied under standard lightning voltage of both positive and negative polarity. Insulating standoff, a mechanical component designed to provide structural support while electrically isolating two parts. This standoff consists of a combination of materials and features that ensure both mechanical stability and electrical insulation. It is constructed primarily from resin and metallic components, each serving a specific purpose.

Figure 3.14: 25cm Insulating Standoffs

### 3.9 Experimental Setup

The final schematic experimental setup is shown in Figure 3.15**.** This experimental setup includes the Marx generator for the generation of standard lightning impulse voltages of both positive and negative polarity. Figure 3.16 shows the actual experimental setup while

Figure 3.17 shows the same setup with an emphasis on how the voltage transformer is connected. As can be seen from Figures 3.16-3.17 The insulating stand-offs are mounted on a properly designed base, as used in practice, and placed on an aluminium plane, positioned parallel to the grounded floor of the laboratory.

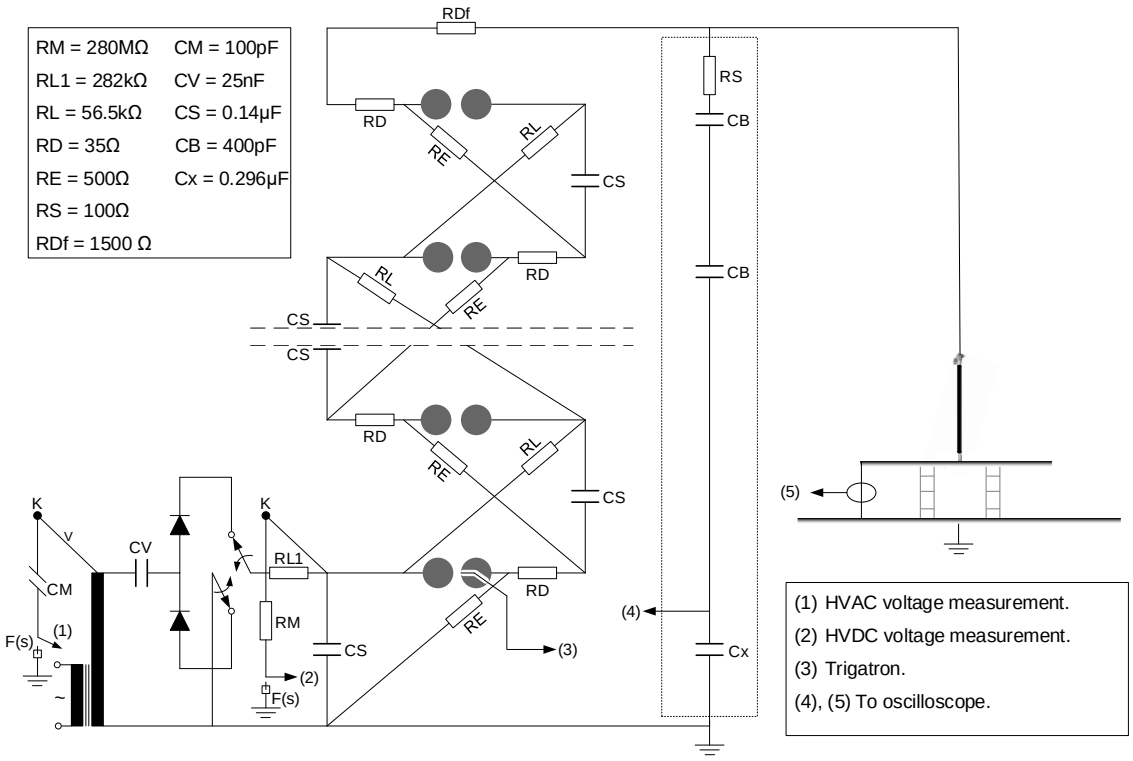


Figure 3.15: Schematic Diagram of Experimental Setup

The plane is grounded through a current transformer, for the measurement of the discharge current. The applied impulse voltage is measured using the capacitive divider of the Marx generator.

In the experimental setup central to this thesis, the Marx generator serves as the primary high voltage generation device. This generator employs capacitors arranged in a specific configuration to multiply input voltage through parallel charging and series discharging, generating the high-voltage impulses required for testing. Notably, one of these capacitors fulfils a dual role: beyond its function in the Marx circuit, it also acts as the high-voltage component of a capacitive voltage divider. This dual-purpose design streamlines the setup by integrating voltage generation and measurement into a single element, enhancing efficiency.

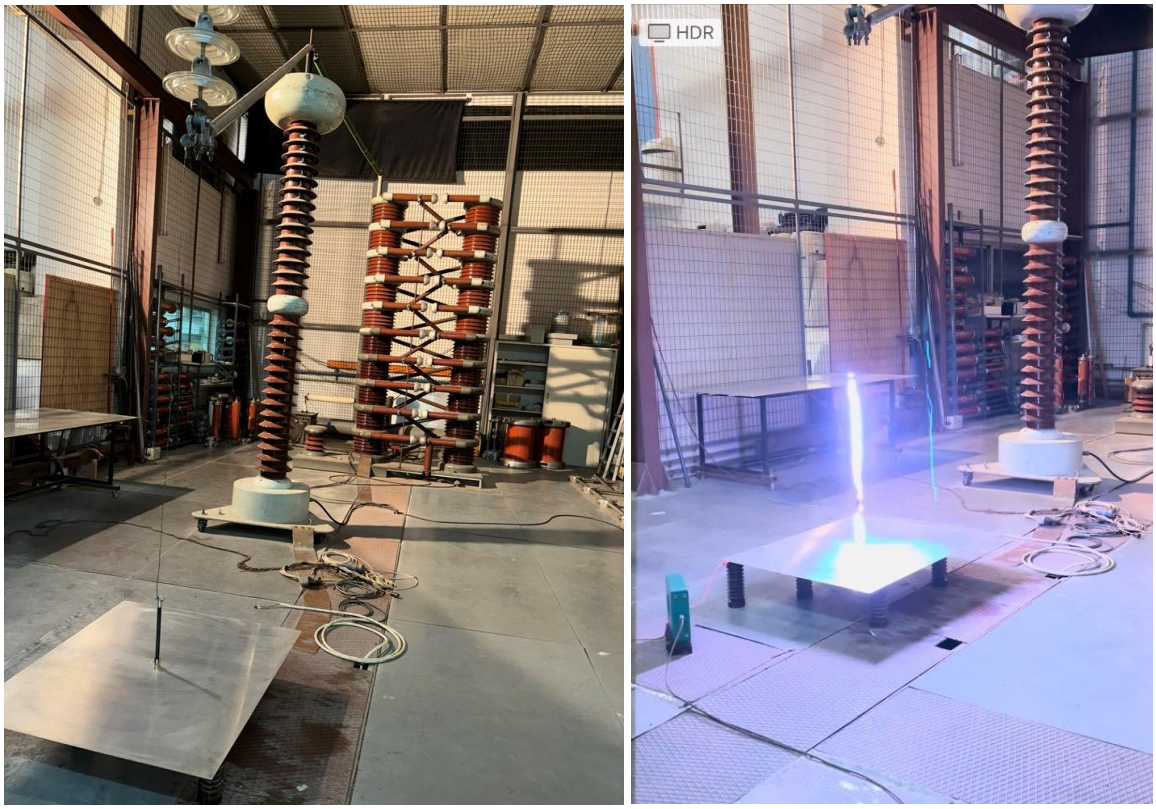


Figure 3.16: Final Experimental Setup


Figure 3.17: Test transformer connection-grounding

The impulse voltage produced by the Marx generator is transmitted to a test electrode suspended from the base of an 11-unit insulator string (a high-voltage string insulator). This electrode, positioned within a test gap, is mechanically adjustable both vertically and

horizontally using a crane. This mobility allows precise control over the electrode's placement, enabling to vary the gap distance and alignment during experiments, which is critical for studying breakdown characteristics under different geometries.

To stabilize the assembly, insulating standoffs of varying lengths (75 cm, 50 cm, and 25 cm) are mounted on a metallic support plate. These standoffs, strategically attached to the plate, provide structural rigidity while maintaining electrical isolation. The plate itself rests atop the insulator cluster, forming a robust foundation that minimizes mechanical vibrations and ensures consistent experimental conditions.

Grounding of the test sample is achieved via specialized cables that route through a current transformer. This transformer measures the transient current during voltage impulses, converting it into a signal suitable for data acquisition. To mitigate electromagnetic interference, shielded cables connect the transformer’s output to a signal attenuator, which scales down the signal magnitude before it is recorded by a high-speed oscilloscope. This measurement chain ensures accurate monitoring of both voltage and current waveforms, essential for analysing discharge dynamics.

# CHAPTER FOUR: ELECTROSTATIC ANALYSIS OF INSULATING STANDOFFS

This section delves into the investigation of the electric field distribution across the surface of an insulating standoff. It emphasizes a realistic approach, incorporating the standoff's precise shape, the inherent characteristics of its material, and its physical length. To achieve this, a three-dimensional digital representation of the standoff is constructed, and electrostatic analysis is performed. For accurate numerical calculations, a detailed tetrahedral mesh is utilized. The core of the study lies in examining the electric field's fluctuations in response to changes in both the material composition and the length of the standoff. By systematically varying these parameters, the research aims to quantify their impact on the electric field's behavior. The findings derived from this analysis are intended to provide meaningful insights into the standoff's operational effectiveness and response, particularly when subjected to varying lightning strike conditions and different standoff lengths.

## 4.1 Introduction

Lightning protection systems utilize insulating standoffs to maintain a safe distance between down conductors and the structure they protect, thereby preventing hazardous side flashes and arcing. These standoffs are crucial for directing the powerful current surge from a lightning strike towards the grounding system, ensuring it doesn't interact with conductive components of the building. A key design consideration is the management of the electric field that develops around the standoff during a lightning event. When substantial currents, often exceeding 200 kA, flow through the down conductor, strong electric fields emerge at the boundary between the conductor, the standoff, and the structure. Improperly controlled, these fields can surpass the insulating capacity of the standoff material or the surrounding air, resulting in partial discharges, insulation failure, or arcing.

In recent times, numerical modelling, particularly using the finite element method, has become increasingly popular for analysing flashover phenomena, driven by experimental findings. Accurately modelling the electric field distribution is fundamental to understanding its characteristics and behavior in this context. Techniques like the charge

simulation method, finite element method, and finite difference method are commonly employed in these numerical studies. Among these, the finite element method is considered particularly effective for calculating the electric field distribution in insulating standoffs. This is due to its simplicity in estimating electromagnetic fields on surfaces of thin structures made of diverse dielectric materials, and its proven success in addressing electrostatic problems involving complex geometries. Software platforms like COMSOL Multiphysics provide the tools necessary for performing these numerical analyses, enabling the solution of finite meshes with complicated geometries and electric field behaviour.

### 4.2 Method of Simulation

A strong, interactive platform for modelling and resolving challenging scientific and engineering issues is provided by COMSOL Multiphysics. Fundamentally, it uses partial differential equations, or PDEs, to faithfully depict a wide variety of physical processes. Users may easily integrate many physics domains that interact with one another thanks to this platform, which simplifies the process of creating Multiphysics models.

By concentrating on the system's physical properties, COMSOL Multiphysics streamlines the process of creating models rather than asking users to manually enter the governing equations. The software can automatically construct the required equations when users define material parameters, apply loads, and set boundary conditions. Additionally, regardless of the underlying computational mesh, these parameters which can be represented as integers or mathematical expressions can be applied directly to geometric elements such as solid domains, borders, edges, and points, providing flexibility and usability[27].

### 4.3 Model Design

To analyse electric field behavior, a computational model was created using COMSOL Multiphysics. This model represents a two-dimensional simulation of insulating standoffs, specifically focusing on three variations of length, all within a 25cm overall dimension as depicted in Figure 4.1. A voltage of 1V was applied to the upper surface of each standoff, while the lower surface was set to ground potential.

The geometric representation within the simulation includes several components: a metal cap, a down conductor fastener, and the surrounding air. Each of these components was assigned distinct material properties, as detailed in the accompanying Table 4.1, to accurately reflect their physical characteristics in the electric field simulation.

Table 4.1: Electrical and mechanical properties of materials used in designed model

| Material Property | Steel | Copper | Epoxy resin/Polymer | Air |
|---|---|---|---|---|
| Permittivity | 1 | 1 | 3.04/2.4 | 1 |
| Electrical Conductivity | 4.03E+07 | 5.9E+07 | 0 | 0 |
| Cofficient of thermal expansion | 12.3E-06 | 17E-06 | - | - |

### 4.4 Mathematical Model

Electric field intensity (E) and Electric Flux density (D) behavior is the subject of electrostatics. When a potential is applied across surface having charge particles, several electric phenomena occur depending upon the nature if surface and properties of the particle such as dielectric.

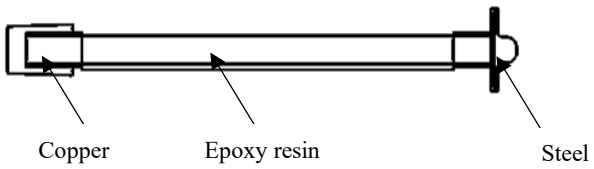


Figure 4.1: 2D geometric model of standoffs

polarization, acceleration of ionization formation, surface charge (leakage current) and so on. According to Gauss Law, flux out of closed volume is equal to the charge contained in the volume. Additionally, Maxwell's equations are the foundation for calculation of electric field[28]. For electrostatic model, following equations 4.1, 4.2 and 4.3 are useful where $\rho$ is electric charge density, V is electric potential and $\epsilon$ is permittivity of material.

$$div\,\vec{D} = \rho \tag{4.1}$$

$$\vec{D} = \epsilon\vec{E} \tag{4.2}$$

$$\vec{E} = -\overrightarrow{Grad}\,V \tag{4.3}$$

Therefore, div $(\epsilon(-\overrightarrow{grad}\,V)) = \rho$ and this equation is also called Poisson equation. If the space charge $\rho = 0$, Poisson equation becomes Laplace's Equation. With the high voltage equipment, space charge is negligible and considered to be zero[29]. For the conductive medium, then Laplace's equation 4.4, 4.5 and 4.6 where $\sigma$ is electrical conductivity.

$$div\,\vec{j} = 0 \tag{4.4}$$

$$\vec{j} = \sigma\vec{E} \tag{4.5}$$

$$div\left(\sigma(-\overrightarrow{grad}V)\right) = 0 \tag{4.6}$$

$$div\overrightarrow{grad} = \frac{d^2V}{dx^2} + \frac{d^2V}{dy^2} + \frac{d^2V}{dz^2} \tag{4.7}$$

$$-div\epsilon\overrightarrow{grad} - div\sigma\overrightarrow{grad} = 0 \tag{4.8}$$

The cartesian coordinates form is given in equation 4.7 and the calculation software determines the electrical potential to obtain the field distribution by solving partial differential equation 4.8 for two dimensions[30]. The overall algorithm simulation flowchart for COMSOL is illustrated in Figure 4.2.

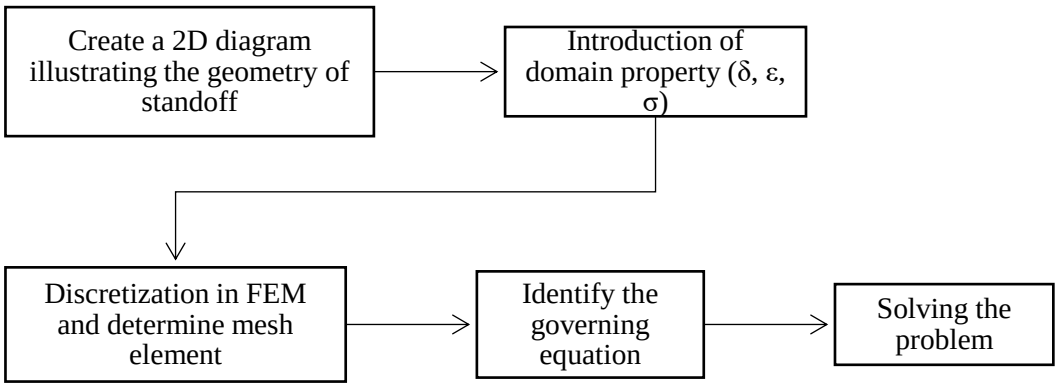


Figure 4. 2: Resolution steps by COMSOL Multiphysics

## 4.5 Meshing

A normal mesh with free triangular pieces calibrated as general physics is utilized for the electrostatic study. To make easier and faster to solve, the normal degree of mesh is chosen over fine (iteration time is lower). And the density of mesh is higher in the corner region as in Figure 4.3.

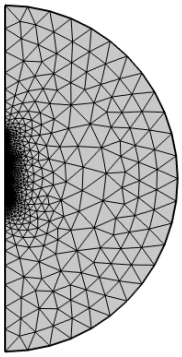

Figure 4.3: Discretization of FEM of insulating Standoffs

## 4.6 Electric Field Distribution

### 4.6.1 Polymer

Figure 4.4 shows the electric field distribution along the 25cm insulating standoffs. The maximum of the electric field strength is observed at the stressed point (*x=20)* i.e. the application point of the lightning impulses. The grounded point is *x=0* as indicated in the graphs. The distribution exhibits a fairly symmetrical profile, suggesting a fairly uniform electric field distribution across the surface, except for the terminal's effects. There is significant peak at both ends *x=0* and *x=20* then at centre from *x=4 to 16*. These high field strength values at the terminals could be points of concern for potential surface discharge inception, when exposed at high voltages. The maximum surface electric field value is 71.84 V/(m·V). This high field at the terminal suggests possible charge accumulation on the surface of the standoffs under test. This could be due to polarization of the materials or the presence of surface charge. Applying a lightning impulse voltage would exacerbate this non-uniformity. The rapid rise time and high magnitude of the impulse would induce a transient surge in the electric field, especially at the edges where the field is already concentrated. This could lead to localized breakdown or flashover initiation at these points. The central region, with its lower field strength, would be less susceptible to such effects.

Figure 4.5 shows the electric field distribution along the 50cm insulating standoffs. The maximum of the electric field strength is observed at the stressed point (*x=45*) i.e. the application point of the lightning impulses. The grounded point is x=0 as indicated in the graphs. The distribution exhibits a fairly symmetrical profile, suggesting a fairly uniform electric field distribution across the surface, except for the terminal's effects.

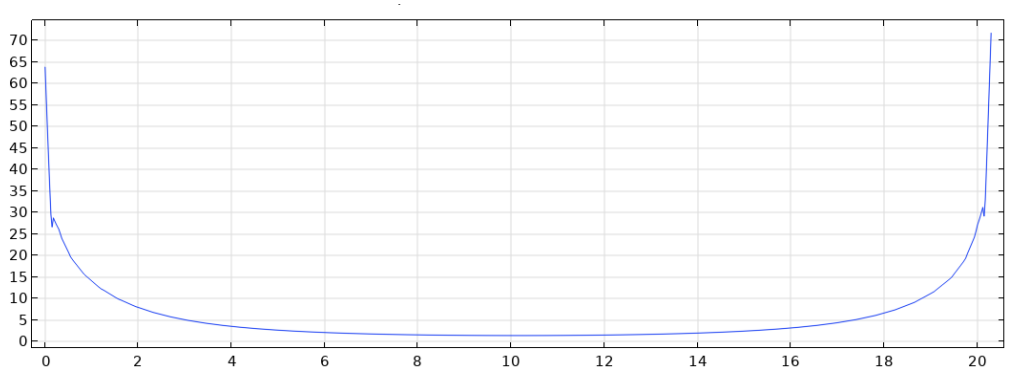


Figure 4.4: Surface electric field on 25cm insulating standoffs

There is significant peak at both ends *x=0* and *x=45* then at centre from *x=8 to 45*. These high field strength values at the terminals could be points of concern for surface discharge inception, when exposed at high voltages. The maximum surface electric field value is *66.7* V/(m·V). This high field at the terminal suggests possible charge accumulation on the surface of the standoffs under test. This could be due to polarization of the materials or the presence of surface charge.

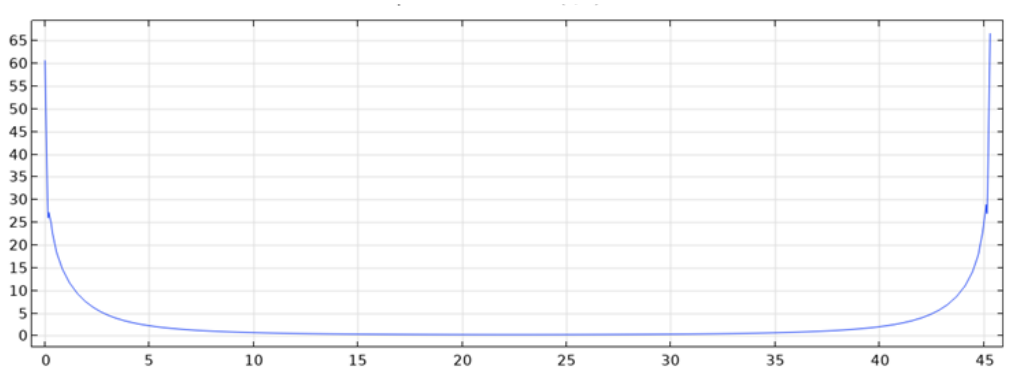


Figure 4.5: Surface electric field on 50cm insulating standoffs

Figure 4.6 shows the electric field distribution along the 75cm insulating standoffs. The maximum electric field strength is observed at the stressed point (*x=70*) i.e. the application point of the lightning impulses. The grounded point is *x=0* as indicated in the graphs. The

distribution exhibits a fairly symmetrical profile, suggesting a fairly uniform electric field distribution across the surface, except for the terminal's effects. There is significant peak at both ends x=0 and x=70 then at centre from *x=10 to 60*. These high field strength values at the terminals could be points of concern for surface discharge inception, when exposed at high voltages. The maximum surface electric filed value is *65* V/(m·V). This high field at the terminal suggests possible charge accumulation on the surface of the standoffs under tests. This could be due to polarization of the materials or the presence of surface charge.

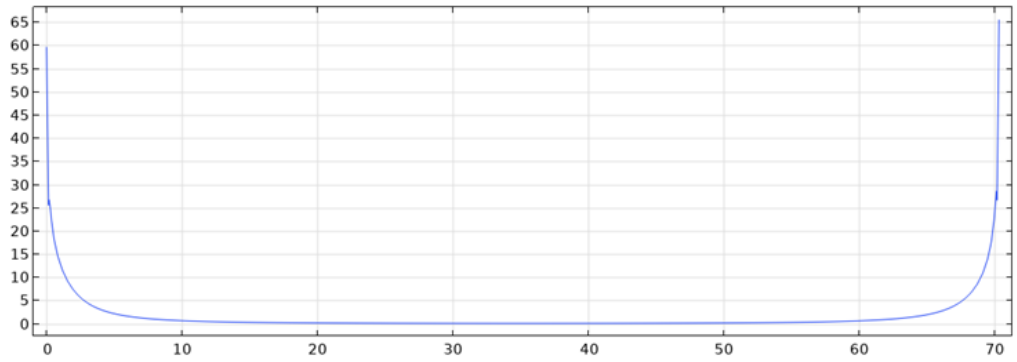


Figure 4.6: Surface electric field on 75cm insulating standoffs

In general, the graph illustrates a typical electric field distribution for an insulating stand-off with significant terminal effects. The high field strength at the terminals is an important consideration in practical applications to ensure the long-term reliability and performance of the insulation system.

### 4.6.2 Resin

Figure 4.7 shows the electric field distribution along the 25cm insulating standoffs. The maximum of the electric field strength is observed at the stressed point (*x=20)* i.e. the application point of the lightning impulses. The grounded point is *x=0* as indicated in the graphs. The distribution exhibits a fairly symmetrical profile, suggesting a fairly uniform electric field distribution across the surface, except for the terminal's effects. There is significant peak at both ends *x=0* and *x=20* then at centre from *x=4 to 16*. These high field strength values at the terminals could be points of concern for potential surface discharge inception, when exposed at high voltages. The maximum surface electric field value is 69 V/(m·V). This high field at the terminal suggests possible charge accumulation on the

surface of the standoffs under test. This could be due to polarization of the materials or the presence of surface charge.

Figure 4.8 shows the electric field distribution along the 50cm insulating standoffs. The maximum of the electric field strength is observed at the stressed point (*x=45*) i.e. the application point of the lightning impulses.

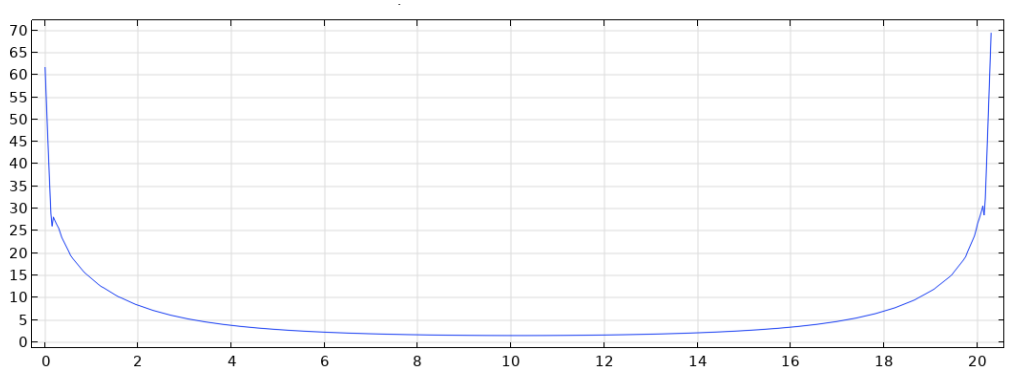


Figure 4.7: Surface electric field on 25cm insulating standoffs

The grounded point is x=0 as indicated in the graphs. The distribution exhibits a fairly symmetrical profile, suggesting a fairly uniform electric field distribution across the surface, except for the terminal's effects. There is significant peak at both ends *x=0* and *x=45* then at centre from *x=8 to 45*. These high field strength values at the terminals could be points of concern for surface discharge inception, when exposed at high voltages. The maximum surface electric field value is *64* V/(m·V). This high field at the terminal suggests possible charge accumulation on the surface of the standoffs under test. This could be due to polarization of the materials or the presence of surface charge.

Figure 4.9 shows the electric field distribution along the 75cm insulating standoffs. The maximum electric field strength is observed at the stressed point (*x=70*) i.e. the application point of the lightning impulses. The grounded point is *x=0* as indicated in the graphs. The distribution exhibits a fairly symmetrical profile, suggesting a fairly uniform electric field distribution across the surface, except for the terminal's effects.

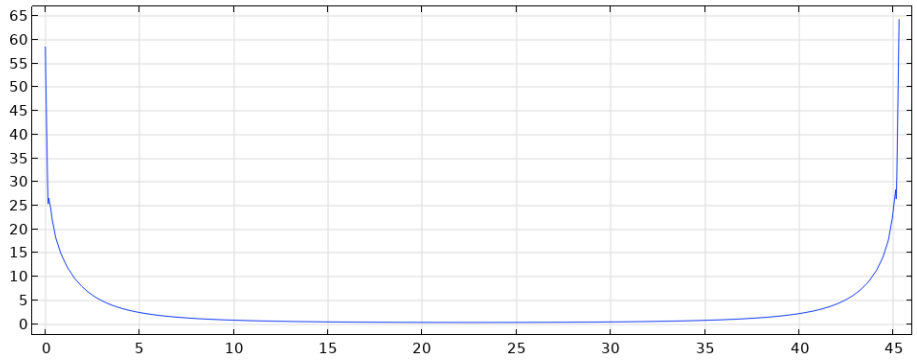


Figure 4.8: Surface electric field on 50cm insulating standoffs

There is significant peak at both ends x=0 and x=70 then at centre from *x=10 to 65*. These high field strength values at the terminals could be points of concern for surface discharge inception, when exposed at high voltages. The maximum surface electric filed value is *63* V/(m·V). This high field at the terminal suggests possible charge accumulation on the surface of the standoffs under tests. This could be due to polarization of the materials or the presence of surface charge.

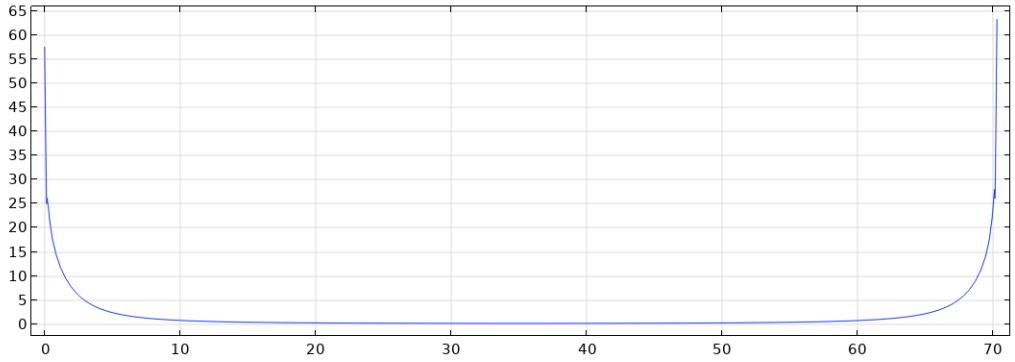


Figure 4.9: Surface electric field on 75cm insulating standoffs

### 4.7 Effect of Material and length on electric field Distribution

From the graphs as shown in Figure 4.10, at constant voltage magnitude, as the length of insulating standoffs increases, the electric field distribution decreases for the both materials (Polymer and Resin). A longer standoff will distribute the voltage over a great distance, reducing the electric filed intensity. For the graphs it is also observed at any length, the resin materials consistently exhibit a lower electric filed distribution compared to the polymer which suggest that the resin material is more effective at distributing the electric

field, is expected to have a higher flashover voltage compared to the polymer materials for same length of standoffs.

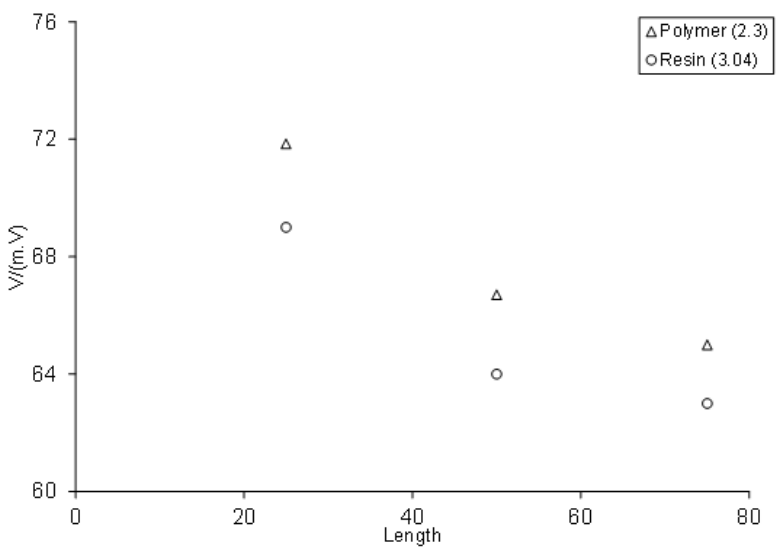


Figure 4.10: Effect of materials on Electric filed distribution

The lower electric field distribution along the standoffs, the higher flashover voltage is likely to be. A lower electric field means the insulator can withstand a higher voltage before reaching its dielectric strength. This inverse relationship highlights the benefit of longer standoffs in distributing potential difference, thereby reducing electric field stress. Moreover, epoxy resin consistently exhibits lower electric field strength compared to polymer at any given length, indicating superior electric field distribution properties.

Polymers and epoxy resins are commonly employed in insulating standoffs due to their inherent dielectric properties, mechanical strength, and environmental resistance. Polymers offer flexibility and cost-effectiveness, while epoxy resins provide enhanced mechanical robustness and thermal stability. Crucially, epoxy resin's higher dielectric constant, as observed in the graph, allows it to more effectively distribute electric fields, minimizing localized stress concentrations. This is paramount in high-voltage applications where preventing electrical breakdown and flashover is critical. The choice between polymer and epoxy resin often depends on specific application requirements, balancing factors like cost, mechanical demands, and desired electrical performance.

# CHAPTER FIVE: MEASUREMENT PROCEDURE

This chapter presents the basic definitions of the experimentally measured characteristics used for the evaluation of the surface dielectric strength and flashover characteristics of insulating standoffs.

## 5.1 Basic definitions

### 5.1.1 Flashover Probability-Flashover Probability Curves

The dielectric behavior of the insulation is defined by the discharge probability as a function of the applied voltage. For insulation design, it is practical to characterize performance using standardized voltage stress profiles defined by time-dependent parameters e.g. double exponential waveforms. The testing protocols simplify these profiles by fixing $T_1$ and $T_2$, reducing variables to only the crest voltage $V$. The most commonly used distribution is the normal distribution and for that the equation for the normal distribution density function is given by equation 5.1.

$$P(f) = \frac{1}{\sigma\sqrt{2\pi}} e^{-\frac{(f_k - f_{av})^2}{2\sigma^2}} \tag{5.1}$$

where, $f_k$ is the $k_{th}$ value of the variables, $f_{av}$ is the average value and σ is the standard deviation.

When the applied voltage ($V$) is the variables the distribution function takes the form as equation 5.2.

$$P(V) = \frac{1}{\sigma\sqrt{2\pi}} e^{-\frac{(V - V_{50})^2}{2\sigma^2}} \tag{5.2}$$

where $V_{50}$, is the voltage which leads to 50 % probability of discharge.

By knowing the $V_{50}$ and σ allows us to calculate value of the probability P(V) for any applied voltage as shown in Figure 4.1.

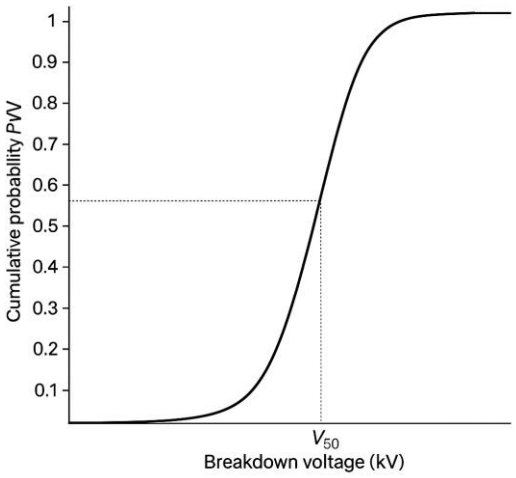


Figure 5.1: Flashover Probability Curve

$$P(f) = \frac{1}{\sigma\sqrt{2\pi}} \int_{-\infty}^{U} \exp\left(-\frac{((U-U_{50})^2}{2\sigma^2}\right) \quad (5.3)$$

### 5.1.2 50% breakdown voltage, $U_{50}$

Breakdown voltage $U_{50}$ is defined as the value of the imposed stress for which the probability of breakdown is 50% [1], i.e. a certain number of impositions under the specific stress leads to a 50% probability of breakdown and a 50% probability of withstand.

### 5.1.3 Flashover voltage, $U_p$

The flashover voltage is defined as the voltage at which the electrical flashover of an insulation occurs [1]. Its value is mainly determined by the mechanism of electrical discharge, from the moment of application of the stress voltage to the moment of flashover. In this work, flashover voltage, $U_p$, was defined as the maximum voltage stressing the insulating stand-offs until flashover, and in fact it is the voltage which eventually causes flashover.

### 5.1.4 Time to flashover, $t_f$

The flashover time is conventionally defined as the time interval between the application of the stress and its collapse [1]. This definition is used as long as no current measurements are performed. In this thesis due to the current measurements, the time at which the maximum current occurs was defined as the time to flashover. At flashover, the spark channel is assumed to bridge the entire gap.

### 5.1.5 Maximum current value, $I_p$

The maximum spark current value or peak current was defined at the time instant when the current value is maximum, at the peak of the current waveform.

### 5.1.6 Voltage at Maximum current Value, $U_{Ip}$

The voltage at the maximum value of the current, is defined as the value of the voltage at the time instant of maximum current, i.e. at the time defined as the flashover time.

## 5.2 Experimentally obtained curves

### 5.2.1 Flashover voltage- time to flashover characteristics, ($U_p$-$t_f$)

Depending on the amplitude of the applied voltage, flashover occurs either during the wavefront or the wave tail of the applied impulse voltage. The voltage-time characteristic, is a graph which, for a series of voltage levels, plots either the instantaneous value or the maximum value of each level as a function of the corresponding decay time, depending on whether it occurs at the front or the tail of the applied voltage. A time-voltage characteristic curve is shown in Figure 5.2. The characteristic voltage-time curve is an important practical property of any insulating device or structure, such as insulators. It provides the basis for determining the level of protection against overvoltage's.

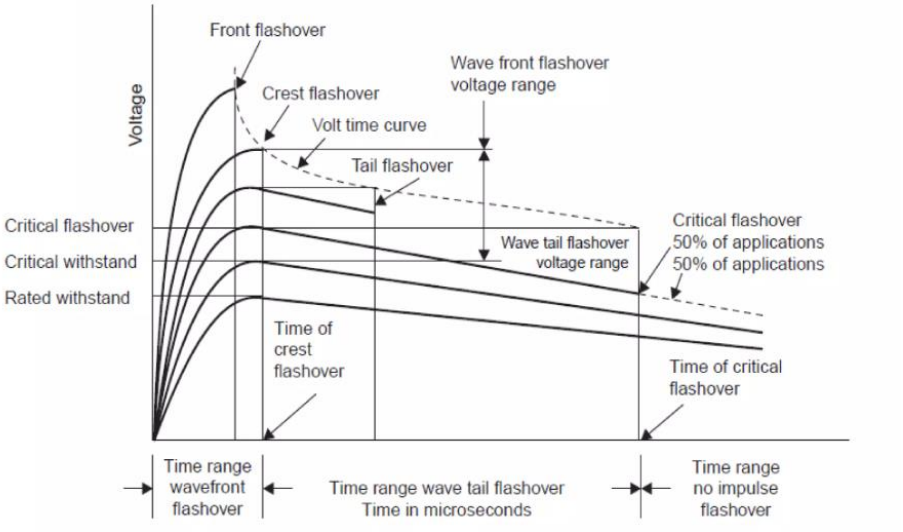


Figure 5.2: Flashover voltage- time to flashover curves

### 5.2.2 Maximum current-flashover voltage, $I_p$-$U_p$

The $I_p$-$U_p$ curves present the maximum current as a function of the flashover voltage The purpose of deriving these curves is to study the current that results for each flashover voltage, current which is a result of this voltage.

### 5.2.3 Maximum current-applied voltage curves, $I_p$-$U_{ap}$

The $I_p$-$U_{ap}$ curves show the maximum current as a function of the applied voltage. The difference with the curves described in the immediately preceding section is that the purpose of deriving these curves is to study the current that results if a given stress voltage value is applied to the standoffs.

### 5.2.3 Spark conductance based on flashover voltage vs applied voltage, $I_p$ /$U_p$ -$U_{ap}$

The $I_p$ /$U_p$ -$U_{ap}$ curves show the spark conductance based on the flashover voltage as a function of the amplitude of the applied voltage.

### 5.2.4 Spark Conduction based on voltage at peak current, $I_p$/U, Ip – $U_{ap}$

The $I_p$/U, Ip – $U_{ap}$ curves show the spark conductance based on voltage at maximum current. The purpose of their extraction is the study of the conductivity presented by the spark at the time of the flashover. This conductivity differs from the conductivity value corresponding to the flashover voltage as at the time of flashover, the voltage is obviously lower than the flashover voltage.

## 5.3 Multiple levels method

The stochastic nature of the flashover phenomenon results in the statistical variation of the breakdown voltage. Therefore, the reliable determination of the flashover voltage is carried out through statistical analysis of the test results. There are three methods of determining the flashover voltage, the multiple levels method, the up and down method and the sequential breakdown method. In this thesis, to determine the surface flashover voltage of the standoffs, the multiple levels method is used.

In applying the method, a voltage of constant value, (voltage level) is imposed on the insulation several times at each of the voltage levels. From the ratio of the number of flashovers observed, to the number of impositions, of the voltage per level, the flashover probability is obtained.

$$P(U_i) = \frac{d_i}{m} \tag{5.3}$$

## 5.4 Impulse voltage waveforms

This thesis examines the surface dielectric behavior of insulating standoffs used to support the down conductors and structures of EILPS under the influence standard lightning impulse voltages. Specifically, the applied voltage waveform is 1.1/50 µs. The waveforms of positive and negative polarity are shown in Figure 5.3 and 5.4, respectively.

## 5.5 Measurement standards

Figures 5.5 and 5.6 demonstrate the measurement procedures obtained during the experiments regarding flashover during the wave tail and the wavefront, respectively.

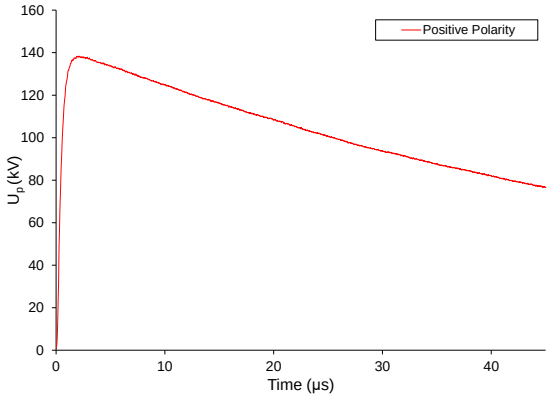


Figure 5.3: Lightning impulse voltage 1.1/50µs (+)

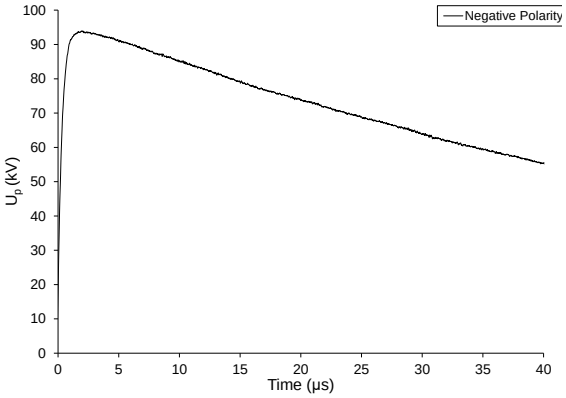


Figure 5.4: Lightning impulse voltage 1.1/50µs (-)

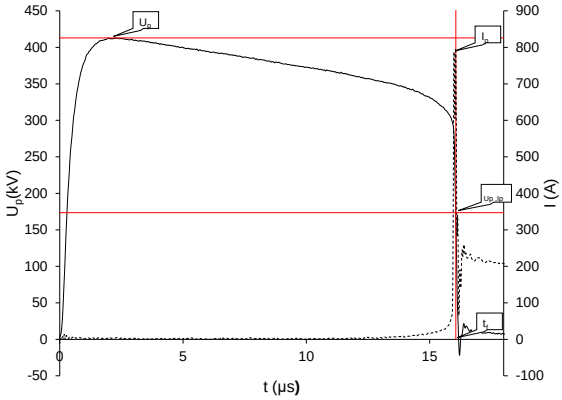


Figure 5.5: V-T curve at lower voltage flashover

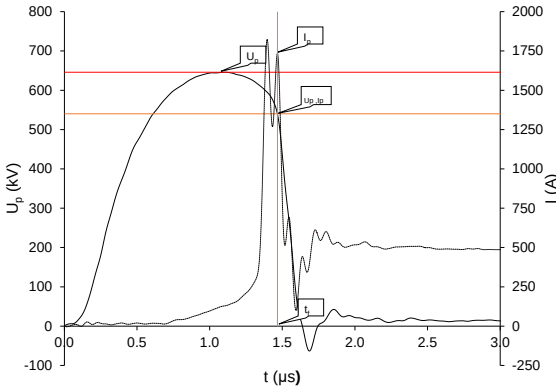


Figure 5.6: V-T curve at higher voltage flashover

### 5.6 Measurement procedures

During experiments on insulating standoffs, flashover characteristics were investigated under both positive and negative polarity. The testing procedure differed significantly between the two polarities.

**Positive Polarity Testing**: Under positive polarity, a progressive voltage application method was employed. The applied voltage was gradually increased from a lower level to a higher level. At each voltage step, the flashover probability was evaluated. This approach allowed for the observation of how the likelihood of flashover increased with increasing voltage, providing a detailed picture of the insulation's performance under rising positive voltage stress.

**Negative Polarity Testing**: The negative polarity testing followed a different protocol. Initially, a high voltage level was applied to the standoff. This initial high voltage application aimed to quickly determine the first flashover event. Because the initial voltage was high, the time to flashover was expected to be short, and the flashover probability was assumed to be 100% or very close to it. Following this initial flashover, the applied voltage was then decreased. This reduction in voltage was implemented to identify the withstand voltage of the insulator. The withstand voltage represents the highest voltage level that the insulator can reliably withstand without flashover. Once the withstand voltage was determined, the applied voltage was incrementally increased again. This second voltage ramp allowed for the collection of data to construct the flashover probability curve and to analyse other relevant insulation characteristics under negative polarity. This complete process provided a comprehensive understanding of the standoff's performance under negative voltage, including the initial flashover behavior, the withstand voltage, and the flashover probability as a function of increasing voltage.

# CHAPTER SIX: EXPERIMENTAL RESULTS

In this chapter, the diagrams extracted from the experimental measurements as well as the conclusions derived from the experimental results are presented. The measurements taken concern the flashover voltage and time, the instantaneous flashover voltage (voltage at maximum current) and the peak current. The results are commented and conclusions are drawn regarding the effect of the amplitude and polarity of applied voltage and the length of insulating standoffs.

## 6.1 Breakdown Probability Curves

Based on the experimental results, the flashover probability curves and their approximation with the normal distribution were constructed. The curves are presented in diagrams 6.1 – 6.6.

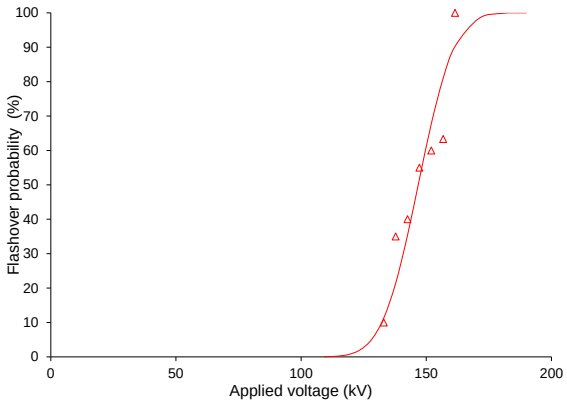


Figure 6.1: 25cm insulating standoff (+)

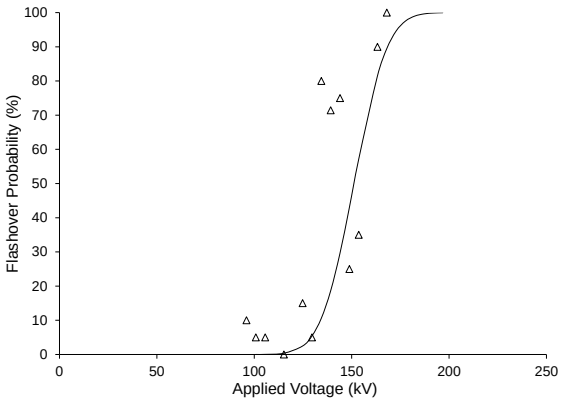


Figure 6.2: 25cm insulating standoff (-)

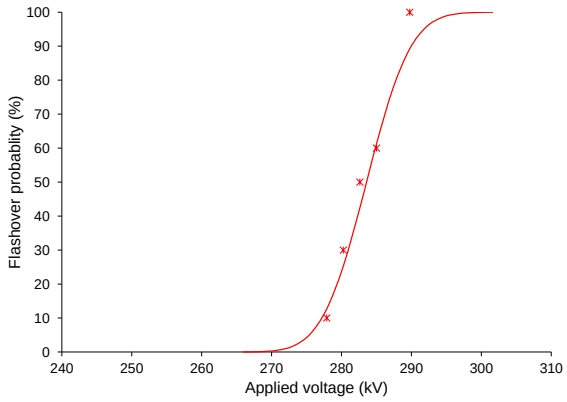


Figure 6.3: 50cm insulating standoff (+)

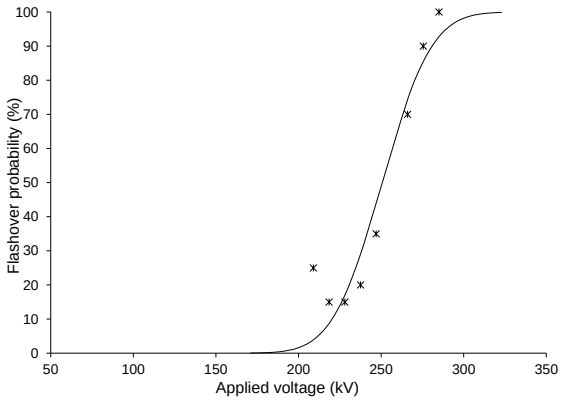


Figure 6.4: 50cm insulating standoff (-)

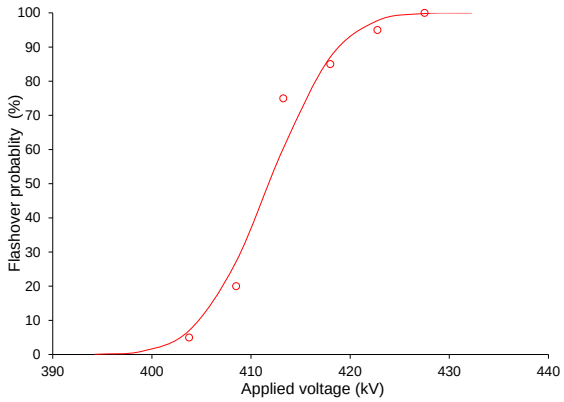


Figure 6.5: 75cm insulating standoff (+)

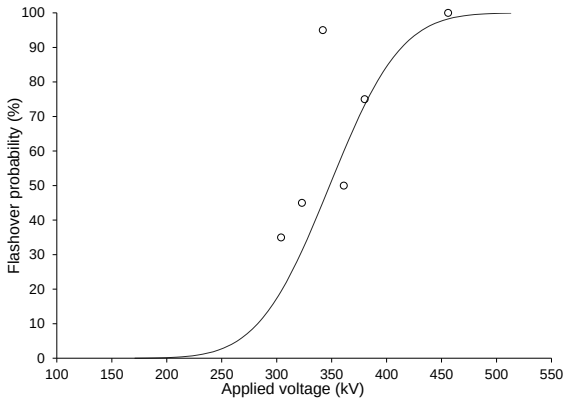


Figure 6.6: 75cm insulating standoff (-)

Listed below, in Table 6.1, for each arrangement, are the values of the 50% flashover voltage ($U_{50}$), standard deviation σ (%) as well as the corresponding atmospheric conditions for both positive and negative polarity.

Table 6. 1: Aggregate results of 1.1/50 μs waveform

| Aggregate results of 1.10/50 μs waveform on insulating standoffs | | | | | | | |
|---|---|---|---|---|---|---|---|
| Sample | Polarity | P (mmHg) | T ($^0$C) | H (gm$^{-3}$) | δ | σ (%) | $U_{50}$ (kV) |
| 25 cm | Positive | 761.5 | 16.75 | 11.15 | 1.0132 | 7.74 | 151.20 |
| | Negative | 768.5 | 17.50 | 11.39 | 1.0199 | 8.59 | 146.78 |
| 50 cm | Positive | 766.0 | 16.00 | 10.00 | 1.0218 | 1.76 | 283.58 |
| | Negative | 763.0 | 16.75 | 11.63 | 1.0152 | 9.43 | 250.56 |
| 75 cm | Positive | 766.0 | 13.50 | 10.27 | 1.0236 | 1.33 | 411.83 |
| | Negative | 763.0 | 16.25 | 10.49 | 1.0170 | 14.69 | 348.18 |

### 6.1.1 Effect of applied voltage polarity on flashover probability curve

In this section the effect of the polarity of the applied voltage on the flashover probability curves is considered. Thus, the flashover probability curves were drawn in a common diagram for both polarities as illustrated in Figures 6.7-6.9.

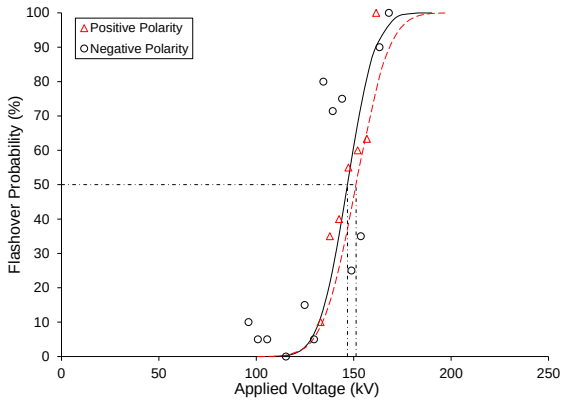


Figure 6.7: 25cm insulating standoff

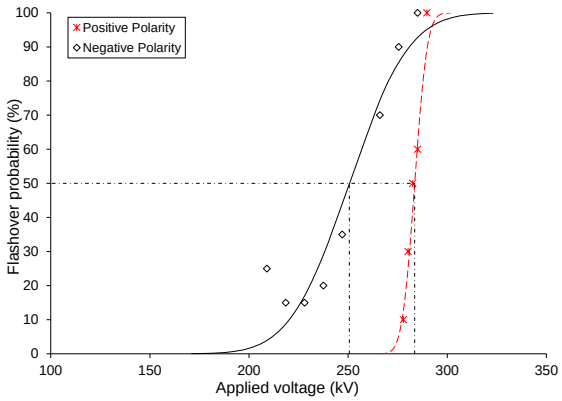


Figure 6.8: 50cm insulating standoff

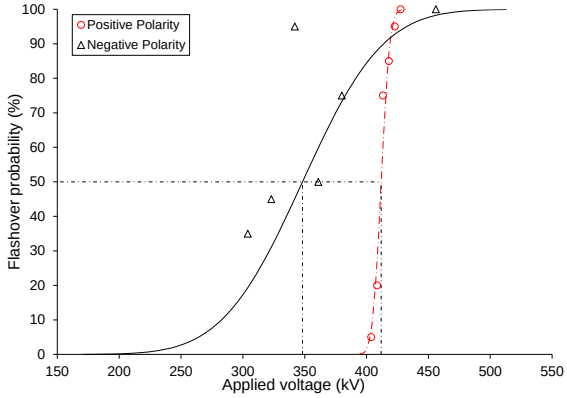


Figure 6.9: 75cm insulating standoff

It is observed that the flashover voltage is higher under positive polarity lightning impulses regarding insulating stand-offs of 25, 50 and 75 cm. Negative impulse create concentrated electron avalanches, leading to faster break down because as negative voltage is applied to standoffs, the surface itself becomes a source of electrons. These electrons initially from the surface gain energy from the electric field and collide with air molecules and these collisions knock out more electrons, which create avalanche of electron and flashover occur. Instead of a concentrated avalanche, a more diffuse "streamer" discharge develops. Because the discharge is spread out, it takes longer for the positive impulse to gather enough energy to completely bridge the gap between the electrodes and cause a flashover. At lower voltages, the initiation of streamers and the effect of space charge plays a significant role, leading to a noticeable difference in flashover probability between positive and negative polarities. But at higher voltages, avalanche process dominates, and the breakdown becomes almost certain, regardless of polarity, leading to the convergence of

the flashover probability curves. The effect of the polarity of applied voltage on the flashover probability distribution of the 25 cm insulating stand-off is rather minimal.

### 6.1.2 Effect of length of standoffs on flashover probability

The flashover probability curves of standoffs differing in length are plotted in Figure. 6.10-6.11 to assess the effect of the length of the standoffs on flashover probability curves.

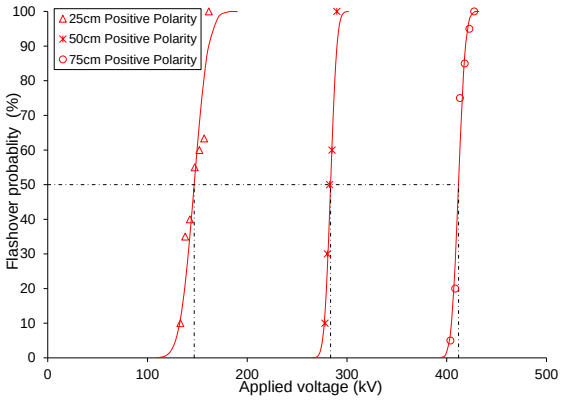


Figure 6.10: 25,50,75cm insulating standoff (+)

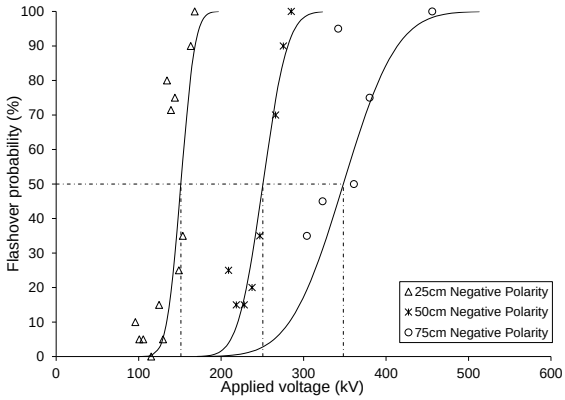


Figure 6.11: 25,50,75cm insulating standoff (-)

The figures 6.10-6.11 clearly demonstrate that for positive and negative polarity the flashover voltage is strongly depended on the length of the insulating standoffs, markedly increasing with the latter. Under negative polarity, larger standard deviations are observed with increasing length. The $U_{50}$ for positive polarity are 146.78kV, 283.58kV and 411.83kV with smaller standard deviations respectively. The $U_{50}$ for negative polarity are 151.20kV, 250.56kV, 348.18kV with larger standard deviation as length increases respectively. It indicates that the 75cm long standoff have higher dielectric strength in both polarity of lightning impulse.

## 6.2 Maximum flashover current -voltage curves, $I_p$-$U_p$

The $I_p$-$U_p$ curves were constructed to enable the study of the discharge current as a function of the flashover voltage. These curves are presented in diagrams 6.12-6.17. The general conclusion drawn from diagrams 6.12 – 6.17 is, as expected, the discharge current increases with increasing applied voltage. It is observed that the increment of the current is fairly proportional to the flashover voltage.

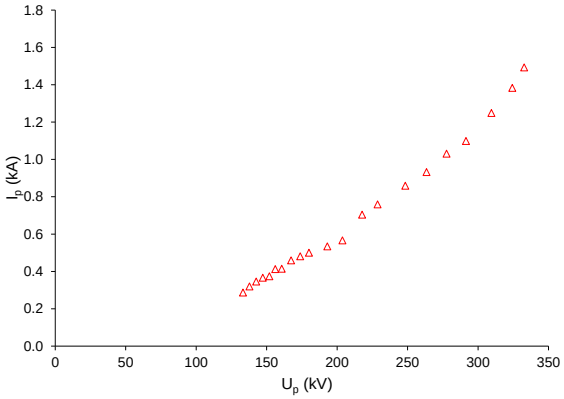


Figure 6.12: 25cm insulating standoff (+)

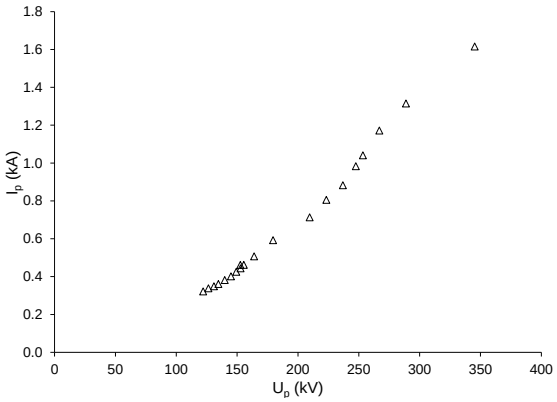


Figure 6.13: 25cm insulating standoff (-)

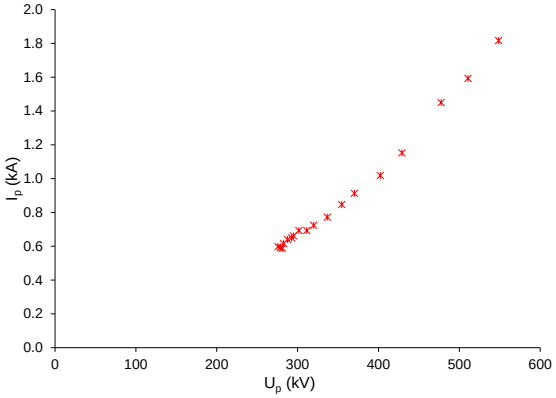


Figure 6.14: 50cm insulating standoff (+)

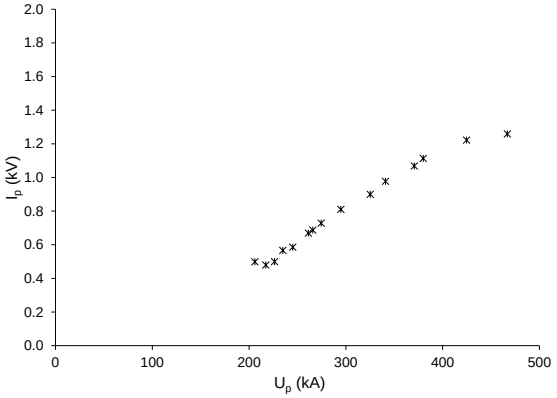


Figure 6.15: 50cm insulating standoff (-)

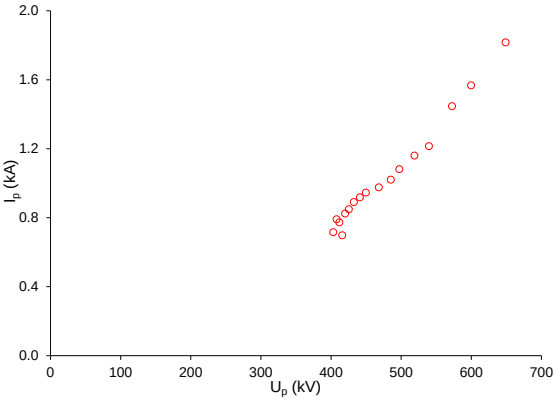


Figure 6.16: 75cm insulating standoff (+)

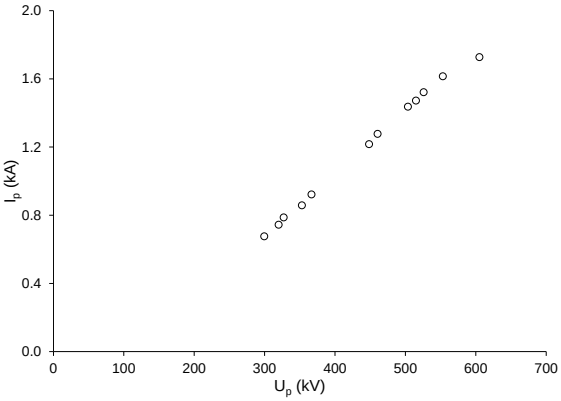


Figure 6.17: 75cm insulating standoff (-)

### 6.2.1 Effect of Polarity on $I_p$-$U_p$ curves

The effect of polarity of the applied voltage on $I_p$-$U_p$ curves, is demonstrated in Figures 6.18-6.20. It can be observed that the current is higher under negative that positive polarity impulses, with the effect being more pronounced as the length of the insulating standoff increases. Current increases linearly with flashover voltage. Negative polarity sees rapid

electron detachment, avalanche growth, and streamer formation, yielding higher currents. Electrons moving from ground and positive ions aid discharge propagation. Positive polarity requires positive ion creation near the electrode, needing a higher field and being sensitive to distance disruptions. As insulator length grows, positive streamer propagation becomes harder, while negative streamers propagate efficiently. This results in larger impulse current magnitude differences. Negative polarity flashovers are faster and more intense than positive polarity flashes. This is due to the free electrons being readily available, and the positive ions helping to propagate the flashover. The positive polarity flashover requires the creation of positive ions, which slows down the process, and requires higher voltage.

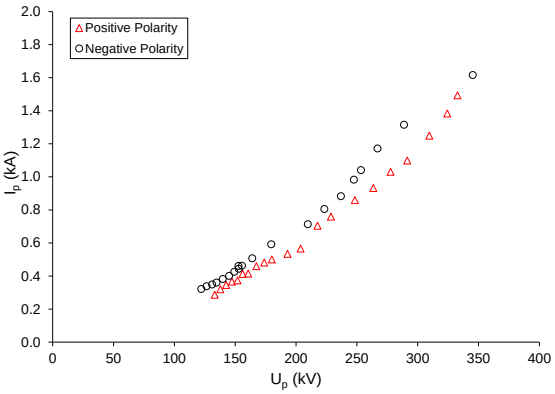


Figure 6.18: 25cm insulating standoff

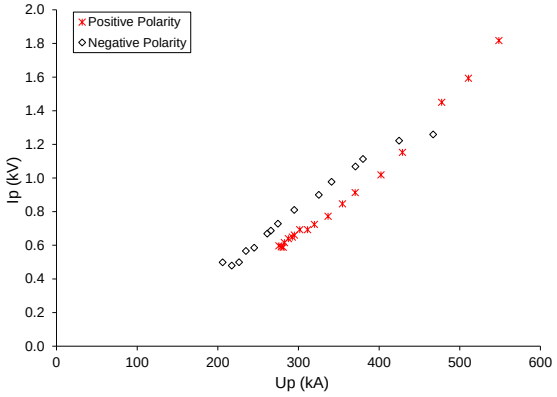


Figure 6.19: 50cm insulating standoff

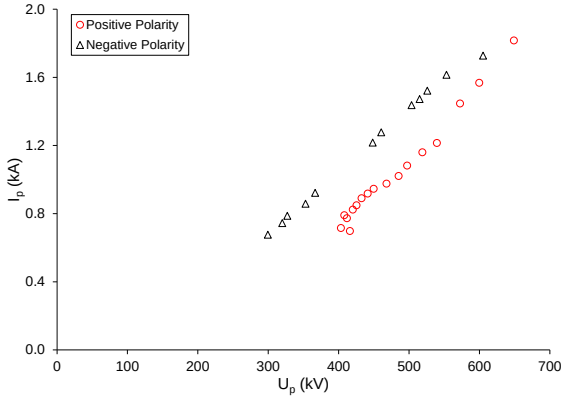


Figure 6.20: 75cm insulating standoff

### 6.2.2 Effect of length of insulating standoffs on $I_p$-$U_p$ curves

In this section the effect of the length of insulating standoffs on the $I_p$-$U_p$. The curves are presented in Figures 6.21-6.22. It is evident that the maximum discharge current, as a

function of the flashover voltage, increases with increasing gap length. For a given voltage, the discharge current tends to be higher for shorter insulator lengths. This is because shorter gaps require less energy to initiate breakdown. However, the fundamental trend of increasing current with increasing voltage holds true for all lengths.

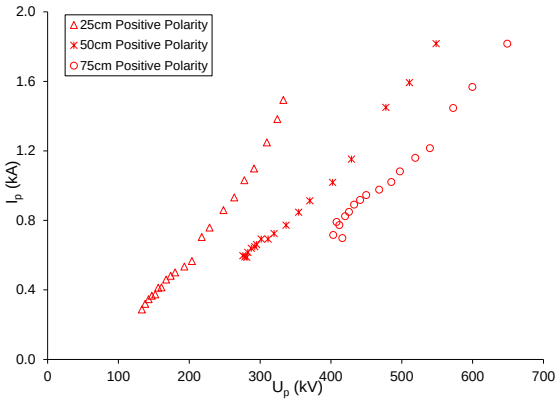


Figure 6.21: 25,50,75cm insulating standoffs (+)

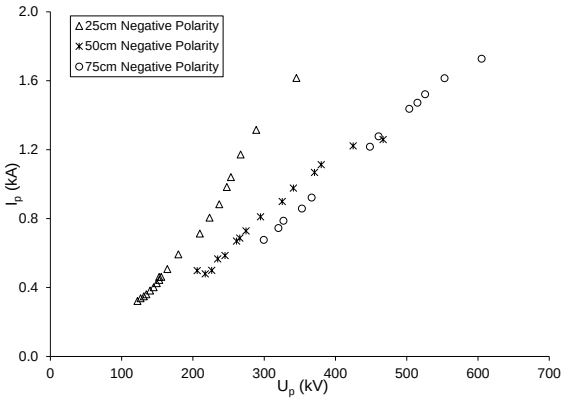


Figure 6.22: 25,50,75cm insulating standoff (-)

### 6.3 Maximum current- applied Voltage curves, $I_p$-$U_{ap}$

The $I_p$-$U_{ap}$ curves were constructed to enable the study of the resulting maximum discharge current as a function of the applied voltage. These curves are presented in diagrams 6.23-6.28.

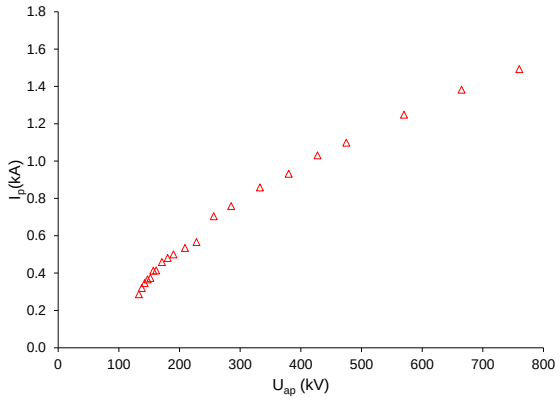


Figure 6.23: 25cm insulating standoff (+)

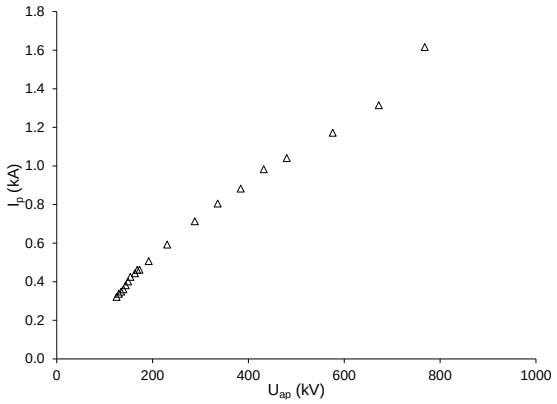


Figure 6.24: 25cm insulating standoff (-)

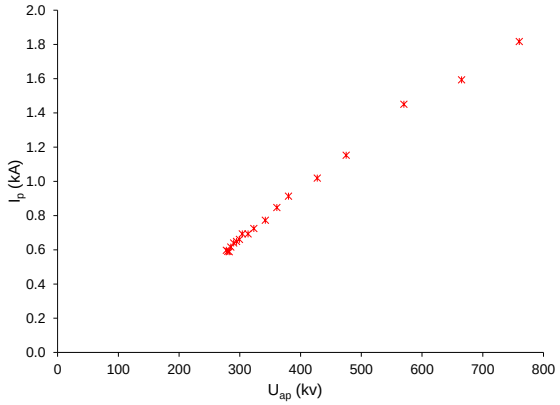


Figure 6.25: 50cm insulating standoff (+)

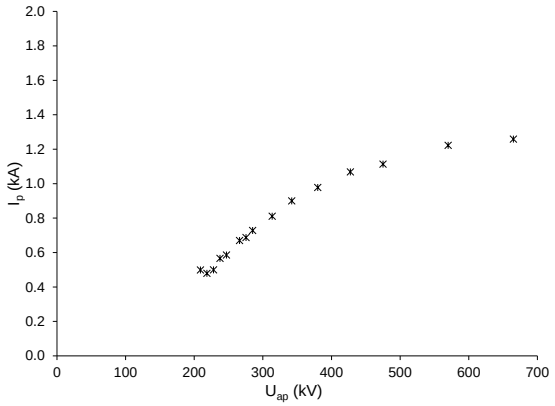


Figure 6.26: 50cm insulating standoff (-)

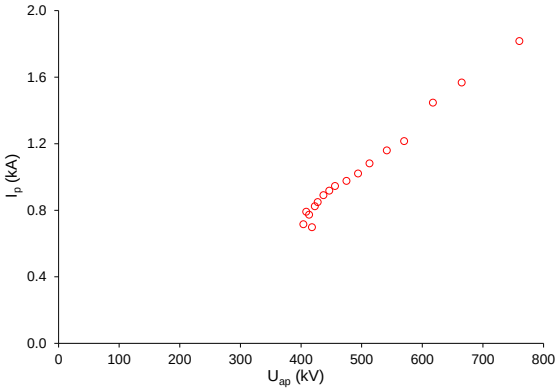


Figure 6.27: 75cm insulating standoff (+)

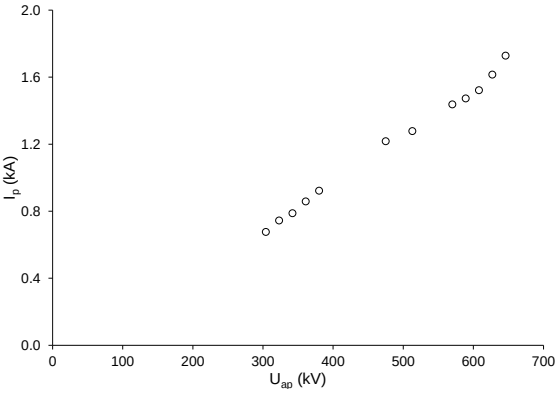


Figure 6.28: 75cm insulating standoff (-)

A general conclusion drawn is the nearly linear increment of the peak current as related to the applied voltage, with an exception of the 50 cm standoff under negative polarity (Figure. 6.26).

### 6.3.1 Effect of Polarity on $I_p$-$U_{ap}$

The curves produced for the purpose of inferring the effect of polarity on the peak current-applied voltage curves are presented in Figures 6.29-6.31.

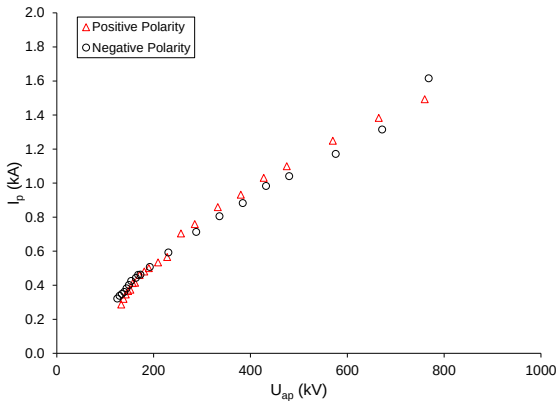


Figure 6.29: 25cm insulating standoff

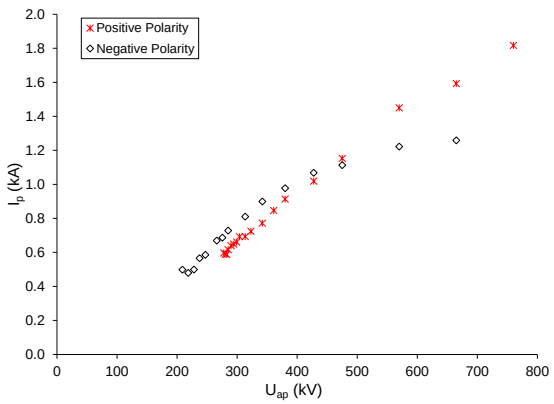


Figure 6.30: 50cm insulating standoff

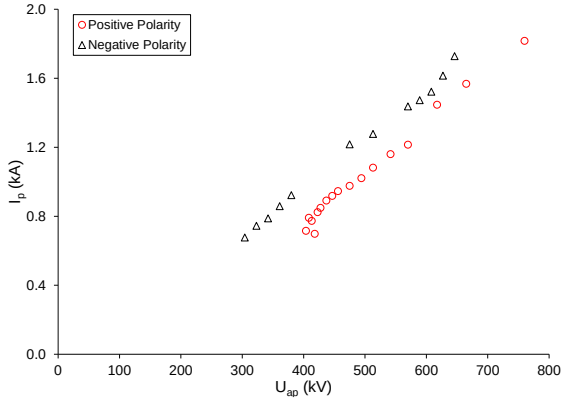


Figure 6.31: 75cm insulating standoff

From the figures above, it can be seen that the curves are relatively close for the two polarities, thus, the polarity effect is fairly minimal, while they may also overlap (figures 6.29 and 6.30). The gap is too short for the inherent differences in streamer propagation between positive and negative polarity to become significantly pronounced. This results in the observed overlap and minimal polarity effect. An exception is the case of the 75cm long standoff (Figure 6.31) where the maximum current is clearly higher under negative than positive polarity impulses.

### 6.3.2 Effect of length on $I_p$- $U_{ap}$

The effect of the length of insulating standoffs is investigated on the maximum discharge current-applied voltage curves can be studied through Figures 6.32-6.33. Under positive polarity impulses slightly higher values of maximum current are observed decreasing gap length. This effect is more pronounced under negative polarity impulses. Under negative polarity, the electrons initiating the discharge move away from the high-voltage electrode. This creates a more favourable condition for streamer propagation, as the positive ions left

behind enhance the electric field ahead of the streamer, promoting further ionization and growth. This effect is amplified in shorter gaps where the field is inherently stronger. With positive polarity, the electrons need to move towards the high-voltage electrode. This can hinder streamer development, as the electrons are effectively moving against the electric field. While a higher field in shorter gaps does increase ionization, it doesn't overcome the fundamental challenge of positive streamer propagation as effectively as in the negative case.

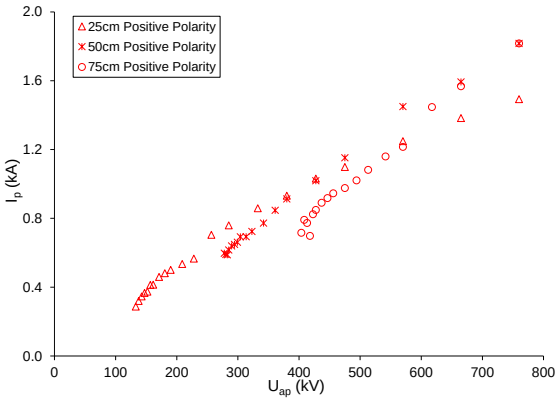


Figure 6.32: 25,50,75cm insulating standoff (+)

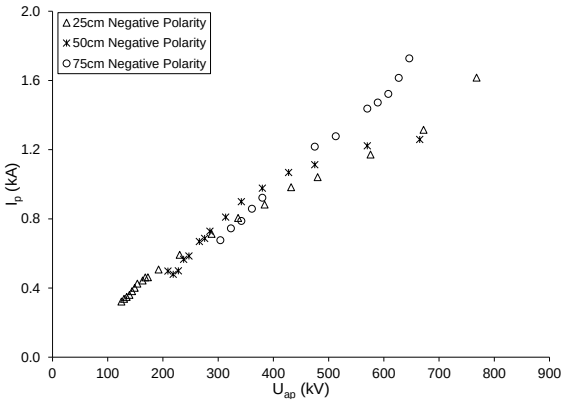


Figure 6.33: 25,50,75cm insulating standoff (-)

## 6.4 Flashover voltage-time characteristics, $U_p$-$t_f$

In this section, the flashover voltage-time characteristics are presented for every insulating standoff under positive and negative polarity of applied voltage in Figures 6.34-6.40.

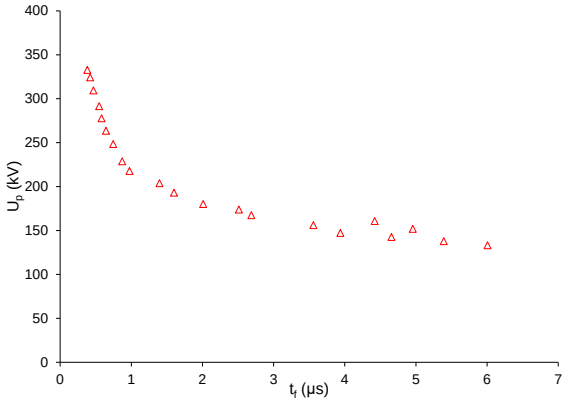


Figure 6.34: 25cm insulating standoff (+)

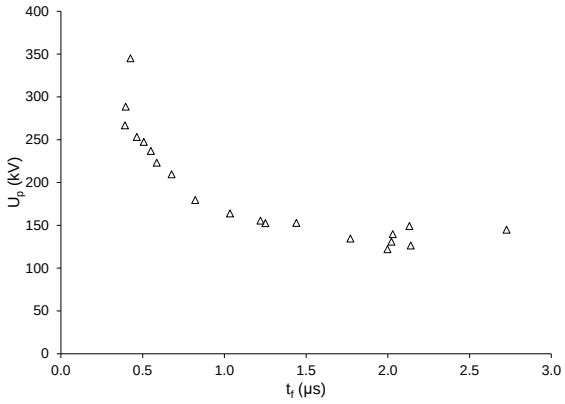


Figure 6.35: 25cm insulating standoff (-)

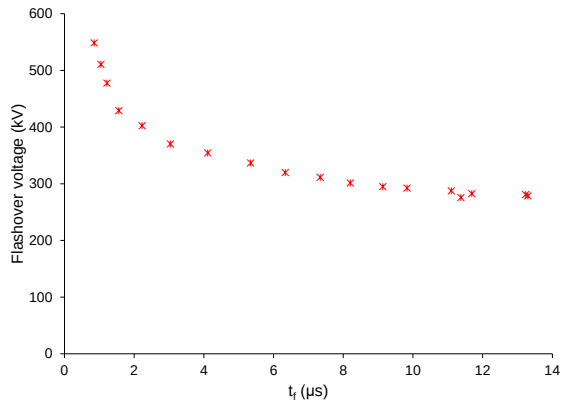


Figure 6.36: 50cm insulating standoff (+)

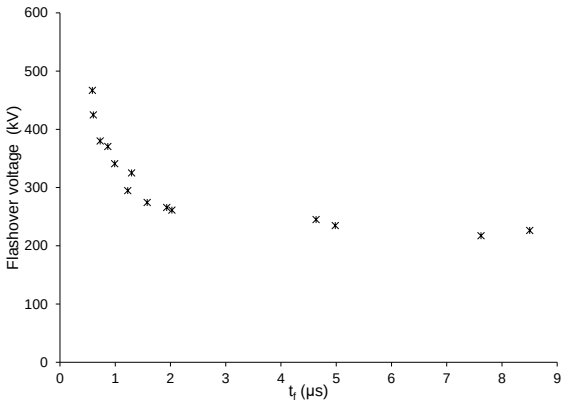


Figure 6.37: 50cm insulating standoff (-)

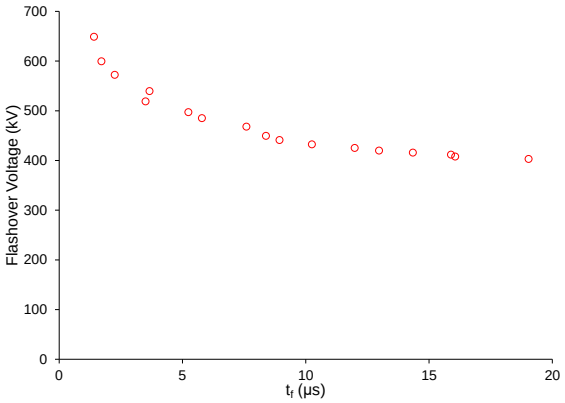


Figure 6.38: 75cm insulating standoff (+)

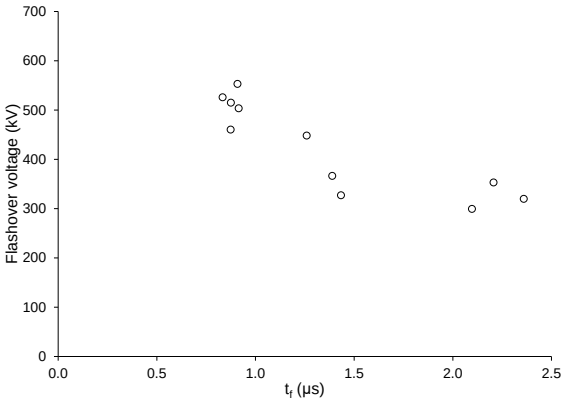


Figure 6.39: 75cm insulating standoff (-)

From diagrams 6.34 – 6.49 it is observed that with increasing applied voltage, flashover voltage increases while the time to flashover decreases, reaching a minimum value for the highest applied voltage levels. At higher levels the breakdown voltage increases but the breakdown time stabilizes. At lower levels of applied voltage, large dispersion of the time to flashover was observed, leading to higher time lags.

### 6.4.1 Effect of Polarity on $U_p$-$t_f$

In this section, the characteristics $U_p$-$t_f$ curves are presented for each with the effect of polarity as affecting parameter, as shown in Figures 6.40-6.42. It is evident that for the same time to flashover, the flashover voltage is higher under positive than negative polarity impulses, indicating better withstand capability compared to negative impulses. For higher voltages and shorter decay times, the effect of polarity on the $U_p$-$t_f$ characteristics is less pronounced, as the curves tend to coincide. The negative polarity curve appears to have a

steeper slope, implying that the flashover voltage changes more rapidly with respect to flashover time compared to positive polarity.

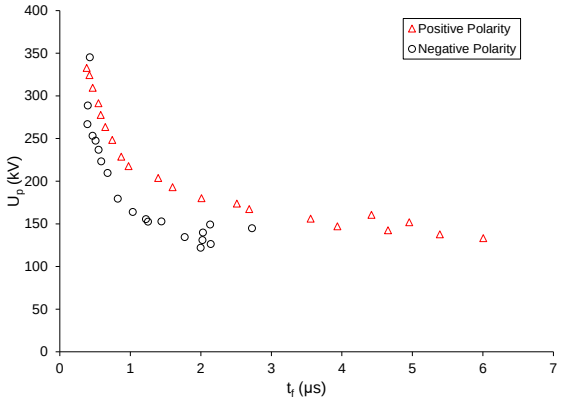


Figure 6.40: 25cm insulating standoff

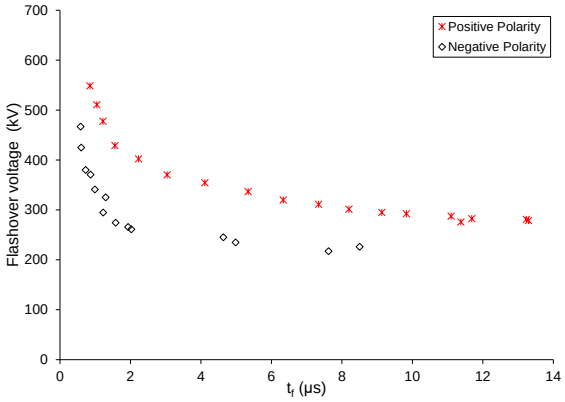


Figure 6.41: 50cm insulating standoff

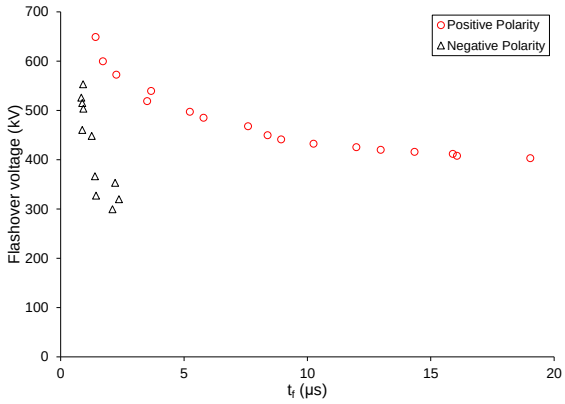


Figure 6.42: 75cm insulating standoff

### 6.4.2 Effect of length on $U_p$-$t_f$

In this section, in diagram 6.43 -6.44, the effect of the length of standoffs on $U_p$-$t_f$ is examined. With increasing gap length, the flashover voltage increases markedly. Also, longer times to flashover are observed with increasing gap length and the curve shift right of the existing curves. The difference in flashover voltage between the different lengths is substantial. This highlights the importance of considering insulator length in the design of insulation systems.

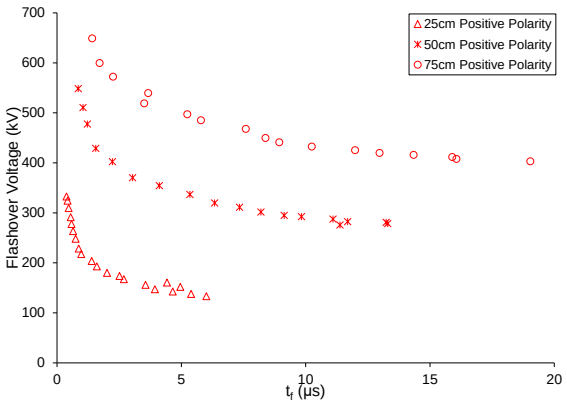


Figure 6.43: 25,50,75cm insulating standoff (+)

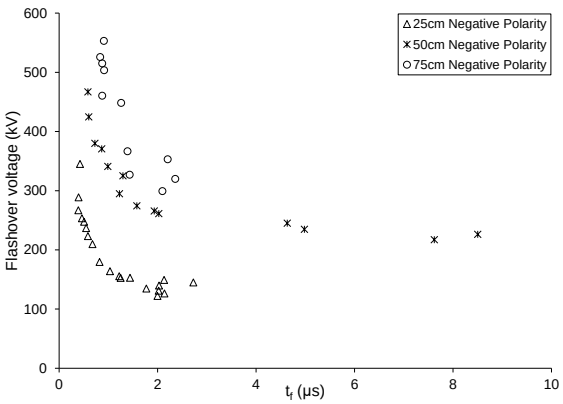


Figure 6.44: 25,50.75cm insulating standoff (-)

## 6.5 Spark conductance as a function of the applied voltage, $I_p/U_p$-$U_{ap}$

The purpose of extracting the $I_p/U_p$-$U_{ap}$ curves is to study the conductance of the spark channel at flashover. Figures 6.45-6.50 show the spark conductance curves for each insulator and polarity of applied voltage. It is observed that spark conductivity increases with increase in applied voltage.

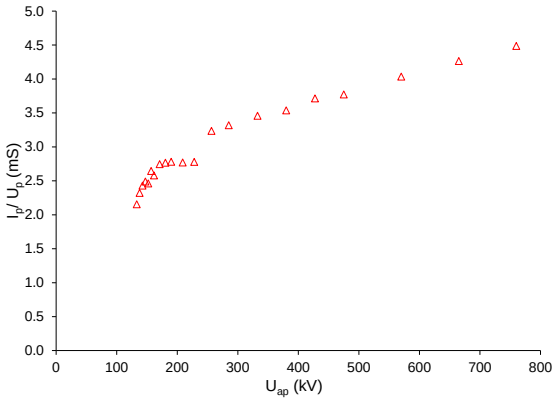


Figure 6.45: 25cm insulating standoff (+)

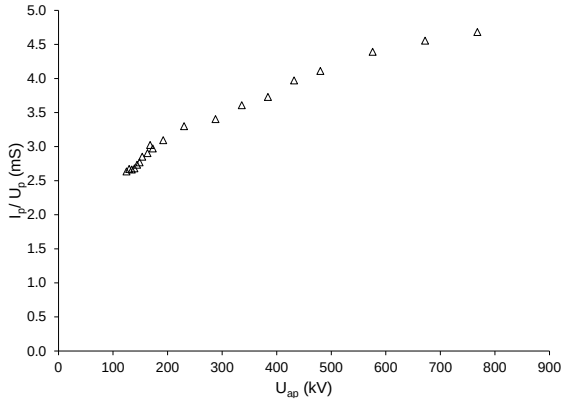


Figure 6.46: 25cm insulating standoff (-)

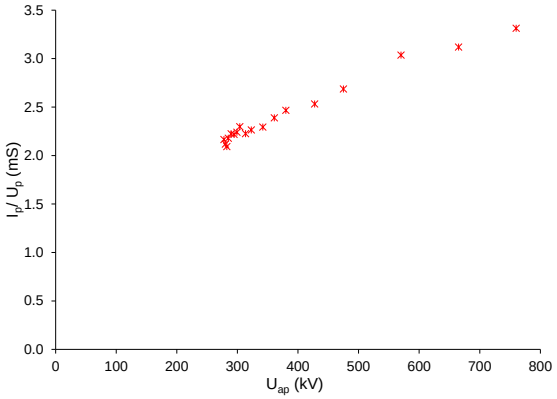


Figure 6.47: 50cm insulating standoff (+)

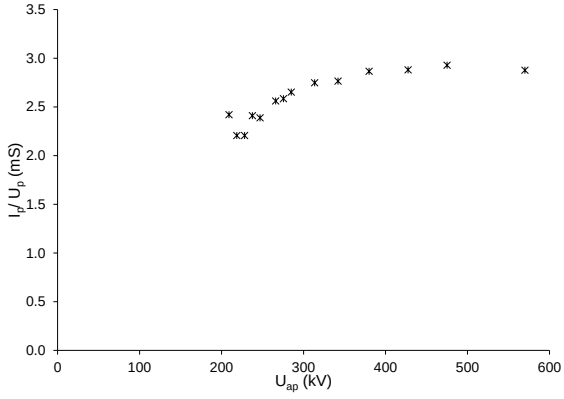


Figure 6.48: 50cm insulating standoff (-)

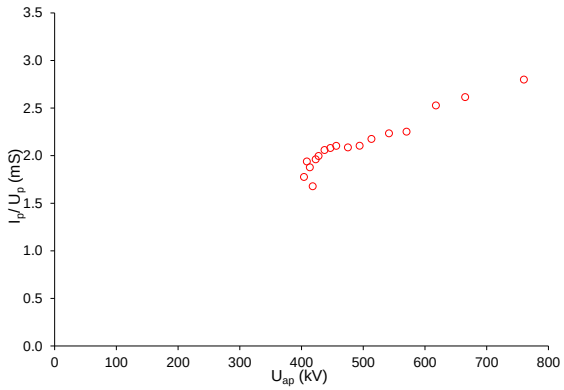


Figure 6.49: 75cm insulating standoff (+)

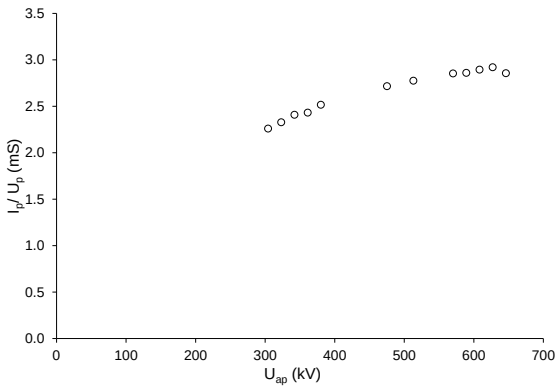


Figure 6.50: 75cm insulating standoff (-)

### 6.5.1 Effect of polarity on $I_p/U_p$-$U_{ap}$

In this section, the curves $I_p/U_p$-$U_{ap}$ curves are presented for each standoff to investigate the effect of polarity, as shown in Figures 6.51-6.53.

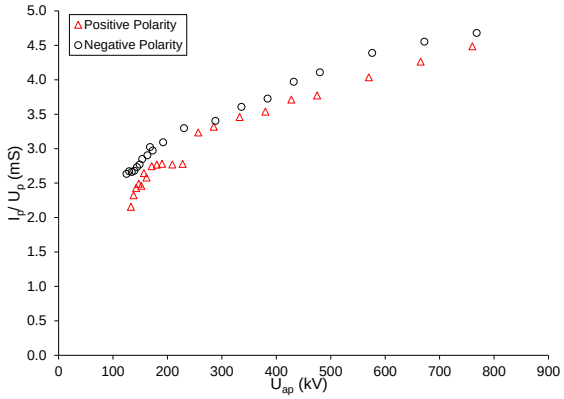


Figure 6.51: 25cm insulating standoff

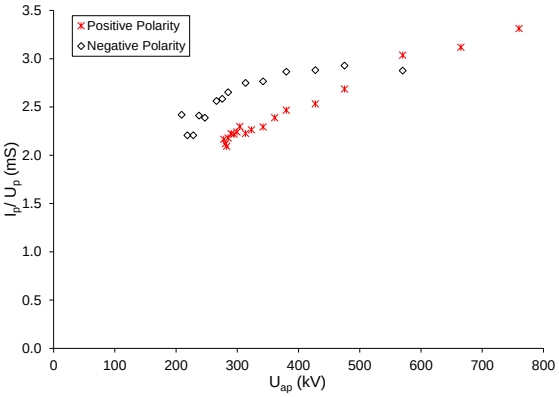


Figure 6.52: 50cm insulating standoff

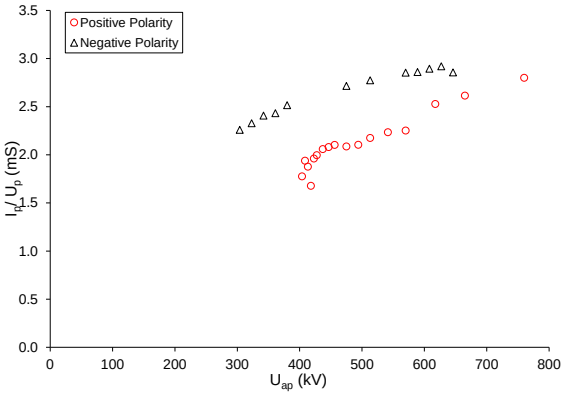


Figure 6.53: 75cm insulating standoff

Under negative polarity, the conductance of the spark channel is generally higher. This is more pronounced for higher gap lengths, especially for lower levels of applied voltage.

It was observed that under negative polarity, the discharge tent to develop on the surface of the insulating standoff, while under positive polarity it developed mostly through the air, away from the surface. This, together with the fact that higher values of conductance of the spark channel are observed under negative polarity impulses, suggest that the surface of the insulating standoff enhances the development of the discharge, resulting in higher conductivity. The positive polarity curve exhibits lower conductance compared to negative polarity, especially at lower voltages.

### 6.5.2 Effect of length on $I_p/U_p$-$U_{ap}$

In this section, in diagrams 6.54 -6.55, the effect of the length of standoffs on $I_p/U_p$-$U_{ap}$ curves is examined. Both positive and negative polarity lightning impulse flashover graphs demonstrate a clear trend: spark conductance ($I_p/U_p$) rises with applied voltage ($U_{ap}$) for all insulator lengths (25cm, 50cm, and 75cm). This is attributed to the increased ionization driven by stronger electric fields, forming a denser plasma channel. Shorter insulators consistently show higher conductance at a given voltage due to reduced air volume and higher current density after breakdown. However, the conductance-voltage relationship is non-linear, exhibiting saturation at high voltages.

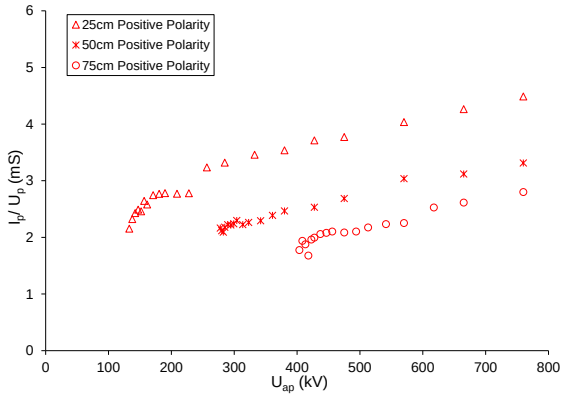


Figure 6.54: 25,50,75cm insulating standoff (+)

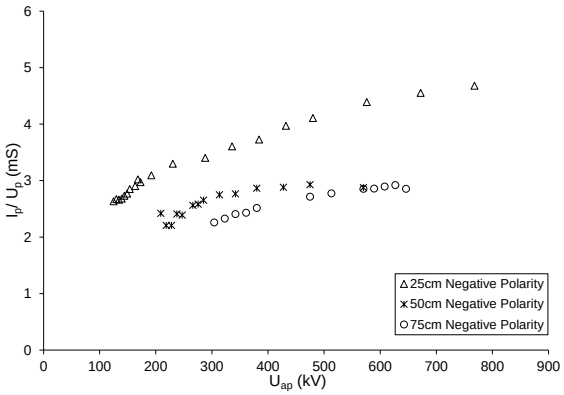


Figure 6.55: 25,50,75cm insulating standoff (-)

Polarity-specific differences arise in streamer development. Negative polarity features cathode-initiated streamers with complex branching, while positive polarity involves anode-initiated, more directed streamers. These variations, influenced by electron availability and field distribution, impact spark conductance patterns.

The initiation point of streamers significantly alters the plasma channel formation dynamics. These polarity-dependent differences are crucial for understanding and mitigating flashover in high-voltage systems.

# CHAPTER SEVEN: CONCLUSION

Insulating standoffs are critical components used in electrically insulated lightning protection systems (ILPS), providing essential support and maintaining electrical isolation between conductive parts. These devices are designed to prevent undesired flashover and facilitate the safe operation of various structures, particularly in environments prone to lightning strikes. Their notable role in enhancing the safety and efficiency of systems across multiple industries including aerospace, power distribution, and renewable energy underscores their significance in modern engineering practices. Constructed from a variety of materials such as metal, plastic, and thermoset composites, insulating standoffs exhibit distinct properties tailored to meet specific operational requirements.

Overvoltages due to lightning strikes, which are simulated using lightning impulse voltages, are a relatively common phenomenon and cause significant failures, since they stress the system. In order to maintain the performance of the system we use lightning protection systems.

However, the stochasticity of the phenomenon and consequently the impossibility of knowing the overvoltage that will appear in the system has led to the study of the dielectric behavior of standoffs under the influence of standard lighting impulses. This experiment was done conducted to investigating the effect of positive polarity and negative polarity of lightning impulses on different gap length of standoffs. The lightning impulse voltage was produced by Marx generator and applied to the fastener of insulating standoffs. The standoff was grounded through a suitable cable that passes the current transformer for discharge current measurements. The output of current transformer ends up via a suitable shielded cable with signal attenuator to the oscilloscope. With all this equipment, the flashover characteristics of the insulating standoffs on each polarity was investigated. The number of shots is applied on each voltage level and using multi-level method, the probability of the flashover is measured. The peak current and flashover voltage as well as the voltage at peak current was measured as described and different curves are plotted which describes the flashover characteristics of the insulating standoffs. In this thesis, insulating standoffs of different lengths (25, 50 and 75cm) have been investigated under

standard lightning impulse voltages, 1.2/50 μs, of both polarities. Experimental results on the lightning impulse flashover characteristics of the standoffs are assessed and discussed.

As we observed in the flashover probability curve $U_{50}$ for positive polarity are greater than negative polarity. And it is clearly observed that for both polarities' flashover voltage is strongly dependent on the length of standoffs, markedly increasing with latter. Under the negative polarity, larger standard deviation was observed with increasing length. It can be concluded that the maximum discharge current is significantly higher under negative polarity compared to positive polarity, particularly with increasing insulating standoff length. The observed higher flashover voltage ($U_{50}$) and better withstand capability under positive polarity, contrasted with the higher discharge currents and increased variability under negative polarity (particularly in longer standoffs), necessitate a design approach that prioritizes maximizing separation distance while specifically accounting for the more demanding conditions presented by negative impulses.

The maximum current increase linearly with flashover voltage across all insulating standoff length. For a given voltage, short length exhibits higher discharge current.

The polarity effect on flashover current with applied voltage is minimal, with curve for positive and negative impulse closely aligning or overlapping. However, with longer standoffs, like 75cm, negative polarity clearly yields higher maximum currents.

For the same time to flashover, the flashover voltage is higher under positive than negative polarity impulses, indicating better withstand capability compared to negative impulses. For higher voltages and shorter decay times, the effect of polarity on the $U_p$-$t_f$ characteristics is less pronounced. With increasing the gap length $U_p$-$t_f$ curves shift to the right of the existing curve. The negative polarity curves appear to have steeper slope implying that the flashover voltage changes more rapidly with respect to flashover time to compared to positive polarity.

The conductance of the spark increases with increasing applied voltage linearly for both polarities of the applied impulse voltage. The positive polarity exhibits lower conductance compared to negative polarity, especially at lower voltages. For same applied voltage markedly higher gap conductance is evident for shorter insulating standoffs. Generally higher gap conductance indicates the lower dielectric strength of standoffs.

Material selection should focus on insulators exhibiting consistently high dielectric strength and stable performance irrespective of impulse polarity. Preference should be given to materials demonstrating lower conductance, particularly at lower voltages, as higher conductance is indicative of reduced dielectric strength. For applications employing longer standoffs, materials that exhibit minimal performance variability and lower discharge currents under negative polarity are paramount for achieving enhanced system reliability

The study highlights the critical influence of gap length and impulse polarity on the surface dielectric performance of insulating standoffs under lightning impulse voltages. Positive polarity generally enhances flashover withstand capability, while negative polarity introduces greater variability, particularly in longer standoffs. These insights underscore the importance of tailored design and material selection for standoffs in lightning protection systems, ensuring reliability across diverse operational conditions.

I have tested multiple voltage levels on different lengths of insulating standoffs, and noting that IEC 62035 lacks specific voltage classifications, we can't solely rely on maximum discharge current for categorization. Instead, considering a 95% flashover probability ($U_{95}$) and the corresponding maximum discharge current, we can classify insulating standoffs for different Lightning Protection Levels (LPL) based on their performance.

Table 7. 1 Classification Of insulating based on LPL

| **Length of Insulating Standoffs** | **Lightning Protection Level** |
|---|---|
| 75cm | LPL-1 |
| 50cm | LPL-2 |
| 25cm | LPL-3/4 |

# CHAPTER EIGHT: SUGGESTION FOR FURTHER RESEARCH

The results obtained from this laboratory thesis have yielded conclusions of considerable importance, yet they underscore the necessity for continued and expanded research. While the current study provides a foundational understanding, it is evident that a more comprehensive investigation is warranted to fully elucidate the subject matter. Specifically, the scope of future research should encompass a detailed examination of the impacts of environmental factors. Crucially, the experimental evaluation of the effects of pollution, humidity, and varying atmospheric conditions is paramount. These elements are known to significantly influence electrical behavior, and therefore their inclusion is essential for a more complete and accurate understanding of the observed phenomena.

Future research could look into protective coatings, insulation methods, or material improvements to increase flashover resist based on the flashover likelihood curves. Investigations into surface treatments or field-grading techniques may provide workable answers for improving standoffs performance when exposed to high voltage. Future research should examine the effects of sustained electrical stress and frequent lightning discharges on material deterioration, mechanical integrity, and electrical characteristics over time in order to evaluate long-term reliability.

Further research should delve into the impact of various waveform parameters, such as rise time and peak value, on flashover characteristics. Studying the dielectric strength of standoffs of different materials will enable the selection of optimal materials for specific applications. Research should explore the long-term performance of novel materials under various stress conditions, including electrical, thermal, and mechanical.

Studying the spark path during electrical discharge using camera and its correlation with electrical characteristics of the discharge provides valuable insights into the breakdown mechanism. Advanced imaging techniques and synchronized electrical measurements should be employed to capture the dynamics of the discharge process with high temporal and spatial resolution.

Flashover Modeling of insulating standoffs using ATP-EMTP offers a powerful tool for simulating and analysing the electrical behavior of these components. Future research should focus on validating and refining these models using experimental data, enabling the

accurate prediction of flashover performance under complex operating conditions. This multifaceted approach to research will ultimately contribute to the development of more robust and reliable insulating standoffs for future power systems.

## REFERENCE


[1] "IEC 60060-1:2010, High Voltage Test Techniques-Part 1: General definitions and test requirements.

[2] *Lightning protection guide*. Dehn + Söhne, 2014.

[3] *ICPADM 2015: 2015 IEEE 11th International Conference on the Properties and Applications of Dielectric Materials: 19-22 July, 2015, University of New South Wales, Sydney, Australia*. IEEE, 2015.

[4] P. N Mikropoulos, Lightning Protection Systems, Thessaloniki, 2009."

[5] *IEEE CMD2012: Proceedings of 2012 IEEE International Conference on Condition Monitoring and Diagnosis: Bali-Indonesia, September 23-27, 2012*. IEEE, 2012.

[6] Equiptest, "Lightning Protection: What It Is and Why You Need It," Equiptest, [Online]. Available: https://www.equiptest.co.uk/lightning-protection-what-it-is-and-why-you-need-[Accessed: 25-12-2024].

[7] AT3W, "What are the effects of a lightning strike on structures and supply lines," AT3W Blog. [Online]. Available: https://at3w.com/en/blog/what-are-the-effects-of-a-lightning-strike-on-structures-and-supply-lines [Accessed: 27-12-2024].

[8] *Protection against lightning. Part 1, General principles = Protection contre la foudre. Partie 1, Principes généraux*. International Electrotechnical Commission, 2010.

[9] Ingesco, "Lightning Rod Function: How Does It Work," Ingesco, [online]. Available: https://www.ingesco.com/en/print/1575 [Accessed: 04-01-2025].

[10] Ingesco, "Down Conductor," Ingesco, [online]. Available: https://www.ingesco.com/en/products/down-conductor/. [Accessed: 04-01-2025].

[11] Meister International, "Standoff Insulator," [online]. Available: https://meisterintl.com/collections/standoff-insulator [Accessed: 10-01-2025].

[12] IEC, *INTERNATIONAL STANDARD NORME INTERNATIONALE Protection against lightning-Part 3: Physical damage to structures and life hazard Protection contre la foudre-Partie 3: Dommages physiques sur les structures et risques humains*. 2010. [Online]. Available: www.iec.ch

[13] H. Jin, I.-A. Tsekmes, J. Wu, A. R. Mor, and J. Smit, "The Effect of Frequency on the dielectric Strength of Epoxy Resin and Epoxy Resin based nanocomposites."

[14] Y. Zhang *et al.*, "Flashover performance test with lightning impulse and simulation analysis of different insulators in a 110 kV double-circuit transmission tower," *Energies (Basel)*, vol. 11, no. 3, Feb. 2018, doi: 10.3390/en11030659.

[15] P. N. Mikropoulos, P. T. Tsouris, and G. K. Aristotelous, “Experimental investigation of the lightning impulse flashover of a typical MV overhead line insulator,” in *2022 IEEE International Conference on High Voltage Engineering and Applications, ICHVE 2022*, Institute of Electrical and Electronics Engineers Inc., 2022. doi: 10.1109/ICHVE53725.2022.9961582.

[16] P. K. Samaras, E. T. Staikos, Z. G. Datsios, P. N. Mikropoulos, T. E. Tsovilis, and N. D. Kokkinos, “Evaluation of the Electric Stress on an Insulating Down-Conductor Caused by Lightning Strikes through ATP-EMTP Simulations,” in *2023 IEEE Industry Applications Society Annual Meeting, IAS 2023*, Institute of Electrical and Electronics Engineers Inc., 2023. doi: 10.1109/IAS54024.2023.10407000.

[17] Aristotelous George Petros Tsouris, “Experimental investigation of the flashover characteristics of typical medium-voltage line insulators under lightning impulse voltages.,” 2020.

[18] R. Brocke and O. Beierl, “Influence of humidity and pollution on the dielectric strength of components used in Isolated LPS,” in *2014 International Conference on Lightning Protection, ICLP 2014*, Institute of Electrical and Electronics Engineers Inc., Dec. 2014, pp. 351–358. doi: 10.1109/ICLP.2014.6973147.

[19] *Lightning parameters for engineering applications. 549*. CIGRE, 2013.

[20] *ICEPE 2018: 2nd International Conference on Energy, Power and Environment: Theme: Towards Smart Technology: ICEPE-2018: June 1-2, 2018, venue: State Convention Center (Pine Wood Hotel Annex) European Ward, Rita Road, Shillong, Meghalaya 793001*. IEEE, 2018.

[21] D. I. Kovalev, E. M. Voronkova, and D. V. Golubev, “Evaluation of the dielectric strength of the insulation of innovative busbar conductors with a voltage class of 6 (10) kV,” in *IOP Conference Series: Earth and Environmental Science*, IOP Publishing Ltd, Feb. 2022. doi: 10.1088/1755-1315/990/1/012047.

[22] Pereira, M.G., Freitas, M.A.V. and da Silva, N.F. (2011) The Challenge of Energy Poverty: Brazilian Case Study. Energy Policy, 39, 167-175. http://dx.doi.org/10.1016/j.enpol.2010.09.0

[23] G. N. Alexandrov and Y. A. Gerasimov, “SWITCHING AND LIGHTNING SURGE DIELJtCPRIC STRENGTH OF UHV INSULATING SUSPENSION SETS.”

[24] P. N. Mikropoulos, Laboratory Exercises inHigh Voltage Technology,

Thessaloniki,08.

[25] John. Kuffel and Peter. Kuffel, *High Voltage Engineering Fundamentals, 2nd Edition*. Newnes, 2000.

[26] Karafyllas Athanasios, “Experimental investigation of the dielectric behaviour of rod-rod and rod-plane air gaps under Lightning Impulse voltages.,” AUTH, 2016.

[27] V. T. Kontargyri, I. F. Gonos, I. A. Stathopoulos, and A. M. Michaelides, “Simulation of the electric field on high voltage insulators using the finite element method,” in *12th Biennial IEEE Conference on Electromagnetic Field Computation, CEFC 2006*, IEEE Computer Society, 2006, p. 373. doi: 10.1109/CEFC-06.2006.1633163.

[28] O. Ghermoul, H. Benguesmia, and L. Benyettou, “FINITE ELEMENT MODELING FOR ELECTRIC FIELD AND VOLTAGE DISTRIBUTION ALONG THE CAP AND PIN INSULATORS UNDER POLLUTION,” *Diagnostyka*, vol. 24, no. 2, 2023, doi: 10.29354/diag/159517.

[29] E. Nicolopoulou, V. T. Kontargyri, and I. A. Stathopulos, “ELECTRIC FIELD AND VOLTAGE DISTRIBUTION AROUND COMPOSITE INSULATORS,” 2011. [Online]. Available: https://www.researchgate.net/publication/229441111

[30] H. Huang, B. N. Hoffman, and S. G. Demos, “Three-dimensional modeling of electric-field enhancement in multilayer dielectric gratings arising from inadvertent flaws,” *Opt Express*, vol. 32, no. 8, p. 14211, Apr. 2024, doi: 10.1364/oe.506111.

# APPENDIX A: PUBLICATION NOTIFICATION

Gmail

Gyanendra Kurmi <kurmigyanendra321@gmail.com>

**[IOEGC16] Editor Decision**

1 message

**Suwarna Lingden** <conference-noreply@ioe.edu.np> 28 March 2025 at 23:05
To: Gyanendra Kumar Kurmi <kurmigyanendra321@gmail.com>, Basanta Kumar Gautam <basanta.gautam@pcampus.edu.np>

Gyanendra Kumar Kurmi, Basanta Kumar Gautam:

We are pleased to inform you that your manuscript titled "Gyanendra Kumar Kurmi Experimental Investigation of the dielectric strength of the insulating standoffs of electrically insulated lightning protection system under standard lightning impulse voltages" submitted to 16th IOE Graduate Conference is **Accepted** for presentation in the Conference as well as inclusion in the Peer-Reviewed Proceedings. Please note that inclusion in hard copy proceedings is contingent upon your timely response to further edits, if any, during the publication process.

With Warm Regards,
IOEGC-16 Editorial Team

**IOE Graduate Conference**
**[Placeholder for Publication Information]**

# Experimental Investigation of the dielectric strength of the insulating standoffs of electrically insulated lightning protection system under standard lightning impulse voltages

Gyanendra Kumar Kurmi a, Basanta Kumar Gautam [b],

[a,b] *Department of Electrical Engineering, Pulchowk Campus, Institute of Engineering, Tribhuvan University, Nepal*
[a] 079mspse010.gyanendra@pcampus.edu.np,

**Abstract**
Electrically insulated lightning protection systems (LPS) utilize insulating standoffs and insulated conductors to maintain the required separation distance from grounded objects. This paper investigates the dielectric strength of insulating standoffs in electrically insulated lightning protection systems (EILPS) under standard lightning impulse voltages. These standoffs are crucial for protecting structures, electrical equipment, and personnel from lightning strikes. The study aims to assess their ability to maintain insulation properties during real-world lightning events. The dielectric strength of these standoffs is influenced by factors such as material properties, geometry, environmental conditions, and applied voltage waveforms. By testing the dielectric strength of these standoffs, it is possible to minimize the risk of failure and ensure that the system remains functional in the event of a lightning strike. This paper presents laboratory experiments to assess the effect of polarity on 25 cm standoffs under standard lightning impulse voltage (1.2/50 µs) conditions, and analyze experimental data to predict breakdown voltage, discharge current, and flashover time.

**Keywords**
Insulating standoffs, flashover, Lightning impulse voltage, Electrically insulated protection system, dielectric strength

## 1. Introduction

Lightning strikes pose a significant threat to electrical infrastructure, potentially leading to power outages, equipment damage, and safety hazards. A lightning protection system's purpose is to shield buildings from mechanical or electrical fire damage and prevent injuries or fatalities to occupants[1]. Electrically insulated lightning protection systems (EILPS) are designed to mitigate the impact of lightning strikes by providing a safe path for the lightning current to flow to the ground through down conductors connected to the air termination and earth termination centres. Insulating stand-offs are typically structured with a high-dielectric strength core material, i.e., a polymer or silicone composite designed to withstand extreme voltages and transient surges. The structure of stand-offs typically consists of three primary sections, as shown in Figure 1, a base for mounting, an insulating column and fasteners. The base and the fastener are often constructed from metal to hold the structure and down conductors, respectively. The insulating column is made from epoxy resin, which elevates the component being mounded away from the conductive base, preventing electrical current flow.

**Figure 1:** 25cm Insulating standoff

Insulating stand-offs are essential in EILPS to maintain electrical insulation between live conductors and grounded structures. They support and isolate lightning protection system components, preventing conductors from becoming grounded and thus preventing fires or system failures. These stand-offs ensure proper dissipation of lightning energy and maintain separation from structures and grounded objects[2]. The National Engineering Laboratory conducted lightning impulse flashover tests on

composite and glass insulators, recording the discharge path and 50% impulse flashover voltage, and calculating electric fields using the finite element method[3]. The behaviour of insulating materials under lightning impulse conditions differs significantly from that under stable or gradually increasing voltages. By ensuring that materials can withstand sudden spikes in voltage and lightning strikes, testing under lightning impulse conditions reduces the chance of system failure [4].Therefore, accurately predicting the flashover performance of insulating stand-offs under lightning surge is of great importance for insulation coordination. Several factors affect the lightning flashover of insulating stand-offs, including polarity, wave shape, geometrical and electrical properties, and atmospheric and environmental conditions.[5]. For testing stand-offs, the crossed-conductor electrode arrangement is employed, which serves as a reference air gap[6].Subsequent studies further investigated the dielectric behaviour of crossed-conductor air gaps and proposed test procedures for determining the equivalent separation distance of insulating components[7][8]. The latter is crucial for the reliability of electrically insulated LPS. However, in service, the stand-offs are stressed by positive and negative standard fast front over-voltages related to lightning current, and there is a lack of adequate experimental investigation on the flashover characteristics of insulating stand-offs under this condition. Thus, for a better understanding of the flashover mechanism of insulating stand-offs, the lightning impulse discharge characteristics of 25 cm stand-offs are experimentally investigated. Based on measurements of the discharge current, the effects of lightning impulse voltage polarity and amplitude on discharge inception are discussed

## 2. Experimental Arrangement

Standard lightning impulse voltage (1.2/50$\mu$s) of both polarities was applied to typical 25 cm insulating stand-offs using a 10-stage Marx Generator 1MV/7KJ (Figure 2). The stand-offs were placed on an aluminium metal plate (100 cm x 100 cm) at a height of 50 cm from the ground of the AUTH laboratory in Thessaloniki. The applied impulse voltage and discharge current were recorded (Figure 2) using a capacitor divider of the Marx generator and a Pearson 301X current transformer, respectively, along with a LeCroy WR64Xi oscilloscope. Disruptive discharge was conducted by applying the multilevel test method according to IEC 60060-1 STD. In applying the method, a voltage of constant value, (voltage level) is imposed on the standoff several times at each of the voltage levels. From the ratio of the number of flashover observed to the number of impositions (n), the determined voltage per level, and the flashover probability is obtained. A line of the best fit is drawn, representing the overall trends of the data. $U_{50}$ is determined at z=0 and $\sigma$ is deterimend at z=1. Breakdown probability distributions were thus produced using a minimum of twenty voltage applications at various voltage levels that increased in amplitude; the related breakdown characteristics, including breakdown percentage and duration, as well as discharge current, were measured. The stand-offs were further overstressed by applying impulse voltages at levels significantly higher than those corresponding to 100% flashover probability. This allowed for an examination of how the figure's distributions of the discharge characteristics were affected by an increase in the applied voltage's amplitude. The overall experimental setup of the experiment is shown in Figure 2 and Figure 3 shows the flashover on the insulating stand-offs, respectively.

**Figure 2:** Overall Experimental setup

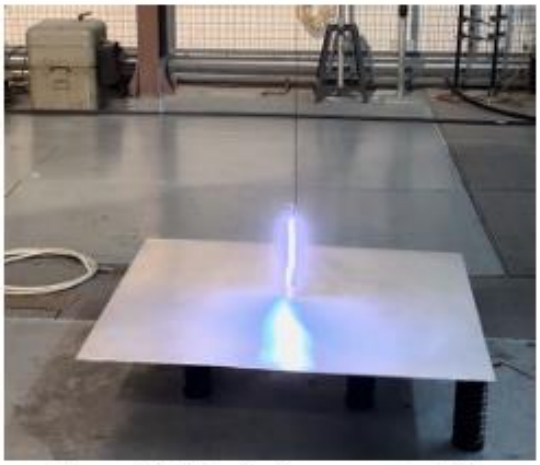

**Figure 3:** Surface flashover over standoffs

Experiments were carried out under ambient atmospheric conditions (T=16.75 $^{0}$C, P=761.50 mmHg, H=11.15 gm$^{-3}$)

## 3. RESULT AND DISCUSSION

Through the oscillograph monitoring of the applied voltage and discharge current with an oscillograph, salient discharge characteristics of the identified stages of the breakdown process were acquired, as seen in Figure 4.

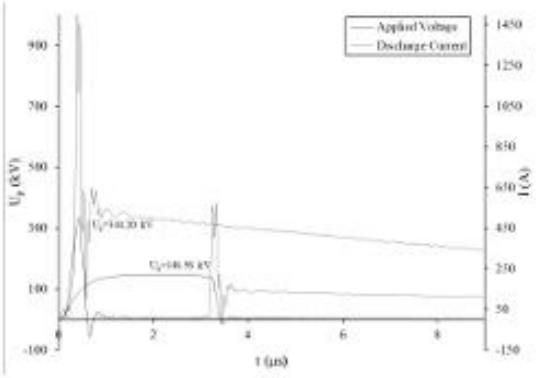


**Figure 4:** Applied voltage and discharge current oscillographs records

**Table 1:** $U_{50}$ and $\sigma$ for positive and negative polarity

| Polarity | $U_{50}$ (%) | $\sigma$ (%) |
|---|---|---|
| Positive | 151.20 | 8.59 |
| Negative | 146.78 | 7.74 |

### 3.1 Flashover Probability curve

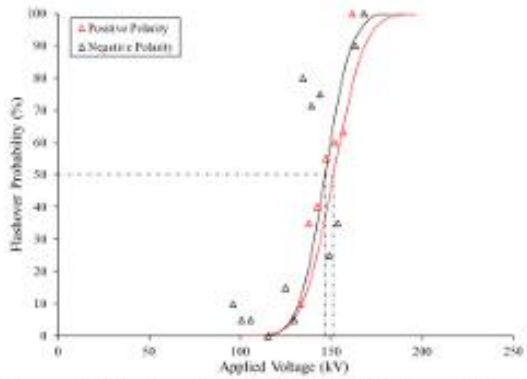


**Figure 5:** Flashover Probability distribution of 25 cm insulating standoff curve

The Positive polarity curve is located to the right of the negative polarity curve, indicating that a higher applied voltage is needed for the same flashover probability with a positive impulse. The steep curve suggests a rapid increase in flashover probability with increasing voltage, suggesting a less dispersed breakdown mechanism. The positive polarity curve is located to the right of the negative polarity curve, suggesting a slightly slower increase in flashover probability. Negative surface charges on the dielectric material strengthen the applied field, whereas positive charges under positive polarity often counteract it. Negative polarity also allows electrons to traverse a longer path in the high-field region, promoting efficient electron avalanches and faster streamer propagation as the cathode continuously supplies electrons.

### 3.2 Maximum current-flashover voltage curve, $I_p$-$U_p$

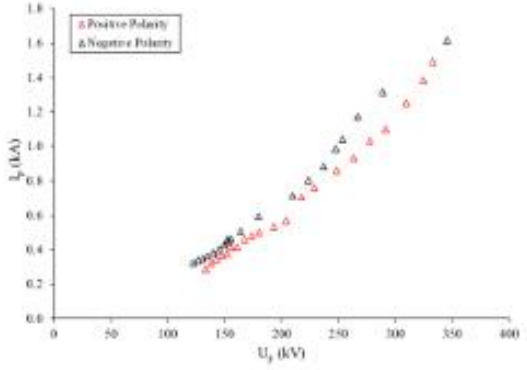


**Figure 6:** Maximum current-flashover voltage curve

The negative polarity curve shows a higher maximum current under negative polarity-imposed voltage for insulating stand-offs. Both positive and negative data sets follow a liner trend, suggesting a direct correlation between flashover voltage and maximum current. Positive data points are tightly clustered along a straight line, while negative data show a slightly steeper trend line. In general, maximum current tends to be higher for negative polarity compared to positive polarity for a given flashover voltage.

### 3.3 Maximum current- applied Voltage curves, $I_p$-$U_{app}$

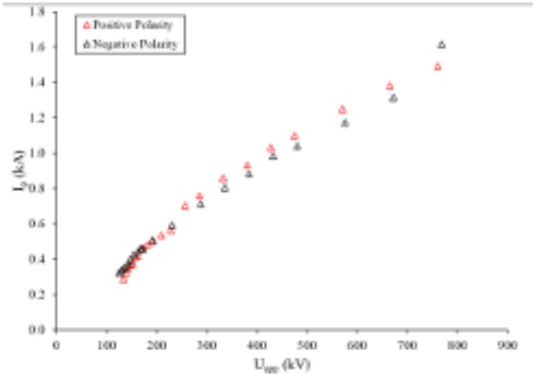


**Figure 7:** Maximum current with applied voltage curve

From the figures above, it can be seen that the curves are relatively close for the two polarities, while they may also overlap.

### 3.4 Flashover voltage and time to flashover characteristics curves, $U_p$-$t_f$

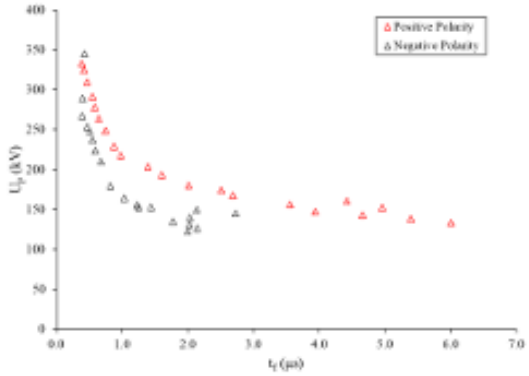


**Figure 8:** Flashover voltage with time to flashover curve

It becomes clear that the effect of polarity is more important for lower voltage levels, as the negative-polarity curve appears lower than the positive one. This means that for the same breakdown time, the breakdown voltage is lower under negative polarity applied voltages and suggests that standoffs are more susceptible to flashover under negative polarity, indicating better withstand capability compared to negative impulse. For higher voltages and shorter decay times, the effect of polarity on the voltage-time ($U_p$-$t_f$)curves is noticeably smaller, as the curves tend to coincide. For both polarities, there's a general trend of decreasing flashover voltage as the flashover time increases.

### 3.5 Spark conduction curves based on breakdown voltage per level, $I_p/U_p$ – $U_{app}$

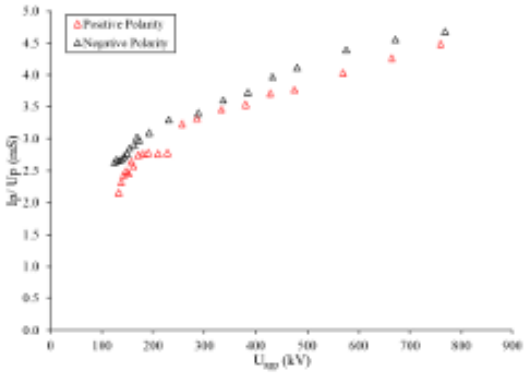


**Figure 9:** Spark conduction with applied voltage curve

The negative polarity curve shows a higher conductance ($I_p/U_{app}$)across most of the applied voltage range, especially at lower voltages. This implies that under negative impulses, the material conducts more readily for a given voltage. The positive polarity curve exhibits lower conductance compared to negative polarity, especially at lower voltages. This indicates that the material is less conductive under positive impulses.

### 3.6 Spark Conduction Curves Based on Voltage at Peak Current per flashover Voltage Level, $I_p/U_p$, $I_p - U_{app}$

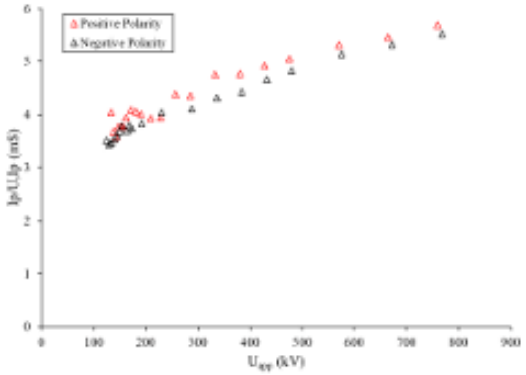


**Figure 10:** Spark conduction at maximum current with applied voltage curve

The difference is relatively small. Flashover voltage might be slightly lower for positive polarity due to the slightly higher conductance at lower voltages.

## 4. Conclusion

This paper evaluates the dielectric strength of insulating standoffs, focusing on the effects of positive and negative lightning impulse polarity on 25 cm standoffs. The results indicate that negative polarity yields a lower $U_{50}$ than positive polarity. This highlights the importance of considering the effects of polarity in insulation coordination and design. Analysis of the $U_{p\text{-}t}$ (presumably voltage time to flashover) curves reveals that at higher flashover voltage levels, the curves tend to converge for all standoff. The effect of polarity is more pronounced at lower voltage levels, where the negative polarity curve lies below the positive one. Further investigation is needed to determine the dielectric strength of insulating standoffs under various conditions, including non-standard lightning impulse voltages, different environmental conditions, varying geometries, and indirect lightning impulses.

## Acknowledgments

This work was supported by the School of Electrical Engineering and computer engineering (High Voltage Laboratory), Aristotle University of Thessaloniki, Greece.

## References

[1] Bojan Franc, Ivo Uglešić, and Božidar Filipović-Grčić. Application of lightning location system data for designing the external lightning protection system. In *CIGRE International Colloquium on Lightning and Power systems*, 2014.

[2] Pavlos K. Samaras, Evangelos T. Staikos, Zacharias G. Datsios, Pantelis N. Mikropoulos, Thomas E. Tsovilis, and Nikolaos D. Kokkinos. Evaluation of the electric stress on an insulating down-conductor caused by lightning strikes through atp-emtp simulations. In *2023 IEEE Industry Applications Society Annual Meeting, IAS 2023*. Institute of Electrical and Electronics Engineers Inc., 2023.

[3] Zijian Li, Yao Yao, Xueming Zhou, Zhiqiang Feng, Jianjin Fu, and Yi Kan. Research on insulator lightning flashover arc- establishing model. In *2023 4th International Conference on Power Engineering, ICPE 2023*, pages 92–97. Institute of Electrical and Electronics Engineers Inc., 2023.

[4] Ralph Brocke and Ottmar Beierl. Probability of insulation failures in isolated lps according to the used insulation technologies. In *2011 International Symposium on Lightning Protection*, pages 31–35. IEEE, 2011.

[5] Ralph Brocke and Ottmar Beierl. Influence of humidity and pollution on the dielectric strength of components used in isolated lps. In *2014 International Conference on Lightning Protection (ICLP)*, pages 351–358. IEEE, 2014.

[6] Ottmar Beierl, Ralph Brocke, and Claudia Rother. Simplified electrical test procedures for components of isolated lps. In *2010 30th International Conference on Lightning Protection (ICLP)*, pages 1–9, 2010.

[7] Ottmar Beierl, Ralph Brocke, and Claudia Rother. Simplified electrical test procedures for components of isolated lps. In *2010 30th International Conference on Lightning Protection, ICLP 2010*. Institute of Electrical and Electronics Engineers Inc., 2 2017.

[8] Fridolin H Heidler and Wolfgang J Zischank. Necessary separation distances for lightning protection systems—iec 62305-3 revisited. *X SIPDA*, 91103, 2009.

# APPENDIX B: PLAGIARISM REPORT



## Gyanendra Kumar Kurmi

### Experimental Investigation of the Dielectric Strength of the Insulating Stand-offs of Electrically I

Tribhuvan University

**Document Details**

Submission ID
trn:oid:::3117:450693452

Submission Date
Apr 20, 2025, 3:18 PM GMT+5:45

Download Date
Apr 20, 2025, 3:19 PM GMT+5:45

File Name
Experimental Investigation of the Dielectric Strength of the Insulating Stand-offs of Electrically I....pdf

File Size
4.8 MB

76 Pages

18,815 Words

102,219 Characters

iThenticate Page 1 of 83 - Cover Page Submission ID trn:oid:::3117:450693452

# 9% Overall Similarity

The combined total of all matches, including overlapping sources, for each database.

## Match Groups

- 152 Not Cited or Quoted 9%
  Matches with neither in-text citation nor quotation marks
- 0 Missing Quotations 0%
  Matches that are still very similar to source material
- 0 Missing Citation 0%
  Matches that have quotation marks, but no in-text citation
- 0 Cited and Quoted 0%
  Matches with in-text citation present, but no quotation marks

## Top Sources

- 6% Internet sources
- 6% Publications
- 0% Submitted works (Student Papers)

## Integrity Flags

**0 Integrity Flags for Review**

No suspicious text manipulations found.

Our system's algorithms look deeply at a document for any inconsistencies that would set it apart from a normal submission. If we notice something strange, we flag it for you to review.

A Flag is not necessarily an indicator of a problem. However, we'd recommend you focus your attention there for further review.

iThenticate Page 2 of 83 - Integrity Overview Submission ID trn:oid:::3117:450693452

## Match Groups

- 152 Not Cited or Quoted 9%
  Matches with neither in-text citation nor quotation marks
- 0 Missing Quotations 0%
  Matches that are still very similar to source material
- 0 Missing Citation 0%
  Matches that have quotation marks, but no in-text citation
- 0 Cited and Quoted 0%
  Matches with in-text citation present, but no quotation marks

## Top Sources

6% Internet sources
6% Publications
0% Submitted works (Student Papers)

## Top Sources

The sources with the highest number of matches within the submission. Overlapping sources will not be displayed.

| | | |
|---|---|---|
| 1 | Internet | ikee.lib.auth.gr <1% |
| 2 | Internet | www.slideshare.net <1% |
| 3 | Internet | hdl.handle.net <1% |
| 4 | Publication | Yaqi Zhang, Licheng Li, Yongxia Han, Yaoxuan Ruan, Jie Yang, Hansheng Cai, Gan... <1% |
| 5 | Internet | kingsmillindustries.com <1% |
| 6 | Internet | www.dehn-international.com <1% |
| 7 | Internet | www.pts.ir <1% |
| 8 | Publication | Pradipta Ghosh, Biswajit Chakraborty, Sovan Dalai, Saibal Chatterjee. "Simulation... <1% |
| 9 | Publication | Elya B. Joffe, Kai-Sang Lock. "Grounds for Grounding", Wiley, 2023 <1% |
| 10 | Publication | N S Othman, M N K H Rohani, W A Mustafa, C L Wooi et al. "An Overview on Overv... <1% |

| | | |
|---|---|---|
| 11 | Publication | Y.A. Gerasimov. "Switching and lightning surge dielectric strength of UHV insulati... <1% |
| 12 | Publication | Hani Benguesmia, Nassima M'ziou, Ahmed Boubakeur. "Simulation of the potenti... <1% |
| 13 | Publication | E. Kuffel, W.S. Zaengl, J. Kuffel. "Overvoltages, testing procedures and insulation c... <1% |
| 14 | Publication | Pantelis N. Mikropoulos, Petros P. Tsouris, Michalis K. Angeli, Fotini C. Knai. "Expe... <1% |
| 15 | Publication | Pavlos K. Samaras, Evangelos T. Staikos, Zacharias G. Datsios, Pantelis N. Mikropo... <1% |
| 16 | Publication | P. N. Mikropoulos, P. T. Tsouris, G. K. Aristotelous. "Experimental investigation of ... <1% |
| 17 | Internet | www.researchgate.net <1% |
| 18 | Internet | repositories.nust.edu.pk <1% |
| 19 | Publication | Pantelis N. Mikropoulos, Petros P. Tsouris. "Modelling of the Positive Lightning I... <1% |
| 20 | Publication | Kurt Feser. "Transient Behaviour of Damped Capacitive Voltage Dividers of Some ... <1% |
| 21 | Publication | Paul Hoole, Samuel Hoole. "Lightning Engineering: Physics, Computer-based Test... <1% |
| 22 | Publication | Yaqi ZHANG, Yongxia HAN, Jie YANG, Yaoxuan RUAN, Yifan LIAO, Gang LIU, Lei JIA... <1% |
| 23 | Publication | B. Thangabalan, Supriyo Das. "The Effect of Lightning on Insulator Flashover Char... <1% |
| 24 | Publication | Nicolopoulou, Eleni, Ioannis Stathopulos, and Ioannis Gonos. "Experimental inves... <1% |

| | | |
|---|---|---|
| 25 | Publication | |
| "Sustainable Energy and Technological Advancements", Springer Science and Bus... | | <1% |
| 26 | Publication | |
| E KUFFEL. "Generation of high voltages", High Voltage Engineering Fundamentals... | | <1% |
| 27 | Internet | |
| wiredspace.wits.ac.za | | <1% |
| 28 | Internet | |
| ir.library.oregonstate.edu | | <1% |
| 29 | Internet | |
| ntnuopen.ntnu.no | | <1% |
| 30 | Publication | |
| He, Li. "Source Strength Impact Analysis on Insulator Flashover under Contamina... | | <1% |
| 31 | Publication | |
| Nicolopoulou, E. P., I. N. Ztoupis, E. Karabetsos, I. F. Gonos, and I. A. Stathopulos. ... | | <1% |
| 32 | Internet | |
| pdfcoffee.com | | <1% |
| 33 | Internet | |
| acikbilim.yok.gov.tr | | <1% |
| 34 | Internet | |
| researcharchive.vuw.ac.nz | | <1% |
| 35 | Internet | |
| www.adhesivesmanufacturer.com | | <1% |
| 36 | Internet | |
| steamradio.com | | <1% |
| 37 | Publication | |
| An Introduction to Lightning, 2015. | | <1% |
| 38 | Internet | |
| www.win.tue.nl | | <1% |

| | | |
|---|---|---|
| 39 | Publication | |
| Vasily Y. Ushakov. "Insulation of High-Voltage Equipment", Springer Science and ... | | <1% |
| 40 | Internet | |
| eprints.utar.edu.my | | <1% |
| 41 | Internet | |
| pure.tue.nl | | <1% |
| 42 | Publication | |
| "Lightning", Springer Science and Business Media LLC, 2021 | | <1% |
| 43 | Publication | |
| Rai, Vijaya, Kamlesh Pandey, and Komal Wadhwa. "Designing of multistage impul... | | <1% |
| 44 | Internet | |
| erewhon.superkuh.com | | <1% |
| 45 | Internet | |
| ir.knust.edu.gh | | <1% |
| 46 | Internet | |
| www.lisleapex.com | | <1% |
| 47 | Internet | |
| www.mdpi.com | | <1% |
| 48 | Internet | |
| www.orosha.org | | <1% |
| 49 | Publication | |
| S. Wada. "Analysis of breakdown mechanisms of long air gaps under positive lon... | | <1% |
| 50 | Publication | |
| Albrecht, Peter. "Strategy for emissions - and instability prevention in gas turbine... | | <1% |
| 51 | Publication | |
| FELCZAK MARIOLA. "Threshold flexoelectric deformations in homeotropic nemati... | | <1% |
| 52 | Publication | |
| P. N. Mavroidis, P. N. Mikropoulos, C. A. Stassinopoulos. "Discharge characteristic... | | <1% |

| | | |
|---|---|---|
| 53 | Publication | |
| Pradipta Ghosh, Arup Kumar Das, Sovan Dalai, Saibal Chatterjee. "The effects of n... | | <1% |
| 54 | Publication | |
| Xiaolong Li, Chen Cao, Xin Lin. "Influence of conducting particle on DC flashover c... | | <1% |
| 55 | Internet | |
| core.ac.uk | | <1% |
| 56 | Internet | |
| d-nb.info | | <1% |
| 57 | Internet | |
| researchspace.ukzn.ac.za | | <1% |
| 58 | Internet | |
| www.geotechnicaldivision.co.za | | <1% |
| 59 | Internet | |
| www.ijert.org | | <1% |
| 60 | Publication | |
| "Handbook of Self-Cleaning Surfaces and Materials", Wiley, 2023 | | <1% |

# ANNEX

## Sample Experimental Data

| Date | Levels | Pressure (mm Hg) | Temperature (°C) | Absolute humidity h (gr/m³) | δ | κ | Polarity | $t_{max}$ | $R_1$ (Ω) | $R_{tr}$ (Ω) | $R_2$ (Ω) | $C_T$ (pF) | $C_C$ (μF) | Stages | η (theor) | η (meas) |
|---|---|---|---|---|---|---|---|---|---|---|---|---|---|---|---|---|
| Sunday, December 1, 2024 | | 760.50 | 16.00 | 10.33 | 1.01 | 0.99 | Positive | 2.15 | 34.20 | 1500.00 | 511.00 | 200.00 | 0.14 | 10.00 | 0.9583 | 0.9600 |

| No. | $U_R$ (kV$_{RMS}$) | Calculations | | | | | | | Measurements | 1 | 2 | 3 | 4 | 5 | 6 | 7 | 8 | 9 | 10 | 11 | 12 | 13 | 14 | 15 | 16 | 17 | 18 | 19 | 20 |
|---|---|---|---|---|---|---|---|---|---|---|---|---|---|---|---|---|---|---|---|---|---|---|---|---|---|---|---|---|---|
| 1 | 61.50 | P (%) | $U_p$ (V) | $t_i$ (μs) | $U_i$ (V) | $t_b$ (μs) | $U_{i,b}$ (V) | $I_p$ (A) | $t_b$ (μs) | | | | | | | | | | 12.79 | | | | | | | | | | |
| | | 5.00 | 379.05 | #DIV/0! | -4.86 | 12.79 | 248.00 | 1240.00 | $U_p$ (V) | 379.00 | 380.00 | 379.00 | 379.00 | 379.00 | 379.00 | 379.00 | 379.00 | 379.00 | 379.00 | 379.00 | 379.00 | 379.00 | 379.00 | 379.00 | 379.00 | 379.00 | 379.00 | 379.00 |
| | | $U_{R,m}$ (kV) | $\sigma_{UP}$ (%) | $\sigma_{ti}$ (%) | $\sigma_{Ui}$ (%) | $\sigma_{tb}$ (%) | $\sigma_{U,b}$ (%) | $\sigma_{Ip}$ (%) | $I_p$ (A) | | | | | | | | | | 1240.00 | | | | | | | | | | |
| | | 590.40 | 0.06 | #DIV/0! | -447.21 | #DIV/0! | #DIV/0! | #DIV/0! | $U_{i,b}$ (V) | | | | | | | | | | 248.00 | | | | | | | | | | |
| | | 591.29 | | | | | | | $t_i$ (μs) | | | | | | | | | | | | | | | | | | | | |
| | | η | 0.9614 | | | | | | $U_i$ (V) | 0.00 | 0.00 | 0.00 | 0.00 | 0.00 | 0.00 | 0.00 | 0.00 | 0.00 | -97.16 | 0.00 | 0.00 | 0.00 | 0.00 | 0.00 | 0.00 | 0.00 | 0.00 | 0.00 |
| 2 | 62.00 | P (%) | $U_p$ (V) | $t_i$ (μs) | $U_i$ (V) | $t_b$ (μs) | $U_{i,b}$ (V) | $I_p$ (A) | $t_b$ (μs) | 3.95 | | 3.60 | 9.30 | 6.24 | | | 6.92 | 4.45 | | 11.15 | | | | | | | 6.13 | | |
| | | 40.00 | 380.75 | #DIV/0! | -20.54 | 6.47 | 271.00 | 1353.75 | $U_p$ (V) | 382.00 | 379.00 | 383.00 | 379.00 | 379.00 | 380.00 | 380.00 | 380.00 | 382.00 | 380.00 | 380.00 | 382.00 | 382.00 | 382.00 | 382.00 | 382.00 | 382.00 | 379.00 | 380.00 | 380.00 |
| | | $U_{R,m}$ (kV) | $\sigma_{UP}$ (%) | $\sigma_{ti}$ (%) | $\sigma_{Ui}$ (%) | $\sigma_{tb}$ (%) | $\sigma_{U,b}$ (%) | $\sigma_{Ip}$ (%) | $I_p$ (A) | 1460.00 | | 1460.00 | 1325.00 | 1315.00 | | | 1345.00 | 1390.00 | | 1210.00 | | | | | | | 1325.00 | | |
| | | 595.20 | 0.35 | #DIV/0! | -138.85 | 40.90 | 5.89 | 6.10 | $U_{i,b}$ (V) | 292.00 | | 290.00 | 265.00 | 267.00 | | | 269.00 | 278.00 | | 242.00 | | | | | | | 265.00 | | |
| | | 593.94 | | | | | | | $t_i$ (μs) | | | | | | | | | | | | | | | | | | | | |
| | | η | 0.9580 | | | | | | $U_i$ (V) | -32.11 | 0.00 | -29.36 | -72.91 | -49.84 | 0.00 | 0.00 | -55.08 | -36.03 | 0.00 | -86.33 | 0.00 | 0.00 | 0.00 | 0.00 | 0.00 | 0.00 | -49.06 | 0.00 | 0.00 |
| 3 | 62.50 | P (%) | $U_p$ (V) | $t_i$ (μs) | $U_i$ (V) | $t_b$ (μs) | $U_{i,b}$ (V) | $I_p$ (A) | $t_b$ (μs) | | | 6.50 | | 4.06 | | 10.82 | | 3.56 | | | | | | | | | | | |
| | | 20.00 | 383.70 | #DIV/0! | -9.97 | 6.23 | 276.25 | 1381.25 | $U_p$ (V) | 383.00 | 383.00 | 387.00 | 383.00 | 386.00 | 388.00 | 384.00 | 384.00 | 383.00 | 383.00 | 383.00 | 383.00 | 383.00 | 383.00 | 383.00 | 383.00 | 383.00 | 383.00 | 383.00 | 383.00 |
| | | $U_{R,m}$ (kV) | $\sigma_{UP}$ (%) | $\sigma_{ti}$ (%) | $\sigma_{Ui}$ (%) | $\sigma_{tb}$ (%) | $\sigma_{U,b}$ (%) | $\sigma_{Ip}$ (%) | $I_p$ (A) | | | 1375.00 | | 1450.00 | | 1230.00 | | 1470.00 | | | | | | | | | | | |
| | | 600.00 | 0.39 | #DIV/0! | -228.52 | 53.12 | 7.88 | 7.88 | $U_{i,b}$ (V) | | | 275.00 | | 290.00 | | 246.00 | | 294.00 | | | | | | | | | | | |
| | | 598.55 | | | | | | | $t_i$ (μs) | | | | | | | | | | | | | | | | | | | | |
| | | η | 0.9577 | | | | | | $U_i$ (V) | 0.00 | 0.00 | -92.32 | 0.00 | -33.27 | 0.00 | -84.59 | 0.00 | -29.26 | 0.00 | 0.00 | 0.00 | 0.00 | 0.00 | 0.00 | 0.00 | 0.00 | 0.00 | 0.00 | 0.00 |
| 4 | 63.00 | P (%) | $U_p$ (V) | $t_i$ (μs) | $U_i$ (V) | $t_b$ (μs) | $U_{i,b}$ (V) | $I_p$ (A) | $t_b$ (μs) | | | | | | | | | 7.60 | | | | | 8.83 | 5.11 | | | | | |
| | | 15.00 | 387.95 | #DIV/0! | -8.68 | 7.18 | 275.33 | 1376.67 | $U_p$ (V) | 388.00 | 388.00 | 388.00 | 388.00 | 388.00 | 388.00 | 388.00 | 388.00 | 387.00 | 388.00 | 388.00 | 388.00 | 388.00 | 390.00 | 386.00 | 388.00 | 388.00 | 388.00 | 388.00 | 388.00 |
| | | $U_{R,m}$ (kV) | $\sigma_{UP}$ (%) | $\sigma_{ti}$ (%) | $\sigma_{Ui}$ (%) | $\sigma_{tb}$ (%) | $\sigma_{U,b}$ (%) | $\sigma_{Ip}$ (%) | $I_p$ (A) | | | | | | | | | 1365.00 | | | | | 1365.00 | 1400.00 | | | | | |
| | | 604.80 | 0.18 | #DIV/0! | -250.28 | 26.41 | 1.47 | 1.47 | $U_{i,b}$ (V) | | | | | | | | | 273.00 | | | | | 273.00 | 280.00 | | | | | |
| | | 605.17 | | | | | | | $t_i$ (μs) | | | | | | | | | | | | | | | | | | | | |
| | | η | 0.9606 | | | | | | $U_i$ (V) | 0.00 | 0.00 | 0.00 | 0.00 | 0.00 | 0.00 | 0.00 | 0.00 | -61.26 | 0.00 | 0.00 | 0.00 | 0.00 | -70.52 | -41.84 | 0.00 | 0.00 | 0.00 | 0.00 | 0.00 |

## Flashover Probability Curve Data

| Breakdown Probability Curve | | | | | | |
|---|---|---|---|---|---|---|
| No. | Up,th (kV) | **P (%)** | Hm/a | Class | Condition | N/dist |
| 0 | 237.50 | 0 | 242.25 | | | 0.00 |
| 0 | 247.00 | 0 | 251.75 | | | 0.00 |
| 0 | 256.50 | 0 | 261.25 | | | 0.00 |
| 1 | 266.00 | 0 | 270.75 | 5.00 | 276.69 | 0.02 |
| 2 | 275.50 | 0 | 276.69 | 10.00 | 276.69 | 5.27 |
| 3 | 277.88 | 10 | 279.06 | 15.00 | 279.06 | 12.66 |
| 4 | 280.25 | 30 | 281.44 | 20.00 | 279.06 | 25.25 |
| 5 | 282.63 | 50 | 283.81 | 25.00 | 279.06 | 42.45 |
| 6 | 285.00 | 60 | 287.38 | 30.00 | 279.06 | 61.24 |
| 7 | 289.75 | 100 | 292.13 | 35.00 | 281.44 | 89.21 |
| 8 | 294.50 | 95 | 296.88 | 40.00 | 281.44 | 98.58 |
| 9 | 299.25 | 100 | 301.63 | 45.00 | 281.44 | 99.92 |
| 10 | 304.00 | 100 | 152.00 | 50.00 | 281.44 | 100.00 |
| | | | | 55.00 | 283.81 | |
| | | | | 60.00 | 283.81 | |
| | | | | 65.00 | 287.38 | |
| | | | | 70.00 | 287.38 | |
| | | | | 75.00 | 287.38 | |
| | | | | 80.00 | 287.38 | |
| | | | | 85.00 | 287.38 | |
| | | | | 90.00 | 287.38 | |
| | | | | 95.00 | 287.38 | |
| | | | | 100.00 | 296.88 | |
| | | | | Average If | 283.58 | |
| | | | | $\sigma_{if}$ (%) | 1.76 | |

## Summary of Results

| Result Condition | | | | | | | | | | | | | |
|---|---|---|---|---|---|---|---|---|---|---|---|---|---|
| No | Uo (kV) | P (%) | Up,th (kV) | Uinst,w (kV) | σUi(%) | $U_{I,w}$ (kV) | $\sigma_{UI}$ (%) | tb (μs) | σtb(%) | $U_{I,lp,w}$ (kV) | $\sigma_{U,Ip}$ (%) | $I_p$ (kA) | $\sigma_{Ip}$ (%) |
| 1 | 28.00 | 0 | 266.00 | 264.88 | 0.25 | 0.00 | #DIV/0! | #DIV/0! | #DIV/0! | #DIV/0! | #DIV/0! | #DIV/0! | #DIV/0! |
| 2 | 29.00 | 0 | 275.50 | 273.77 | 0.00 | 0.00 | #DIV/0! | #DIV/0! | #DIV/0! | #DIV/0! | #DIV/0! | #DIV/0! | #DIV/0! |
| 3 | 29.25 | 10 | 277.88 | 275.72 | 0.15 | -6.34 | -307.95 | 11.38 | 4.69 | 135.71 | 11.38 | 0.60 | 3.08 |
| 4 | 29.50 | 30 | 280.25 | 278.64 | 0.35 | -21.88 | -168.57 | 13.30 | 41.59 | 128.04 | 6.21 | 0.59 | 7.84 |
| 5 | 29.75 | 50 | 282.63 | 281.06 | 0.48 | -36.97 | -104.76 | 13.24 | 16.94 | 132.44 | 5.93 | 0.59 | 4.06 |
| 6 | 30.00 | 60 | 285.00 | 282.58 | 0.20 | -39.94 | -85.63 | 11.69 | 15.39 | 141.82 | 5.14 | 0.62 | 5.13 |
| 7 | 30.50 | 100 | 289.75 | 287.50 | 0.33 | -64.52 | -14.67 | 11.10 | 15.87 | 147.92 | 3.82 | 0.64 | 4.71 |
| 8 | 31.00 | 95 | 294.50 | 292.45 | 0.31 | -55.70 | -25.25 | 9.83 | 9.59 | 150.78 | 5.28 | 0.65 | 3.89 |
| 9 | 31.50 | 100 | 299.25 | 294.94 | 0.98 | -55.62 | -10.17 | 9.13 | 10.88 | 159.93 | 7.33 | 0.66 | 5.29 |
| 10 | 32.00 | 100 | 304.00 | 301.53 | 0.34 | -51.04 | -12.80 | 8.20 | 13.52 | 172.10 | 7.16 | 0.69 | 4.70 |
| 11 | 33.00 | 100 | 313.50 | 311.28 | 0.36 | -23.69 | -103.94 | 7.34 | 12.77 | 165.43 | 5.47 | 0.69 | 7.01 |
| 12 | 34.00 | 100 | 323.00 | 319.79 | 0.33 | -21.22 | -103.54 | 6.34 | 10.52 | 185.40 | 6.13 | 0.72 | 6.32 |
| 13 | 36.00 | 100 | 342.00 | 336.71 | 0.22 | -19.08 | -103.62 | 5.34 | 10.98 | 204.90 | 7.29 | 0.77 | 7.70 |
| 14 | 38.00 | 100 | 361.00 | 354.49 | 0.24 | -15.62 | -104.43 | 4.11 | 14.50 | 227.28 | 7.30 | 0.85 | 7.06 |
| 15 | 40.00 | 100 | 380.00 | 370.25 | 0.22 | -12.24 | -106.34 | 3.04 | 20.76 | 245.84 | 5.89 | 0.91 | 6.89 |
| 16 | 45.00 | 100 | 427.50 | 402.33 | 0.20 | -12.18 | -88.31 | 2.23 | 22.45 | 274.09 | 7.41 | 1.02 | 5.63 |
| 17 | 50.00 | 100 | 475.00 | 428.98 | 0.13 | -3.96 | -177.80 | 1.56 | 3.24 | 305.90 | 1.23 | 1.15 | 4.21 |
| 18 | 60.00 | 100 | 570.00 | 477.49 | 0.31 | -3.73 | -177.97 | 1.22 | 5.36 | 341.47 | 1.48 | 1.45 | 0.84 |
| 19 | 70.00 | 100 | 665.00 | 510.72 | 0.60 | -3.73 | -179.80 | 1.04 | 15.06 | 363.93 | 3.32 | 1.59 | 6.60 |
| 20 | | | | | | | | | | | | | |

## Characteristics Curve Table

| Table of Characterstics Curve | | | | | | | | | | |
|---|---|---|---|---|---|---|---|---|---|---|
| No | Uo (kV) | P (%) | $U_{p,th}$ (kV) | $U_{inst,w}$ (kV) | $\sigma_{Ui}$ (%) | U-T | 1/tb | v (m/µs) | U-T/U50 | Uinst/U50 |
| 1 | 28.00 | 0 | 266.00 | 264.88 | 0.25 | #DIV/0! | #DIV/0! | #DIV/0! | #DIV/0! | 0.93 |
| 2 | 29.00 | 0 | 275.50 | 273.77 | 0.00 | #DIV/0! | #DIV/0! | #DIV/0! | #DIV/0! | 0.97 |
| 3 | 29.25 | 10 | 277.88 | 275.72 | 0.15 | 277.88 | 0.09 | 0.00 | 0.98 | 0.97 |
| 4 | 29.50 | 30 | 280.25 | 278.64 | 0.35 | 280.25 | 0.08 | 0.00 | 0.99 | 0.98 |
| 5 | 29.75 | 50 | 282.63 | 281.06 | 0.48 | 282.63 | 0.08 | 0.00 | 1.00 | 0.99 |
| 6 | 30.00 | 60 | 285.00 | 282.58 | 0.20 | 285.00 | 0.09 | 0.00 | 1.01 | 1.00 |
| 7 | 30.50 | 100 | 289.75 | 287.50 | 0.33 | 289.75 | 0.09 | 0.00 | 1.02 | 1.01 |
| 8 | 31.00 | 95 | 294.50 | 292.45 | 0.31 | 294.50 | 0.10 | 0.00 | 1.04 | 1.03 |
| 9 | 31.50 | 100 | 299.25 | 294.94 | 0.98 | 299.25 | 0.11 | 0.00 | 1.06 | 1.04 |
| 10 | 32.00 | 100 | 304.00 | 301.53 | 0.34 | 304.00 | 0.12 | 0.00 | 1.07 | 1.06 |
| 11 | 33.00 | 100 | 313.50 | 311.28 | 0.36 | 313.50 | 0.14 | 0.00 | 1.11 | 1.10 |
| 12 | 34.00 | 100 | 323.00 | 319.79 | 0.33 | 323.00 | 0.16 | 0.00 | 1.14 | 1.13 |
| 13 | 36.00 | 100 | 342.00 | 336.71 | 0.22 | 342.00 | 0.19 | 0.00 | 1.21 | 1.19 |
| 14 | 38.00 | 100 | 361.00 | 354.49 | 0.24 | 361.00 | 0.24 | 0.00 | 1.27 | 1.25 |
| 15 | 40.00 | 100 | 380.00 | 370.25 | 0.22 | 380.00 | 0.33 | 0.00 | 1.34 | 1.31 |
| 16 | 45.00 | 100 | 427.50 | 402.33 | 0.20 | 427.50 | 0.45 | 0.00 | 1.51 | 1.42 |
| 17 | 50.00 | 100 | 475.00 | 428.98 | 0.13 | 428.98 | 0.64 | 0.00 | 1.51 | 1.51 |
| 18 | 60.00 | 100 | 570.00 | 477.49 | 0.31 | 477.49 | 0.82 | 0.00 | 1.68 | 1.68 |
| 19 | 70.00 | 100 | 665.00 | 510.72 | 0.60 | 510.72 | 0.96 | 0.00 | 1.80 | 1.80 |
| | | | | 548.47 | | | | | | |
| | | | | 0.00 | | | | | | |

## Additional Data

| Additional Diagrams | | | | | | | |
|---|---|---|---|---|---|---|---|
| No | Uo (kV) | Uinst,w (kV) | $U_{,Ip,w}$ (kV) | $I_p$ (kA) | Up/Ip (Ω) | U,Ip/Ip (Ω) | Up/U,Ip |
| 1 | 28.00 | 264.88 | #DIV/0! | #DIV/0! | #DIV/0! | #DIV/0! | #DIV/0! |
| 2 | 29.00 | 273.77 | #DIV/0! | #DIV/0! | #DIV/0! | #DIV/0! | #DIV/0! |
| 3 | 29.25 | 275.72 | 135.71 | 0.60 | 461.84 | 227.33 | 2.03 |
| 4 | 29.50 | 278.64 | 128.04 | 0.59 | 472.01 | 216.90 | 2.18 |
| 5 | 29.75 | 281.06 | 132.44 | 0.59 | 477.83 | 225.16 | 2.12 |
| 6 | 30.00 | 282.58 | 141.82 | 0.62 | 458.86 | 230.30 | 1.99 |
| 7 | 30.50 | 287.50 | 147.92 | 0.64 | 449.56 | 231.31 | 1.94 |
| 8 | 31.00 | 292.45 | 150.78 | 0.65 | 450.80 | 232.42 | 1.94 |
| 9 | 31.50 | 294.94 | 159.93 | 0.66 | 446.28 | 241.99 | 1.84 |
| 10 | 32.00 | 301.53 | 172.10 | 0.69 | 435.24 | 248.41 | 1.75 |
| 11 | 33.00 | 311.28 | 165.43 | 0.69 | 449.18 | 238.72 | 1.88 |
| 12 | 34.00 | 319.79 | 185.40 | 0.72 | 441.69 | 256.07 | 1.72 |
| 13 | 36.00 | 336.71 | 204.90 | 0.77 | 436.04 | 265.34 | 1.64 |
| 14 | 38.00 | 354.49 | 227.28 | 0.85 | 418.73 | 268.46 | 1.56 |
| 15 | 40.00 | 370.25 | 245.84 | 0.91 | 405.44 | 269.21 | 1.51 |
| 16 | 45.00 | 402.33 | 274.09 | 1.02 | 394.96 | 269.07 | 1.47 |
| 17 | 50.00 | 428.98 | 305.90 | 1.15 | 372.25 | 265.45 | 1.40 |
| 18 | 60.00 | 477.49 | 341.47 | 1.45 | 329.31 | 235.50 | 1.40 |
| 19 | 70.00 | 510.72 | 363.93 | 1.59 | 320.60 | 228.46 | 1.40 |